공학박사 학위논문

# Assessment Method of the Fitness of Initial Arrangement Design of a Naval Ship Considering Ship Flooding

침수를 고려한 함정의
초기 배치 설계의 적합성 평가 방법

2019년 8월

서울대학교 대학원
조선해양공학과
김 기 수

# Abstract

## Assessment Method of the Fitness of Initial Arrangement Design of a Naval Ship Considering Ship Flooding

The initial design of the ship follows several stages to meet the design requirements. Generally, it is based on the design requirements and the information of the buses, and it goes through the steps of selecting the main specifications, selecting the line, selecting the main engine, arranging the layout, calculating the ship, and analyzing the performance. The layout design in the above process depends on the information of the mother ship and the experience of the designer. Accordingly, arrangement design was performed according to qualitative evaluation rather than traditionally quantitative evaluation. Because a person manually manages the layout design and evaluates multiple plans, it takes a lot of time to design the layout. Therefore, in this study, we aimed to automate and optimize quantitative evaluation and review of several for the initial arrangement design of a naval ship.

In addition, after the arrangement design, ship calculation process can be done to ensure that the ship has adequate stability during operation. Ship stability is evaluated as intact stability and damage stability. Damage stability is traditionally evaluated considering only the final stage after damage, and there is a lack of evaluation of damage and progress of flooding. In addition, the stability calculation for various things must be

carried out through the ship calculation program, which is a process in which many designers take a lot of work as the layout design. In order to overcome the limitations of the existing ship calculation, this study proposes a method to evaluate the stability of the ship by applying intermediate flood analysis as well as intact and damage stability evaluation and applying it to the arrangement design evaluation process.

In this study, we considered three aspects of stability, vulnerability, and operability for the initial arrangement design of naval ships. According to the requirements for the intact stability of naval ships, the intact stability was investigated. In addition, the damage stability evaluation was carried out considering the recovery of the damage in the general final condition and the intermediate flooding. Intermediate flooding uses PBD (Position Based Dynamics) to calculate the flow rate through the openings in the damaged part and trap, thereby updating the weight and center of gravity of the modified trap. Then, the changed information is substituted into the 6-DOF motion equation to track the behavior of the ship every time step. Through this, it is possible to evaluate the progress of the ship 's flooding through the damage and the damage stability in the process. In order to improve the intact stability and damage stability, GZ curve calculation is accompanied. In this study, trim is considered in addition to GZ value calculation considering existing heave motion.

The vulnerability assessment of the naval ship considers both the vulnerability of the bulkhead and the vulnerability of the rooms. Vulnerability of the bulkhead was considered as the sum of the bursting pressure on the bulkhead with various damage, and the vulnerability of the compartment was taken into account by multiplying the severity of the compartment with the probability that various damage would affect the compartment. In addition, for the two vulnerabilities, we considered the length, width, and height direction damage probability of the five types of damage (ASMs (Anti-Ship

Missiles), torpedoes, mines, collisions, and grounding)

In order to quantitatively evaluate the operability of the naval ship, the movement of the crew and cargos between the compartments of the naval ship was considered. For this, the relation between the shortest distance between each rooms and the compartment was considered. The relationship between the compartments was considered through proximity considering both intimacy assessing the affinity of rooms to be close and antagonism between rooms to be far apart.

The three evaluations described above have been formulated as a problem for the initial layout design of a ship. The optimization problem design variables were set to the location of the bulkhead and deck, the location of the compartment and the location of the corridor, and the objective function was set to minimize the vulnerability of the naval ship and maximize operability. In order to improve stability, we considered maximizing initial GM as an objective function. In this process, constraints on the positions of the bulkheads and decks, the lengths required by the engine, and the constraints on the extent that each compartment has to be minimized are considered, and the location of the compartment is considered as a constraint in the optimization problem. The optimal design of the initial arrangement design of the naval ship was obtained through this, and it was evaluated whether the optimized arrangement design satisfies the damage stability including the intermediate flooding stage.

The initial arrangement design and the ship calculation process described above were developed as one program, and the applicability of this study was confirmed by applying it to the U.S. Navy Destroyer.

Keywords: Arrangement design; Stability evaluation; Intermediate flooding; PBD

(Position Based Dynamics); Vulnerability evaluation; Operability evaluation; Arrangement optimization; Multi-objective optimization; Naval ship

Student number: 2015-30240

# Contents

# Figures

# Tables

# Nomenclature

| | |
|---|---|
| PBD | Position Based Dynamics |
| SPH | Smoothed Particle Hydrodynamics |
| MPS | Moving Particle Semi-Implicit |
| EMPS | Explicit Moving Particle Semi-Implicit |
| CFD | Computational Fluid Dynamics |
| QS | Quasi-Static analysis |
| IFA | Intermediate Flooding Analysis |
| GUI | Graphical User Interface |
| PDM | Position Difference Method |
| RAO | Response Amplitude Operator |
| DOF | Degree of Freedom |
| IMO | International Maritime Organization |
| SOLAS | Safety Of Life At Seas |
| MARPOL | Marine Pollution Treaty |

# 1. Introduction

## 1.1. Research backgrounds

The design of the vessel is carried out in several stages, similar to that of commercial ships, as shown in Figure 1-1. Starting the design of the naval ship essentially begins with the requirements of the shipowner (usually the country). The requirements of naval ships are added to the requirements of normal ship speed, cargo weight, and regulation satisfaction, in addition to those for specific operations [1].

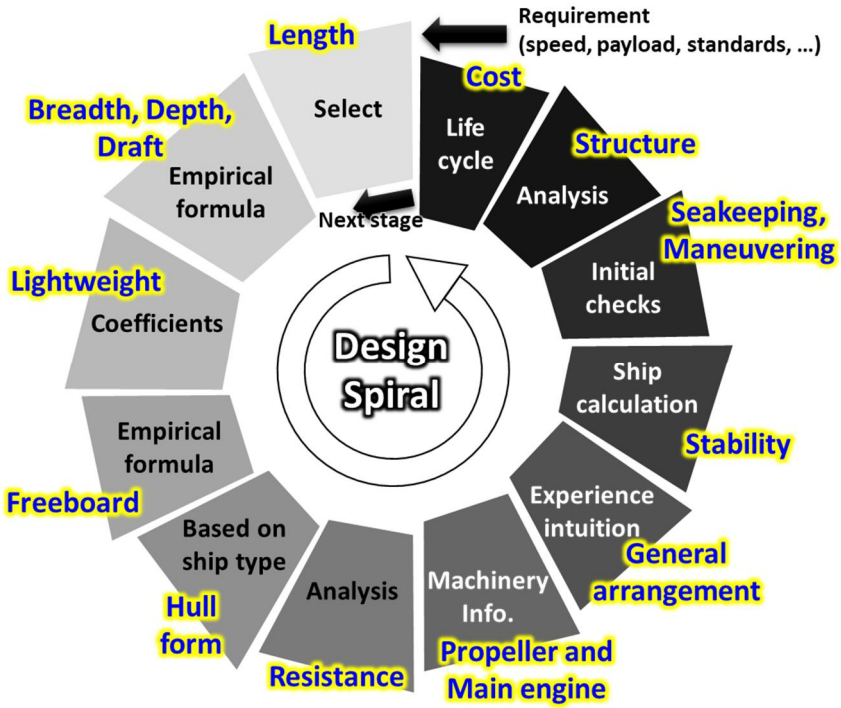


Figure 1-1. Design spiral of naval ships

The initial design of the vessel begins with the selection of the length. Selected

according to the specifications of the parent ship or the designer's experience. Based on the empirical formula and the length of the selected vessel, the remaining main dimensions (width, depth, and water) are then determined. Based on the main dimensions determined, the displacement will be determined through various empirical formulas and areas of the surface are then calculated according to the type of vessel. Subsequent designs were designed to satisfy the surface area, which based on the reference to the different types of ship and the model experiments, resulted in the lines of ships meeting various requirements (mainly with respect to resistance). Then, through empirical methods or model experiments, the ship resistance is calculated, and after the resistance is calculated, the main engine is selected to overcome the resistance and to operate at the required speed. The engine is then loaded, and a number of other auxiliary equipment to run the engine are selected, and the layout design is carried out to deploy the equipment. After the layout design, the weight, center of gravity and distribution of the weight of the naval ship are determined, and the information is used to calculate the ship's stability. After calculating the stability, the analysis of various functions such as self-propulsion performance and operational performance is carried out, and the ship is evaluated for structural strength in the required various loading condition. It will then finally measure the price of the ship. Generally, prices are so important that they are often a requirement, but naval ship is generally not more sensitive to prices than merchant ships because they are prioritized as to whether they are capable of carrying out required operations. Complete the initial design and concept prior to the detailed design through a design spiral with the process described above as a cycle [2].

In particular, the arrangement design is one of the most important parts because it defines the design philosophy of the ship. As such, many compartments, including tanks, rooms, and equipment, are placed in limited space on the ship. There are many

alternatives for the arrangement design, and our hope is to select a better alternative (if possible, the best one) in less time [3]. arrangement designs are generally heavily influenced by the layout design of the parent ships and are conducted by expert experience, so qualitative assessment rather than quantitative assessment is the main factor. Therefore, time is also expended. In order to reduce this time-consuming and to derive the optimal arrangement design through various requirements and quantitative assessments, optimization of the initial arrangement design of a naval ship was conducted in this study. As previously discussed, after the design of the initial arrangement design of the naval ships, the weight and center of gravity of the ship are determined, so the ship calculations are carried out. Ship calculations are traditionally done through calculations of GZ curve and HA curve, and in the case of vessels, they are carried out in accordance with national regulations, unlike commercial vessels. In the case of the South Korea Navy, it is almost similar to the U.S. Navy's stability regulations under the influence of the U.S. Navy [4]. As with general arrangement, a large number of people are required to manually calculate through a program and evaluate stability within each time to write a report. Therefore, the purpose of this study was to help reduce the time of initial design and to select a better design by taking into account the stability of optimization of initial arrangement design of a naval ship, simultaneously proceeding with two steps, and automating them.

For the stability assessment, there are two main categories: intact and damage stability assessment. Damage stability is used to ensure that certain compartments meet certain stability criteria even in their states when they are damaged. However, the criteria are difficult to assess accurately considering only the final state of the damage. Therefore, in this study, it was intended to improve this by means of an intermediate flood analysis. After selection of arrangement design, as described earlier, to evaluate the alternative is

satisfying the criteria of the stability, intermediate flooding analysis is necessary, in order to evaluate how the accident occurred in the event of an accident. If ship is damaged, we have to estimated it can be reach to certain equilibrium position or sinking, and how it takes time to reach to final state. It is also necessary to find out the cause of the accident after the accident and to prepare countermeasures to cope with another accident in the future. The description is shown in Figure 1-2.


Figure 1-2. necessity of the intermediate flooding analysis

In this process, a lot of implementation is required to deploy several alternatives, and a very quick analysis is essential for a quick response to a ship's accident. Therefore, in this study, the rapid intermediate flooding analysis method was proposed. This was then incorporated into the initial arrangement design of naval ships.

## 1.2. Related works

This section summarizes, compares, and analyzes the various related works in which a study similar to this study was conducted before the study for the purposes above. Section

1.2.1 investigated and compared studies related to optimizing ship layout design with this study, and Section 1.2.2 investigated the intermediate flooding analysis not considered in other studies considered for layout design optimization and compared with the methods proposed in this study.

### 1.2.1. Related works for optimizing arrangement design of the naval ship

Several researchers have proposed methods to solve arrangement problems of ships, and in this section, we summarize past studies related to arrangement design in naval architecture.

Byun [5] proposed a rule-based expert system incorporating a knowledge base to support the compartment design of a commercial ship. Shin et al. [6] proposed an expert system to arrange the machinery on a ship. They proposed an expert system to evaluate the feasibility of design alternatives for machinery arrangement. Lee et al. [7], [8] used an improved genetic algorithm to arrange rooms and passages in the superstructure of a naval surface ship taking into account its operability, including the flow of crews and supplies. Boulougouris and Papanikolaou [9] proposed a method to arrange compartments in the hull of a naval surface ship and also proposed methods to assess the stability and survivability. They then formulated an optimization problem for the compartment arrangement and solved it using a multi-objective genetic algorithm (MOGA). Helvacioglu and Insel [10] proposed a multistage expert system to arrange the compartments on a container ship.

Andrews [11] proposed the building block method to perform the initial arrangement design of a naval surface ship. The building block method allows the arrangement design

according to various design requirements and the designer's preferences, and it also enables naval architectural calculations. Nick [12] proposed a method to generate, evaluate, and optimize the compartment arrangement of a naval surface ship. She defined the allocation as the assignment of space (compartment) to a deck of a ship, and the arrangement is used to determine the topology and geometry of the space for the assignment of each deck. Ours et al. [13] proposed an optimization method for the arrangement design of a naval surface ship. They determined a Pareto-optimal set from various objective functions. Parsons et al. [14] conducted zone-deck optimization and detailed room arrangement in the zone-deck through fuzzy optimization and allocation optimization. That is, they performed the arrangement design with two steps: allocation and arrangement. In their study, the relationship between compartments and the requirements of designers were reflected. Roh et al. [15] proposed a method to arrange bulkheads in the hull of a naval surface ship. They formulated an optimization problem for the bulkhead arrangement of which objective functions are to maximize the space for the armament and the structural strength while satisfying stability requirements. Chung et al. [16] proposed a rule-based expert system to optimize the compartments in the pressure hull of a submarine. Shin [17] proposed a method to arrange rooms in the superstructure of a naval surface ship by considering its survivability. He tried to quantify the survivability by using FMEA (Failure Mode and Effective Analysis) and FTA (Fault Tree Analysis). Ju et al. [18] proposed a method to arrange rooms in the superstructure of a naval surface ship. He used the SLP (Systematic Layout Planning) method to solve an optimization problem for the room arrangement of which objective functions are to optimize the survivability and operability. Kim et al. [19] proposed an expert system to arrange the compartments and equipment in the pressure hull of a submarine. The proposed expert system was based on the arrangement evaluation model (AEM) to

evaluate the feasibility of the design alternatives and the arrangement template model (ATM) to store the arrangement information. Kim and Roh [20] proposed an arrangement method of a submarine based on the expert system and the optimization technique. In their study, the arrangement design was mathematically formulated as a three-stage optimization problem for compartments, sub-compartments, and equipment. Jung [21] proposed a method to arrange rooms in the superstructure of a naval surface ship and also proposed a method to evaluate the integrated survivability considering the vulnerability, susceptibility, and recoverability. In addition, Jung et al. [3] performed optimizing the layout design of the naval surface ship considering their stability, operability and survivability.

As seen above, the most relevant studies have focused separately on the compartment (bulkheads or rooms) arrangement in the hull or the superstructure, but not both. Even considering both, the relationship between compartments and rooms cannot be considered true optimization because the layout design optimization has not been carried out as a single problem. Furthermore, not all performance, such as stability, operability, and vulnerability, were considered except Jung et al. [3], even though it is important to consider them simultaneously in the design of naval surface ships. Thus, this study proposes a method to optimally arrange bulkheads and rooms considering the major aspects of the performance as a naval surface ship as mentioned Section 1.1. Table 1-1 shows a summary of related studies and a comparison of those studies with this study.

Table 1-1. Summary of related studies of optimal layout design of a ship and comparison with this study

| Studies | Target | Compartment arrangement | | Consideration of | | | Optimization |
|---|---|---|---|---|---|---|---|
| | | Hull (Bulkhead) | Superstructure (Room) | Stability | Operability | Survivability | |
| Byun [5] | Commercial ship | √ | - | √ | - | - | - |
| Shin et al. [6] | Machinery space | √ (Equipment) | - | - | √ | - | - |
| Lee et al. [7], [8] | Naval surface ship | - | √ | - | √ | - | √ |
| Boulougouris and Papanikolaou [22] | Naval surface ship | √ | - | √ | √ | √ | √ |
| Helvacioglu and Insel [10] | Commercial ship | √ | - | - | - | - | - |
| Andrews [23] | Naval surface ship | √ | √ | √ | √ (User preference) | √ | - |
| Nick [12] | Naval surface ship | - | √ | - | √ | - | √ |
| Oers et al. [24] | Naval surface ship | √ (2D) | √ (2D) | - | √ | √ | √ |
| Parsons et al. [14] | Naval surface ship | √ | √ | | | | |
| Roh et al. [15] | Naval surface ship | √ | - | √ | √ | - | √ |
| Chung et al. [16] | Submarine | √ | - | - | √ | - | √ |
| Shin [17] | Naval surface ship | - | √ | - | - | √ | - |
| Ju et al. [18] | Naval surface ship | - | √ | - | √ | √ | √ |
| Kim et al. [19] | Submarine | √ | - | - | √ | - | - |
| Kim and Roh [20] | Submarine | √ | - | √ | √ | - | √ |
| Jung [21] | Naval surface ship | - | √ | - | - | √ | √ |
| Jung et al. [3] | Naval surface ship | √ | √ | √ | √ | √ | √ |
| This study | Naval surface ship | **√ (integrated)** | | **√ (intermediate flooding analysis)** | √ | √ | √ |

In the case of the stability of some study evaluation as one of them taken into consideration, but a simple intact stability and damage stability to the standards of optimization may have only applied. There was no study taking into account an intermediate flooding analysis. In this study, damage stability, including intermediate flooding analysis, was applied into the arrangement design of a naval ship. Studies related to intermediate flooding analysis were investigated in Section 1.2.2.

### 1.2.2. Related works for intermediate flooding analysis

The intermediate flooding analysis of a ship is a method of calculating the amount of fluid flowing through the damaged part or through openings in the ship, through which the weight and center of gravity of the renewed vessel are used to calculate the movement of the vessel in the next time. Although quasi-static methods have generally been used for intermediate flooding analysis, the quasi-static methods have not been able to detect the dynamic behavior of ships and serious ship movements in the early transmission conditions of the flooding, and more recently a dynamic method has emerged.

The studies using quasi-static analysis were studied as follows. Ruponen et al. [25]–[29] and Dankowski [30]–[32] used the quasi-static method to perform the intermediate flooding simulation. They calculated the equilibrium position of a damaged ship at every time step considering incoming water from damaged holes. They also compared their results with the experimental data. However, they simulated only the intermediate stage of the flooding simulation. In addition, Ruponen used the water plane-based method when calculating the water volume in the damaged compartments [25]. The water volume calculated from the water plane-based method can have some errors for compartments

having a complicated shape because the waterplane area is approximated in the method [26], [28]. That is, he calculated the water volume in the compartment by integrating the derivative of the water volume in the compartment (¼the approximated water plane area * the derivative of the water height in the compartment). And Dankowski used the interpolation method to calculate the water volume from the water height in the compartment under a certain attitude of the ship. These methods require the iterative process to reduce an error caused by approximation or interpolation. Lee et al. [33] calculated the motion of both intact and damaged ships by using the CFD method. They compared simulation results with the experimental data. However, they did not consider the increased weight of incoming water through a damaged hole and the effect of air compression. The air compression influences the flooding speed of water because the air compression due to incoming water can prevent further flooding progress. They mainly focused on the motion itself when the damaged compartments are already filled with seawater at the intermediate flooding stage.

Unlike the quasi-static analysis described above, researches conducted by dynamic methods for flooding analysis is as follows. Strasser et al. [34] conducted an underwater analysis using the CFD method and verified its accuracy by comparing the method with the experimental results of Ruponen [27]. However, there was a disadvantage in accuracy compared to the quasi-static method. Sadat-Hosseini et al. [35] conducted an intermediate flooding analysis using a similar method, and in this study, even the effects of waves being applied to vessels during flooding were taken into account by applying the power up to a wave using CFD. In addition, the study in Lee et al. [33] considered waves by external force in the flooding analysis using CFD. However, using CFD, as in previous studies, takes a lot of time for mesh generation and it is difficult to set the basic condition. Also, the analysis time was too long compared to the quasi-static method. Therefore, to

address these shortcomings, many studies have recently implemented a method to calculate the flow rate along the damaged parts and openings using the existing orifice method, and to analysis the movement of ships using the 6-DOF movement equation. Manderbacka et al. [36] calculates the flow rate through the damaged part and the opening using the hydraulic orifice equation and calculates the movement of the vessel by substituting it for the 6-DOF movement equation, enabling the analysis of flooding under a transfer condition that was not previously analyzed. In addition, in the case of Ypma & Turner [37], similar to the preceding study, the influence on waves was also taken into account while performing analyses relatively quickly, taking into account the waves by an external force. In the previous study of this study, Kim et al. [38] calculated the flow rate through the damaged parts and openings using the dynamic orifice equation and analyzed the movement of the ship's 6-DOF movement by substituting the changed ship's weight and center of gravity with the Cummins equation. It also considered oil spills in the process.

In this study, the advantages of the above mentioned methods were collected and the position based dynamics (PBD) was used to calculate the fluid inside the vessel and the dynamic flow rate, thus renewing the weight and center of gravity of the vessel. By applying updated information to the Cummins equation every time step, dynamic flooding analysis was performed, and waves were considered as external forces using the hydrodynamic coefficient of the Cummins equation. As performing the method proposed in this study, an accurate and rapid intermediate flooding analysis method was proposed, which was carried out in the initial layout design process of the vessel to further assess the damage stability. The relevant studies for flooding analysis and what has been done in this study are as shown in Table 1-2.

Table 1-2. Related works on flooding analysis

| Studies | Method for flooding analysis | | Consideration of oil spill | Consideration of wave loads | Computing time |
|---|---|---|---|---|---|
| Ruponen [25], [27] | Quasi-static | Hydraulic orifice eq. | - | - | Fast |
| Manderbacka et al. [39] | | | - | - | Fast |
| Dankowski et al. [31], [32], [40] | | | - | | Fast |
| Lee [41] | | Dynamic orifice eq. | | | Fast |
| Debra et al. [42] | Experiment | | √ | | N/A |
| Strasser et al. [34] | Dynamic analysis | Eulerian method | | | Slow |
| Hamid et al. [35] | | | | √ | |
| Lee et al. [33] | | | | √ | Slow |
| Manderbacka et al. [36] | | Hydraulic orifice eq. | | | Slow |
| Ypma & Turner [37] | | | | √ | Fast |
| Kim et al. [38] | | Dynamic orifice eq. | √ | √ | Fast |
| This study | | Lagrangian method | √ | √ | Fast |

## 1.3. Research objectives and work scope

For the requirements described in Section 1.1, the studies done in this study is as follows.

First of all, this study considered intact and damage stability and intermediate flooding analysis to assess resiliency as shown in Figure 1-3.

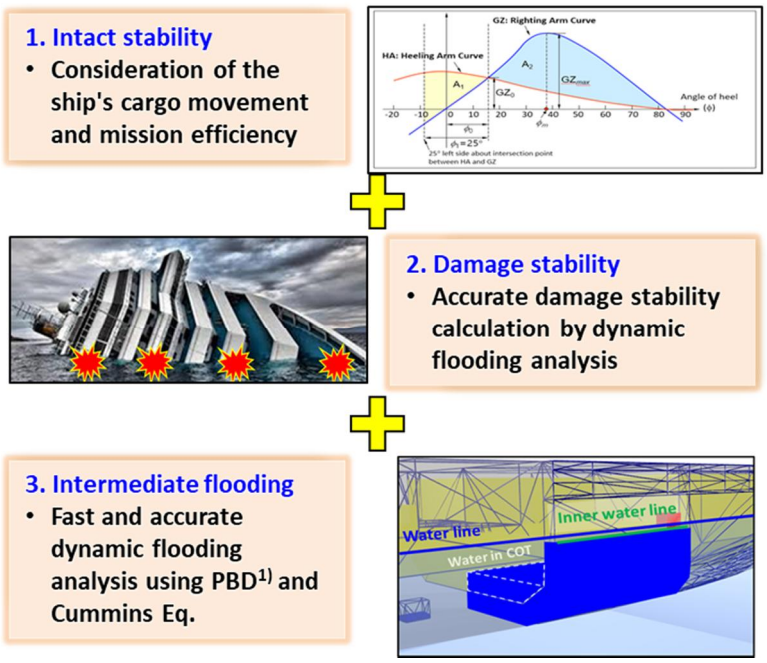


Figure 1-3. Research objectives for stability evaluation

For the vulnerability evaluation, the vulnerability of naval ships due to various damage was calculated by distinguishing between the vulnerability of bulkheads and the vulnerability of rooms. The research objectives for vulnerability evaluation is shown in Figure 1-4.

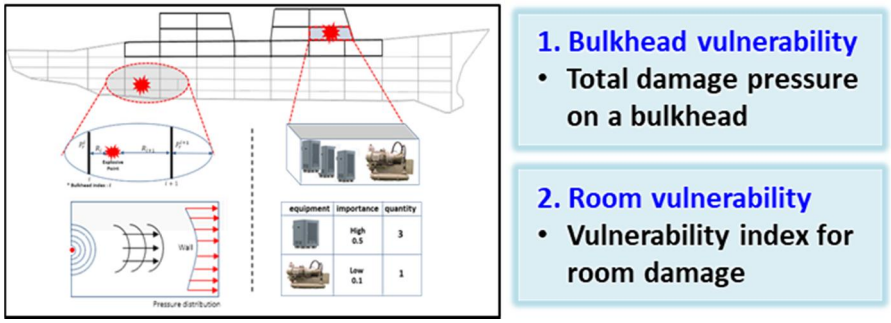


Figure 1-4. Research objectives for vulnerability evaluation

In order to operability evaluation, the spatial efficiency of the ship to increase the armed space was reconsidered, and the efficiency of the goods movement and source movement between rooms was evaluated quantitatively through proximity taking into account intimacy and hostility. In addition, to improve the operability of the compartments and rooms, the rectilinear distance between the interrelated compartments and the compartments was calculated and reflected as operability. The research objectives for operability evaluation is shown in Figure 1-5.

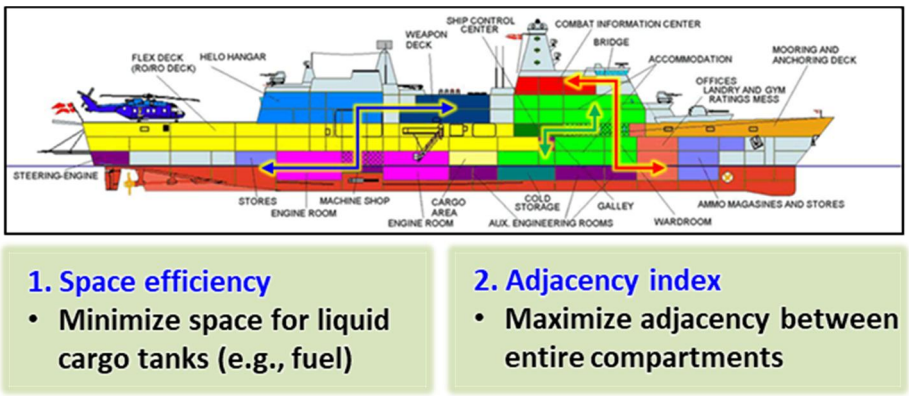


Figure 1-5. Research objectives for operability evaluation

In order to optimize the initial arrangement design of a naval ship, the optimization problem for the layout of bulkheads and superstructure was formulated. Problems for the layout of compartments and rooms were considered by integrating into one. In this process, the stability, vulnerability, and operability described above were taken into account and used to find optimal arrangement design as shown in Figure 1-6.

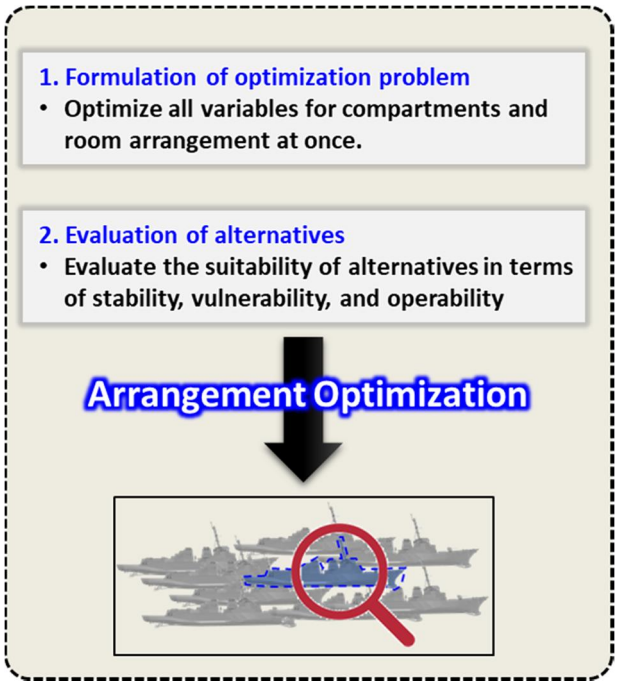


Figure 1-6. Research objectives for optimization of naval ship arrangement

The purpose of this study can be summarized in 6 categories as follows:

- Flow analysis using PBD, and motion analysis using 6-DOF equation for analyzing the intermediate flooding analysis
- Evaluation of damage stability including intermediate flooding analysis
- Evaluation of the vulnerability of a naval ship considering the damage of bulkheads and rooms
- Evaluation of operability in consideration of the relationship between rooms and compartment inside the hull
- Proposed optimization method for initial arrangement design for naval ships

considering stability, vulnerability, and operability

- Development of a program for initial arrangement design for naval ships

# 2. Theoretical backgrounds

For the background and objective of this study introduced in Section 1, theoretical backgrounds for the study items conducted in this study is described in this Section.

## 2.1. Configuration of a framework for evaluation of arrangement for naval ships

In this study, various evaluation factors were considered, programmed, and applied to the optimization of arrangement design of naval ships. For this methodology to an application, a single large framework is required. Therefore, this study proposed and applied a framework consisting of five layers as shown in Figure 2-1.

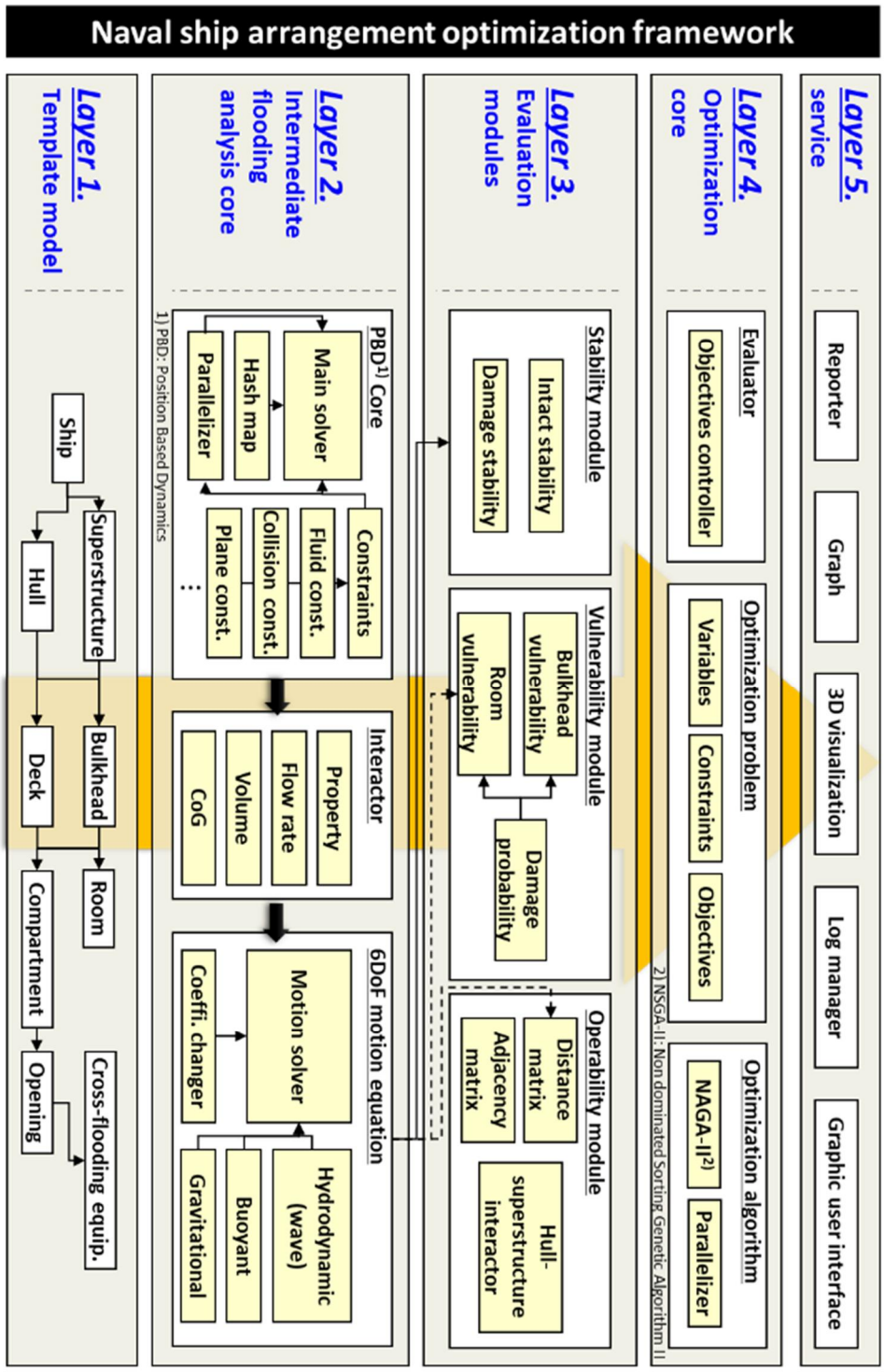


Figure 2-1. Framework for optimization of naval ship arrangement

In this study, offer framework is constructed with layers of a total of five. The first layer is a template model (data structure) which is for stability, vulnerability, and operability evaluation. The second layer is for intermediate flooding analysis using PBD and 6-DOF equation. PBD core used to analysis flow rate and flow movement. And analyzed results were used in 6-DOF equation to solve the movement of a naval ship. In the meantime, the information analyzed in PBD is delivered through the interactor in a 6-DOF equation. The third layer is an evaluation module consisting of three modules for evaluating alternatives for arrangement design. It consists of a stability evaluation module that evaluates the intact stability and damage stability of a naval ship, a vulnerability evaluation module through vulnerability calculations of rooms and bulkheads, and an operability evaluation module through a rooms and compartments relationship, including the results of an intermediate flooding analysis previously calculated from the second layer. The fourth module is the optimization core layer for applying the calculated evaluation elements to the optimization problem in the third module. In this layer, the evaluation elements consist of an evaluator for application from optimization problems, an optimization problem into a single problem, and finally an optimization algorithm for solving a formulated optimization problem. Three assessment modules included in the third layer are utilized when finding the optimal arrangement design of a naval ship. Finally, the fifth layer includes 3D visualization, graphs, etc. for users to effectively evaluate through the proposed methods, including the GUI to utilize them.

The later chapters describe the basic background theory used in each of the layers described earlier and the method by which the theory was used in this study. First, Section 2.2 describes the template model included in Layer 1. Section 2.3 describes the resilient assessment module, including intermediate-stage flooding analysis. Section 2.4 describes the vulnerability assessment and Section 2.5 details how to assess its operability.

Section 2.6 addresses the issue of optimization through the three evaluation factors.

## 2.2. Template model for naval ship

To express specific information, we need a model for domain about specific subject. And the model is called ontology. In other words, ontology is a specification of a conceptualization [43]. For arrangement design of ships, we need to have ontology for the arrangement of ships. And for arrangement design of the naval ship, we need to have ontology for arrangement of naval ship. Ontology gives the concept of a specific domain to object that have to share the information about the domain [44]. Ontology's necessity is as follows:

- To share a common understanding of the structure of information among people or software agents
- To enable reuse of domain knowledge
- To make domain assumptions explicit
- To separate domain knowledge from the operational knowledge
- To analyze domain knowledge

In many books about artificial intelligence, the definition of ontology is vary with each other. There are many definitions of ontology, so that clear concept of ontology is treated in this study. Ontology is composed of a formal explicit description of concepts in a domain of discourse (classes or concepts), and properties of each concept describing

various features and attributes the concept (slot or properties). In practical terms, developing an ontology includes:

- Defining classes in the ontology
- Arranging the classes in a taxonomic (subclass-superclass) hierarchy
- Defining slots and describing allowed values for these slots
- Filling in the values for slots for instances

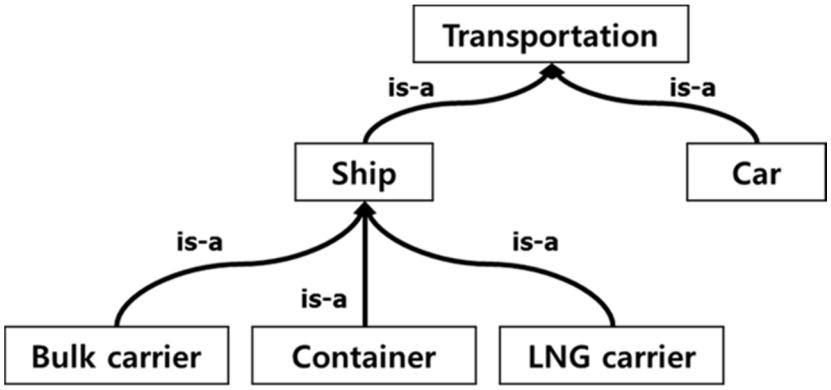


Figure 2-2. Ontology of transportation

Figure 2-2 shows the example of ontology for transportation. In the example, car and ships (bulk carrier, container, and LNG carrier) are described. But it can change the structure as the usage of.

In this study, an ontology is required primarily to evaluate the three performances (resilience, vulnerability, and operability) including the arrangement design of a naval ship. Therefore, the naval ship is described as ontology as shown in Figure 2-3.

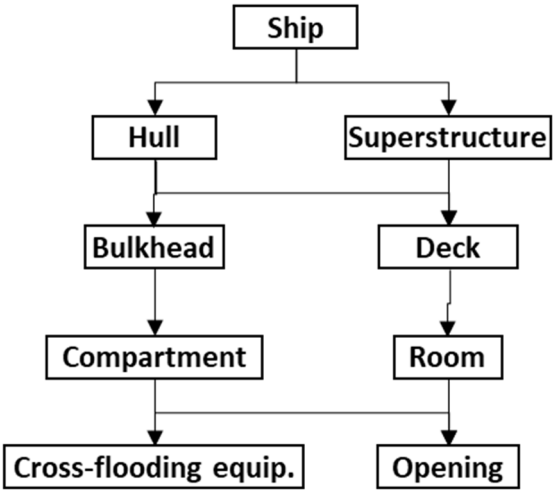


Figure 2-3. Ontology for a naval ship

The ship is first expressed as a hull and superstructure. If the hull consists mainly of bulkheads and decks, it is divided into bulkheads and decks, and the superstructure can also be divided into bulkheads and decks. Actual hull bulkheads and decks exist for structural strength and various performance, but in this study, only the elements for arrangement design, stability, vulnerability, and operability are considered. The hull divided by the bulkhead and deck is divided into sections, and the superstructure is divided into rooms. There are doors or passages between the rooms for the connection, which serve as an opening for flooding. A specific opening also serves as cross-flooding equipment. Hierarchical template model as shown in Figure 2-3.

## 2.3. Stability evaluation

In the case of ordinary ships, such as merchant ships, the stability of the ship is

evaluated in accordance with various international regulations. International regulations are mainly set for the safe operation of ships and for the safety of seafarers and passengers on board the ship, and they are subject to SOLAS or MARPOL, which are mainly prescribed by IMO. However, in the case of a naval ship, it belongs to each country except for special cases, and operates according to the mission designated by the state. Therefore, the evaluation of the stability of these special lines does not comply with the international regulations but follows the standards set by each country. In the case of the Korean Navy, it follows the reference standard [4], which is very similar to that of the U.S. Navy. Therefore, in this study, the satisfaction of existing intact stability was checked. In case of damage stability, intermediate flooding analysis is carried out at each time step during the flooding of the vessel, and its satisfaction is checked.

### 2.3.1. Intact stability evaluation

Intact stability is a standard for judging the stability of a ship when the ship is still floating in the waters. It is similar to the general merchant ship standard. To verify the criteria for the intact stability, a GZ (righting arm) curve, and an HA (heeling arm) curve should be calculated, as shown in Figure 2-4.

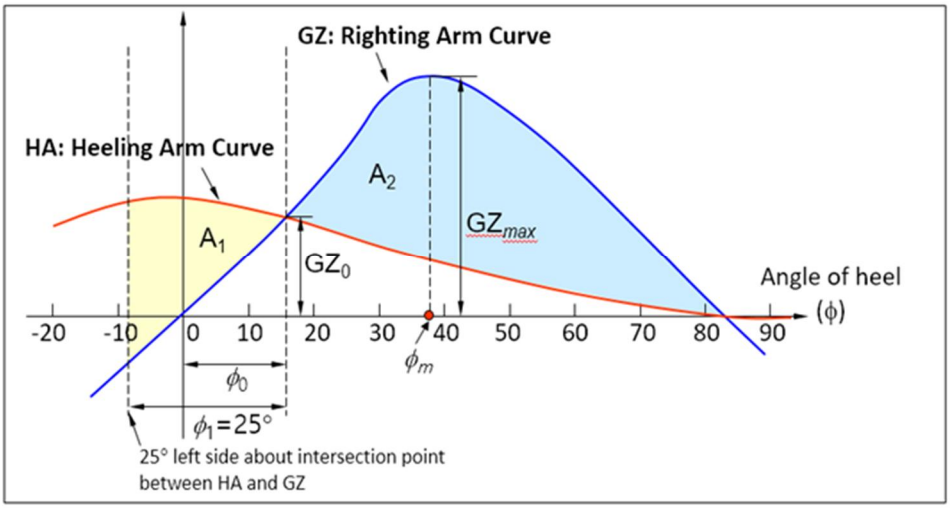


Figure 2-4. GZ and HA curve for intact stability

In Figure 2-4, GZ can be calculated by Eq. (1). HA can also be calculated arithmetically through Eq. (2).

$$GZ = KN - KGsin\theta \tag{1}$$

$$HA = \frac{0.437 \cdot V^2 \cdot A \cdot L \cdot \cos^2 \phi}{2240 \cdot \Delta} \tag{2}$$

In order to understand how to calculating righting arm, we have to understand Figure 2-5. In Figure 2-5, the point '*K*' represents the keel of the ship. If at any angle of the heel ($\theta$), a line parallel to that of GZ is drawn from '*K*', then the point of intersection of this line with the vertical line of action of buoyancy is represented as '*N*'. When calculating heeling arm (HA), '*V*' means ship's velocity in knot unit, '*A*' means projected side area of the ship for wind pressure, '*L*' means the perpendicular distance between the centroid of

'*A*' and half draft, and '∆' means displacement of ship.

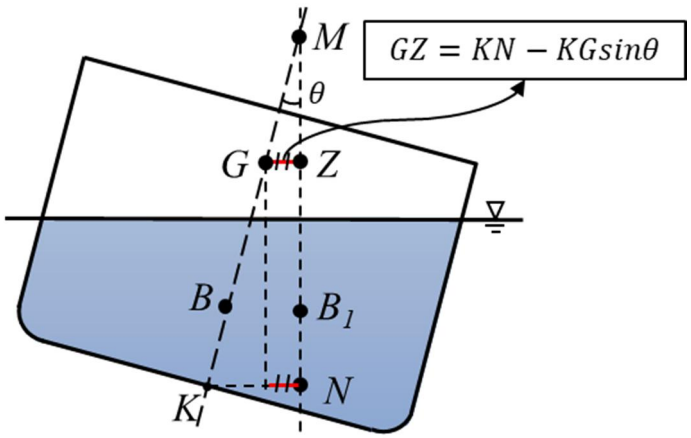


Figure 2-5. Calculating GZ (righting arm) in the external heeling moment

To calculate the GZ curve, the buoyancy and weight changes should be considered for different heel angles. Thus, if the positions of the bulkheads associated with liquid tanks change, the GZ curve should be calculated considering the free surface effect of the liquid tanks [45]. The following three factors [46] are assessed, which are static considerations Eq. (3), initial restoration-related items Eq. (4), and dynamic restoration-related items Eq. (5). These expressions are shown in detail below.

$$GZ_0/GZ_{max} \leq 0.6 \quad (3)$$

$$\text{Ratio between capsizing and restoring energy } (A_2/A_1) \geq 1.4 \quad (4)$$

$$\text{Equilibrium heel angle } (\phi_0) \leq 15 \text{ deg} \quad (5)$$

Eq. (3) , the maximum GZ value and the ratio of the GZ curve to the point at which the HA curve meets can be calculated, which means that $GZ_0$ must be greater than 0.6 of $GZ_{max}$. As expressed in Eq. (4), the initial restoration performance is related to the condition that the point where the initial GZ curve and the HA curve meet is smaller than 15 degrees. Finally, Eq. (5) shows that the ratio of the area between $A_1$ and $GZ_0$ surrounded by HA curves and GZ curves below 25 degrees from $GZ_0$ and the area between the first and second GZ curves and HA curves in the positive direction is 1.4 Must be satisfied. This means that the restorative offset due to buoyancy should be 1.4 times larger than the loss of stability of the ship due to sudden tilts due to the wind. In this study, the optimization is basically performed to satisfy the intact stability.

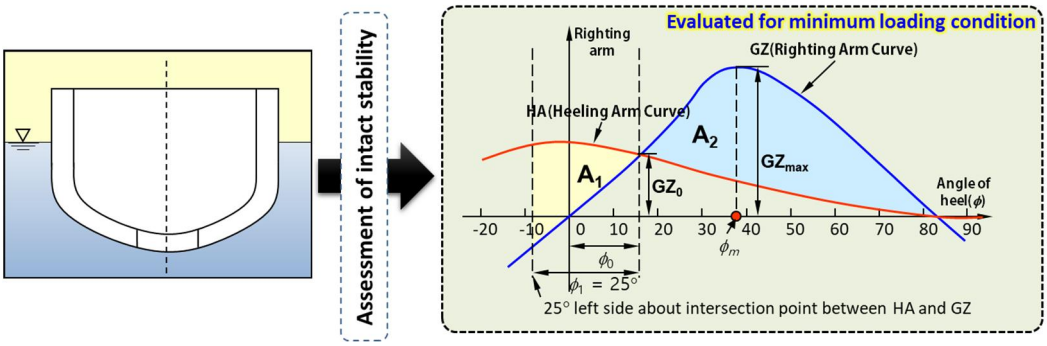


Figure 2-6. Intact stability evaluation

In this study, the satisfaction of intact stability was evaluated at minimum loading condition as shown in Figure 2-6. This is generally more susceptible and vulnerable in terms of stability since the center of gravity of the minimum loading condition is above the full loading condition in the case of a naval ship. Therefore, the optimization process satisfies the minimum loading condition.

### 2.3.2. Damage stability evaluation

The damage stability of a naval surface ship can be roughly checked using a deterministic approach. The basis to determine the extent of flooding is the length of damage to the shell at any point along the ship's length resulting from an attack with a weapon or a collision. In particular, the combatant-type naval surface ships of over 90 m in length should meet criteria for adequate subdivision to resist underwater damage [47]. That is, they should be capable of withstanding to flood from a shell opening equal to 12.5% of the ship's length (longitudinal extent) at any point fore and aft. The maximum transverse extent is assumed to be that caused by penetrating damage to, but not including, any center bulkhead, and the maximum vertical extent is assumed for all decks to be opened because of the effect of the resulting high flooding, free surface, and possible unsymmetrical flooding. With this assumption for the extent of the damage, satisfying the damage stability can be checked with the criteria summarized in Eqs. (6)-(10).

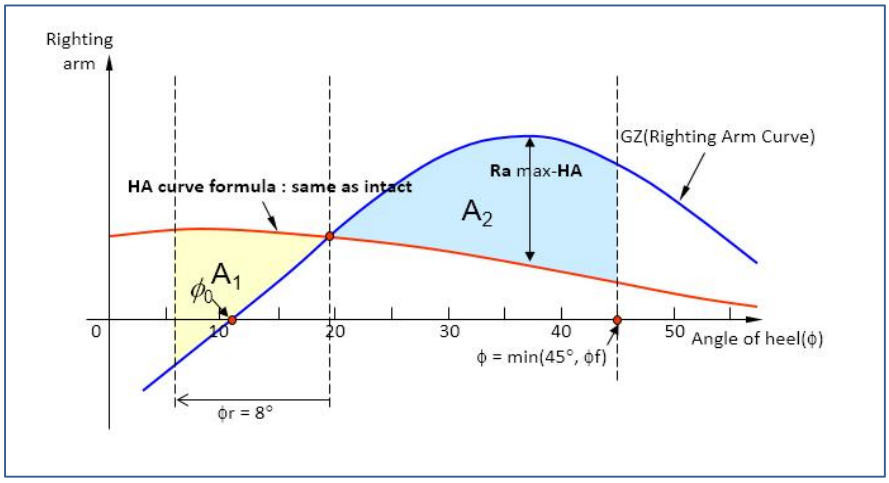


Figure 2-7. GZ and HA curve for damage stability

$$\text{Equilibrium heel angle } (\phi_0) \leq 15 \text{ deg} \quad (6)$$

$$\text{Ratio between capsizing and restoring energy } (A_2/A_1) \geq 1.4 \quad (7)$$

$$GZ_{max} - HA \geq 0.075 \text{ m} \quad (8)$$

$$\text{Area } A_1 \geq 0.02 \text{ m·rad} \quad (9)$$

$$\text{Distance from waterline to margin line} \geq 0.0 \text{ m} \quad (10)$$

It means that the final posture should not be tilted by more than 15 degrees in case of the damage of Eq. (6). As described in Eq. (7), the area enclosed by the HA curve and the GZ curve at the point where the initial GZ curve and the HA curve meet and the point shifted by 8 degrees in the negative direction are defined as $A_1$, If the $A_2$ surrounded by the GZ curve and the HA curve at a small point in $\phi_f$ is greater than 1.4 times the $A_1$, the wind is blown from the damaged state and the restoration of the naval ship due to the sudden tilting disappears This means dynamic stability that the restoring force generated by buoyancy must be larger. Eq. (8) Indicates that the difference between the maximum value of GZ and the HA value at the angle is 0.075 or more, which is a criterion for the magnitude of intact stability. Eq. (9) is a condition related to dynamic stability on condition that the area of $A_2$ mentioned above should be larger than 0.019. Finally, Eq. (10) is a condition that the margin line of the damage should not be flooded in the water. Is the height of the deck. When the deck is submerged in water, it is a criterion to prevent it because the seawater flows through the opening in the upper part of the deck. In this study, the five damage stability criteria are calculated and met at every time step in the intermediate flooding analysis.

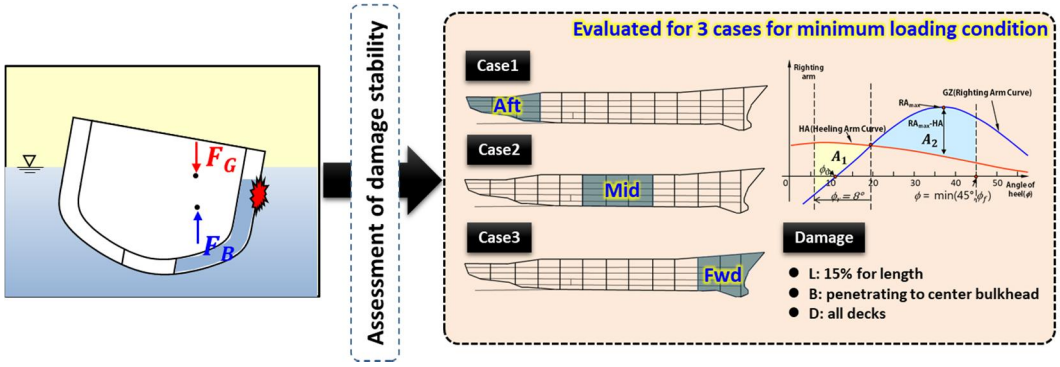


Figure 2-8. Damage stability evaluation

As with intact stability, damage stability is basically more vulnerable in minimum loading condition. In the case of deterministic damage stability of a ship, assuming that all decks are damaged in the half-width direction and height direction in the width direction by 15% in the longitudinal direction, it is assumed that the corresponding compartment is damaged. In this case, there are many cases in the longitudinal direction. However, in this study, three types of damage are selected for the representative aft body, midship, and fore body.

Currently, most ships are subject to the intact and damage stability criteria [48] according to the properties of righting lever curves. However, recent maritime accidents require revision of intact and damage stability standards. Accordingly, IMO [49] intends to announce and regulate second-generation stability standards.

In addition, a recent study [50] has noted the need for improvement in damage stability performance by calculating the damage stability at the time of flooding as well as the final posture. Therefore, in this study, the damage stability criterion value was evaluated every second during the dynamic flooding analysis. In order to reflect this situation, Dynamic flooding analysis was used to evaluate the damage stability even in

the intermediate flooding condition. The damage stability evaluation was evaluated every second through dynamic flooding analysis. This means that every second of the ship is in a steady-state in the process of flooding the ship, and GZ curve and HA curve are created by giving external moment, the results used to evaluate the damage stability.

Figure 2-9 shows the motion of the ship during the flooding process. As mentioned above, damage stability evaluation performed at the final state of the ship. It means that the flooding process was neglected when we evaluate the damage stability. However, the motion of ship can be more severe in the process of the flooding. As seen in Figure 2-9, the most dangerous situation occurred in about 7 sec. Therefore, we have to consider the intermediate of the flooding.

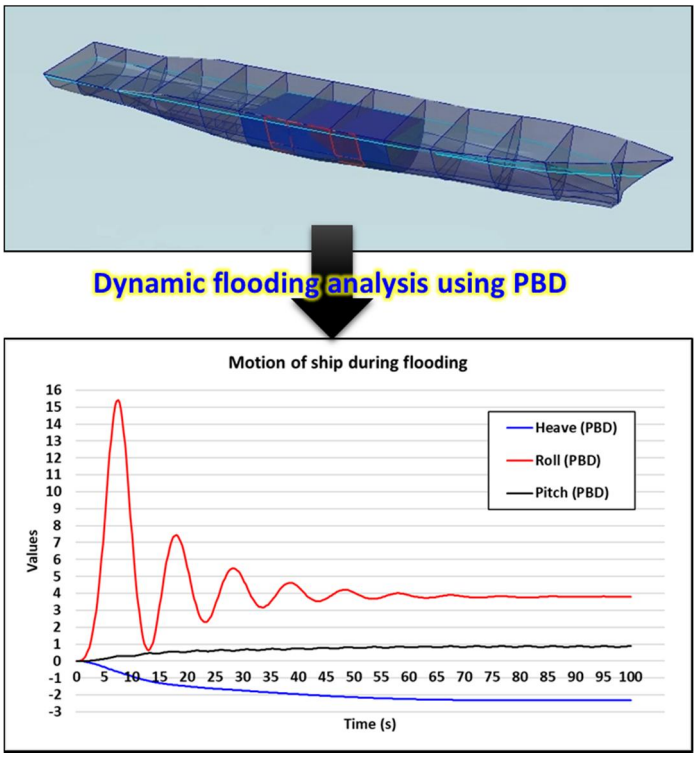


Figure 2-9. Motion of ship during the flooding process

Figure 2-10 shows the GZ curve during the flooding. The first graph shows the GZ curve at 7 sec, the second graph shows GZ curve at 17sec, and the third graph shows GZ curve at the final state. The first and second graph was evaluated first two peaks of the rolling angle. As seen in Figure 2-10, as the flooding progresses, the flooding rate increases, and the overall graph is lowered. However, the initial rolling angle due to dynamic motion is more severe in the initial flooding period. If we look at Figure 2-10 first graph for 7 sec, the result not satisfied the criteria for initial damage stability which should not exceed an initial heeling angle of 15°. From these results, it can be seen that the damage stability must be evaluated during flooding analysis. Therefore, the damage stability evaluation was performed during dynamic flooding analysis proposed in this study.

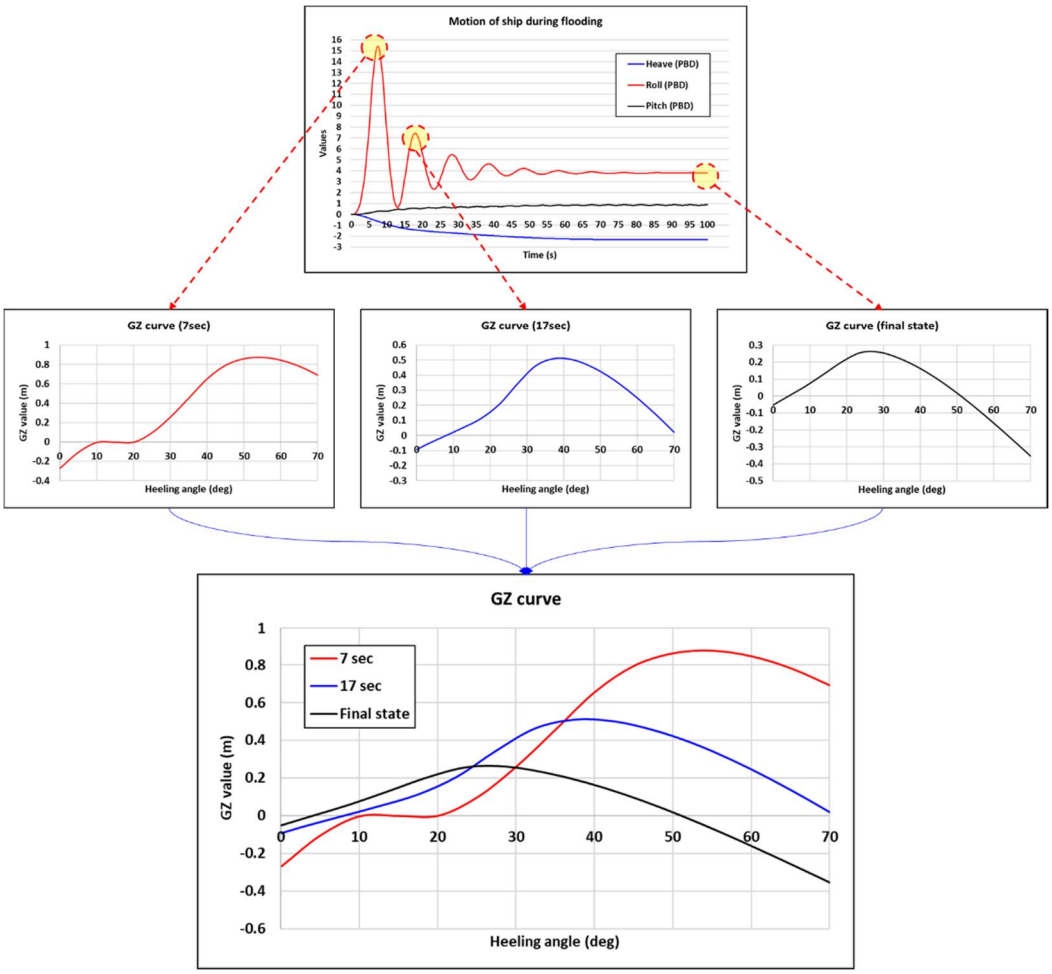


Figure 2-10. GZ curve variation during the flooding

### 2.3.3. GZ Curve calculation considering free trim

Calculating the GZ curve of the ship follows Eq. (1), plotting the value at an angle, giving an external moment in the equilibrium state. This external moment gives the vessel a tilt and equilibrium is in violation. In this process, the equilibrium between buoyancy and gravity is made by adjusting the heave value to match the equilibrium. Since there is only one variable for equilibrium, it can be obtained through the first NR (Newton-Raphson) iteration as Eq. (11). This process is summarized in Figure 2-7.

$$z_{n+1} = z_n - \frac{f_z(z_n)}{f_z'(z_n)} \tag{11}$$

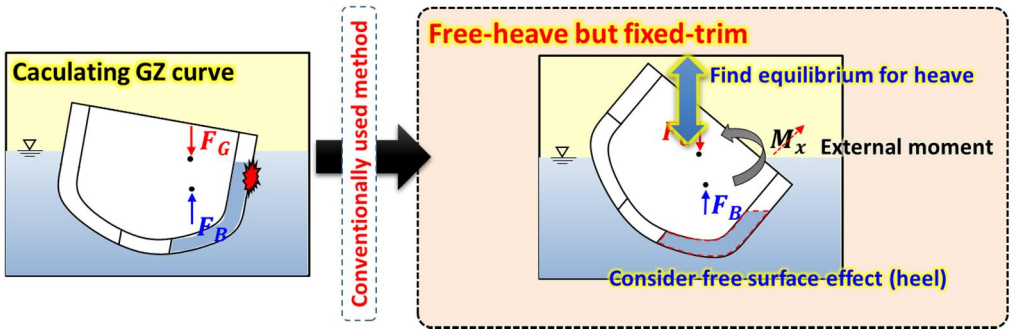


Figure 2-11. GZ curve calculation considering free-heave but fixed-trim

In Eq. (11), '$z_n$' means z position of the ship in '$n$' step, '$f_z$' means equilibrium function of gravity and buoyancy, and '$f_z'$' means derivative of '$f_z$'.

Most commercial programs use this method, which is done on the assumption that the longitudinal shapes are the same. However, if the shape of the longitudinal vessel is different or if the shape of the inner section is large in the longitudinal direction due to

lateral deformation, the equilibrium of the vessel should be found considering the trim as well as the heave. Therefore, in this study, the GZ curve was calculated considering two equilibria of heave and trim. Considering both heave and trim, we can obtain it using 2D NR iteration, which is shown in Eq. (12). This process is summarized in Figure 2-7.

In Eq. (12), '$\phi_n$' means pitching angle of ship in '$n$' step, '$f_\phi$' means equilibrium function of x-axis moment, and '$f'_\phi$' means derivative of '$f_\phi$'.

$$\begin{bmatrix} z_{n+1} \\ \phi_{n+1} \end{bmatrix} = \begin{bmatrix} z_n \\ \phi_n \end{bmatrix} - \begin{bmatrix} \frac{\partial f_z}{\partial z_n} & \frac{\partial f_z}{\partial \phi_n} \\ \frac{\partial f_\phi}{\partial z_n} & \frac{\partial f_\phi}{\partial \phi_n} \end{bmatrix}^{-1} \begin{bmatrix} f_z(z_n, \phi_n) \\ f_\phi(z_n, \phi_n) \end{bmatrix} \tag{12}$$

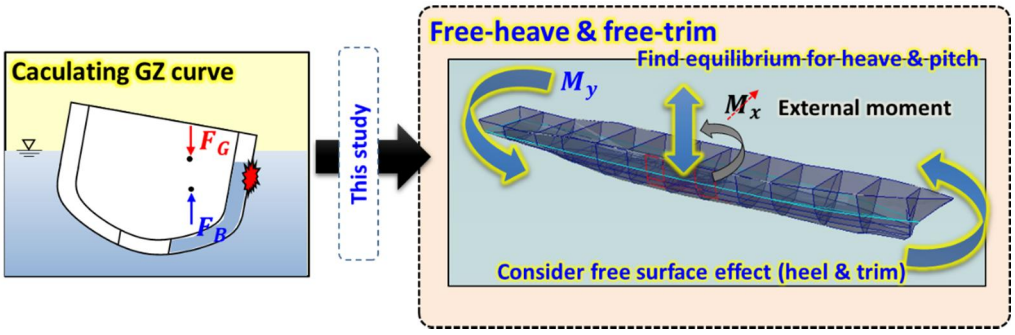


Figure 2-12. GZ curve calculation considering free-heave and trim

When calculating the GZ curve considering the free-trim, there is a large difference from the GZ curve considering only the free-heave in the case where the longitudinal hull shape change due to heeling is large or the shape of the inner compartment is largely changed by heeling. Therefore, we compared the GZ curves with and without free-trim at

the bow, center, and stern as a result.

In order to investigate this effect of the mention above, this study applied this to a 10,000 ton class destroyer and compared the difference between GZ-curve calculation results with and without considering the free-trim. According to the damage criteria described above, GZ curves were compared when free heave & trim was considered or only free heave was considered for forebody, midship, and after body was damaged. Figure 2-13 shows the results of the GZ curve as mentioned above. As seen in the three graph, It can be seen that the free-trim effect must be considered when the longitudinal directional change due to heeling is large.

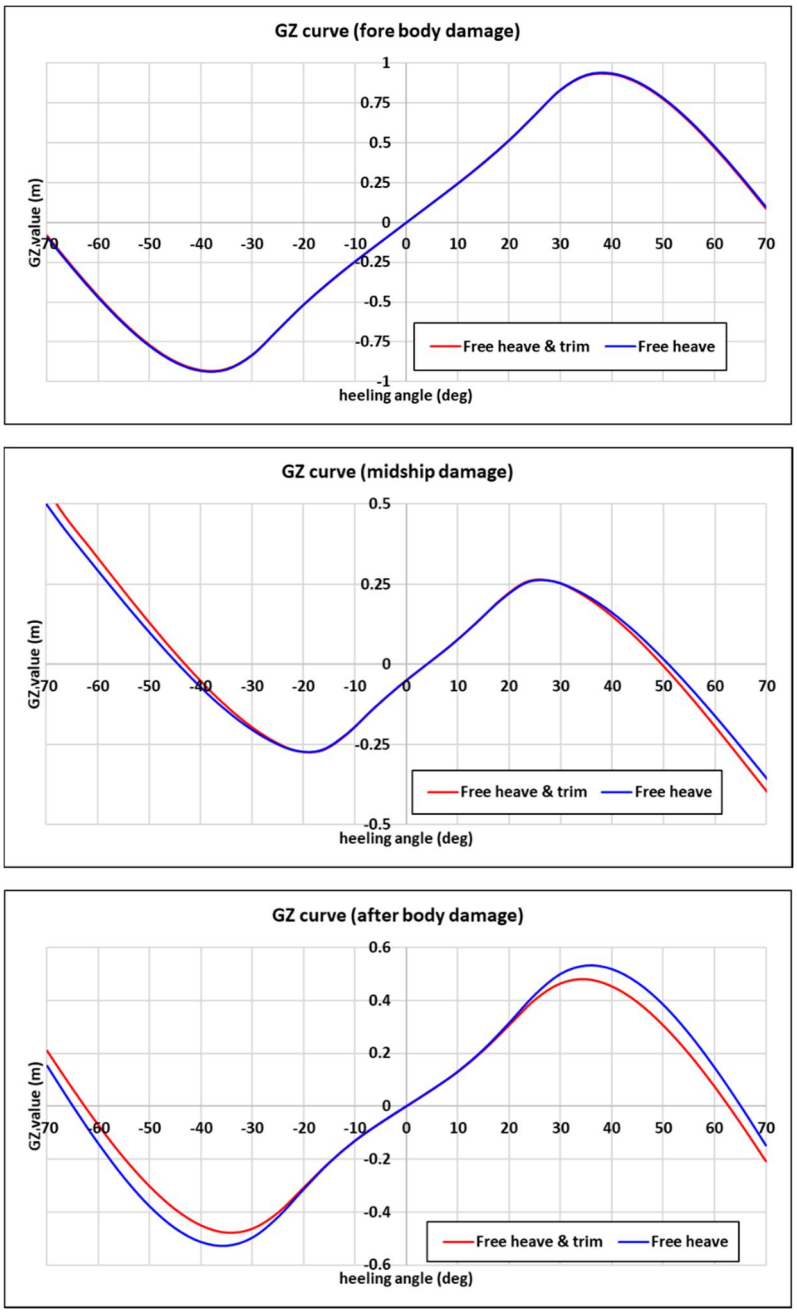


Figure 2-13. GZ curve with or without considering free-trim

### 2.3.4. Intermediate flooding analysis

Traditionally, to assess damage stability, the GZ curve and HA curve were calculated assuming that the vessel was damaged at a specific site and all of the compartments were flooded, and then the five damage stability criteria described in Section 2.3.2 were reviewed if it is satisfied. In general, it is considered that the most serious situation is because the amount of water flooded in the final state of damage is the greatest. However, the naval ship is floating in the water and accompanied by various environmental factors (waves, winds). It is hard to say that this is the most critical. Generally, a more severe condition may occur than the final state due to the initial transit motion of the damage. Therefore, there is an atmosphere that consideration should be given to this.

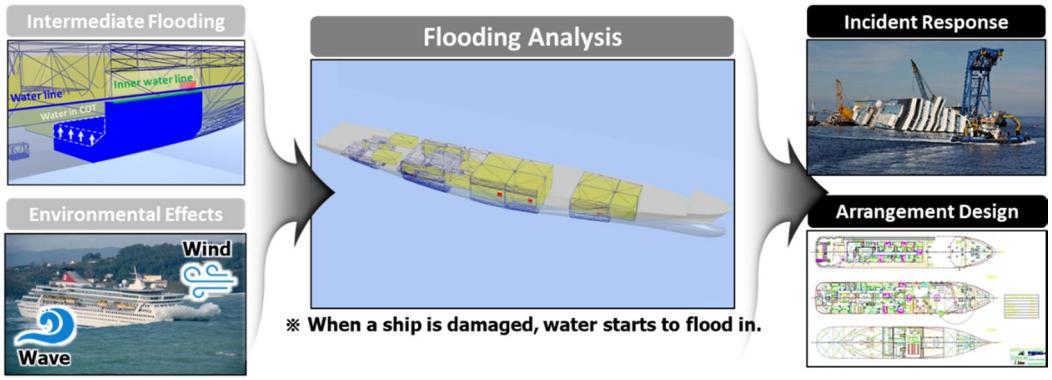


Figure 2-14. Consideration in flooding analysis

As shown in Figure 2-14, flooding analysis was carried out in consideration of the intermediate flooding and various environmental factors, and the results applied to the accident response, post-accident treatment, and optimization of arrangement design for a naval ship as proposed in this study.

Intermediate flooding analysis is divided into two major methods: quasi-static analysis and dynamic analysis. The quasi-static analysis generally calculates the flow rate through the openings in the damaged area or vessel and then updates the weight and center of gravity of the vessel by calculating the amount of water entering or leaving for a certain period of time. We then use the updated weight and center of gravity to find the equilibrium position of the ship.

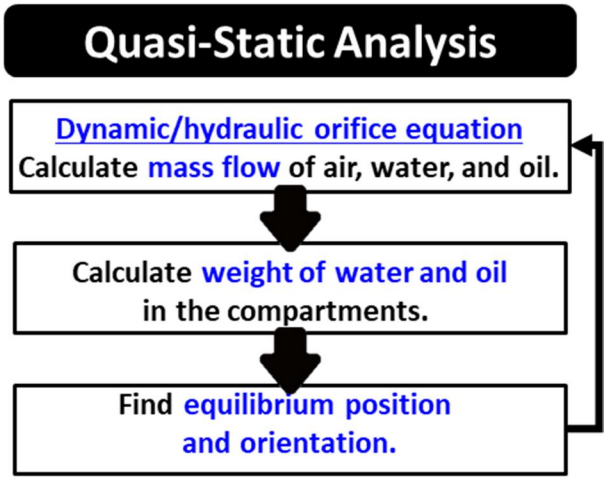


Figure 2-15. Process for quasi-static analysis

Figure 2-15 shows the main process for quasi-static analysis, and many studies have used this method because it is relatively simple and quick to analysis. However, this has the disadvantage that the ship cannot consider the transit situation because it cannot take into account the dynamic effects of the sudden flooding. A detailed description of the quasi-static analysis is given in Appendices A.

For that, there is a fully dynamic method of dynamic analysis using CFD. However, this requires a lot of additional work from problem setting to mesh generation, boundary condition setting, and it takes a long time to analyze, so it is difficult to use it in the layout

design process or accident.

Therefore, in order to overcome the disadvantages of the above two methods and take advantages, this study proposed a modified dynamic flooding analysis method. In this study, the PBD is used to analyze the dynamic behavior of the fluid in a short time, and the weight and the center of gravity of the whole ship are updated by using the flow center and the center of gravity of the fluid in the vessel compartment calculated every hour through the PBD. The updated information is then applied to the Cummins equation to calculate the 6- DOF motion of the ship every time step. This is illustrated schematically in Figure 2-16.

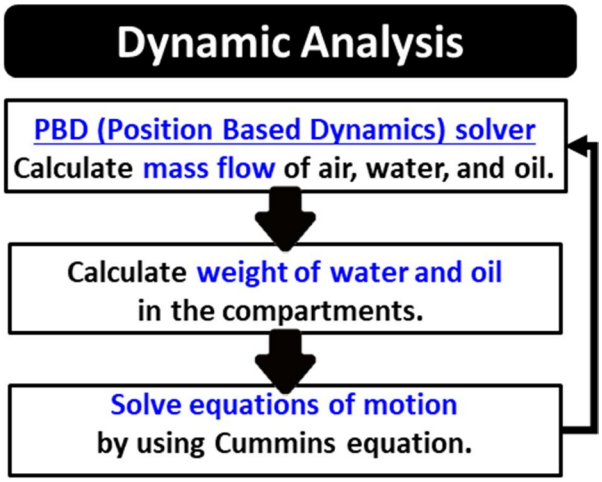


Figure 2-16. Process for dynamic analysis proposed in this study

The dynamic flooding analysis method proposed in this study is able to analyze the dynamic behavior of ship in transit situation and to analyze at high speed compared with CFD.

### (1) Dynamic analysis for intermediate flooding

As described above, this study proposed a new dynamic flooding analysis method. A basic physical model of the ship is needed for the flood analysis proposed in this study. The model includes ship and ship's compartments and damaged opening. This model is a basic 3D mesh model, not an analytical model used in CFD. Therefore, the preparation process for the analysis is simple.

Modeling for analysis and entering the weight distribution of the ship, including liquid weights, including various cargo weights, find the static equilibrium position of the ship. After that, information on the damaged opening (damage size, position, the shape of the damage, etc.) is input to start flooding analysis. When a damage occurs on a ship, various fluids such as water, oil, and airflow in and out through the damaged part. In addition to the damaged part, the same situation occurs in the inside of the ship through various openings. The mass flow of the fluid through the site is calculated every time step, thereby changing the amount of fluid and the center of gravity contained in the ship's compartment. Then, the weight and center of gravity of the entire ship are changed accordingly, and this can be applied to the Cummins equation to calculate the 6-DOF motion of the ship. In this process, the free surface effect of the fluids in the ship due to the movement of the ship is considered. The process of dynamic analysis proposed in this study is shown as Figure 2-17.

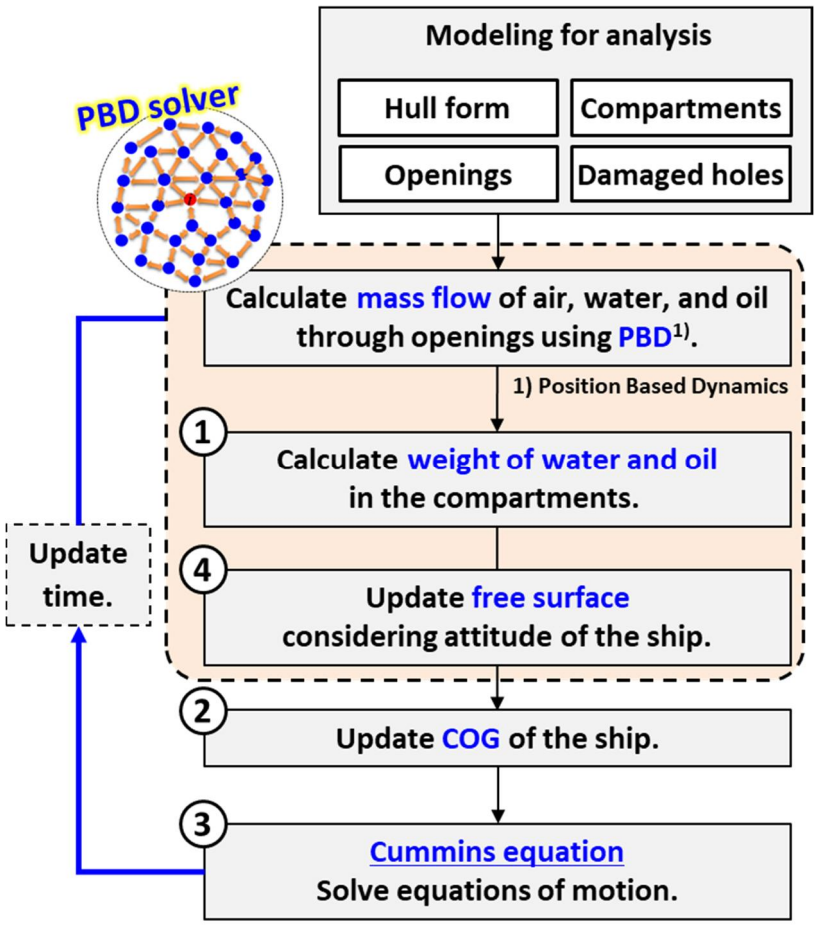


Figure 2-17. Process of dynamic analysis for flooding proposed in this study

The part highlighted by the dashed line in Figure 2-17 is analyzed by PBD.

### (2) Position Based Dynamics for flooding analysis

Position Based Dynamics (PBD) is one of the mesh free particle methods and one of the methods for the analysis of particles in the mesoscale analysis.

In order to understand the PBD method, understanding of the conventional dynamic

fluid analysis methods such as FEM (Finite Element Method) and FVM (Finite Volume Method; References) used in CFD is preceded. It was developed in the mid-1900's and has been actively used in various fluid analyzes to date. In this method, the Navier-Stokes equation and the continuity equation are used as basic governing equations for the fluid analysis, and the problem is analyzed according to the various boundary conditions applied according to the analysis requirement. Although the traditional Eulerian methods employ various integration methods depending on the analysis, the stability expressed in the stability of the analysis up to now is variable depending on the analysis conditions. In addition, careful mesh generation is required for analysis, and analysis time is relatively long. However, it has been developing for a long time, and it has been applied to various analysis problems and has proved to be very accurate. Therefore, there are many commercial programs using this method.

Unlike the Eulerian method, it has recently been developed with the Lagrangian method, which analyzes the nonlinear behavior of fluids and boasts fast analysis speed. The Lagrangian method is divided into several categories, but let's examine the Mesh-free Particle Method (MPM). Unlike the Eulerian method described earlier, the MPM is a method of excluding the mesh for analysis and expressing the fluid in the analysis region as a particle, as the name suggests. Typically, there is SPH (Smoothed Particle Hydrodynamics). This method is the method proposed by Gingold and Monaghan [51]. The basic governing equation is the same as the Eulerian method, but there is no boundary condition, and the boundary is processed by pressure through special treatment. Basically, there is stability problem because it is computed to satisfy Navier-Stokes equation and continuity equation, and it is still developed at present but it is still faster than Eulerian method because there is much computation amount for analysis.

In addition, as a relatively recently proposed method, the accuracy of interpretation is

still improving through the application of various problems. On the other hand, similar to SPH, the Moving Particle Semi-implicit (MPS) method has been proposed by Koshizuka and Oka [52] and is widely used until now. MPS is similar to SPH, but there is a difference in that an implicit method is used in the integration method. In the case of the PBD method, Muller et al. [53] and were developed for early fluid graphics. In the case of the PBD method, instead of the previous SPH and MPS methods, the governing equations are not applied and all of them are replaced with the constraints for the position of the particles so that the stability is always guaranteed and the algorithm is developed for parallelization. It is as fast as possible. However, in the recently developed method, the accuracy still needs to be continuously improved. Table 2-1 summarizes the results of comparing the methods described above. In this study, we used PBD with relatively accurate and very fast analysis speed for flood analysis.

Table 2-1. Comparison of fluid analysis

| Category | Eulerian methods | Lagrangian methods | | |
|---|---|---|---|---|
| | | SPH | MPS | PBD |
| Developed | Early 1940, 1960 | Gingold & Monaghan [51] | Koshizuka & Oka [52] | Muller et al. [54] |
| Governing Eq. | Navier-Stokes equation<br>Continuity equation | Navier-Stokes equation<br>Continuity equation | Navier-Stokes equation<br>Continuity equation | Constraint function |
| Boundary Eq. | Applying boundary conditions | Exerted to pressure | Exerted to pressure | Exerted to constraint |
| Integration | Various | Explicit | Implicit | Explicit |
| Stability | Moderate | Moderate | Moderate | Always stable |
| Computing Speed | Very slow | Slow | Slow | Very fast |
| Accuracy | Relatively high | Moderate | Moderate | Improving |
| Commercial Software | ANSYS, Fluent | LS-Dyna, ABAQUS, Fluidix, etc. | MPS-RYUJIN | NVIDIA Flex |

The PBD was applied in this study to calculate the flow rate and to consider the center of gravity in consideration of the shape of the flow in the dynamic flooding analysis method described above. The traditional approach to simulating dynamic objects has been to work with forces. However, PDB works on positions which makes direct control of positions which makes a collision or kinematic behaviors easier. PBD is a technique for calculating the movement of a set of vertices through 3D space. It is possible to control the integration directly thereby avoiding overshooting and energy gain problems in connection with explicit integration. There are several advantages of PBD. PBD gives control over explicit integration and removes the typical instability problems. The formulation allows the handling of general constraints in the position based setting. The explicit position based solver is easy to understand and implement. In addition, it is fast. However, PBD also has disadvantages comparing other methods. This algorithm is unconditionally stable and provides plausible, however, yet physically inaccurate. The formulation resolves rotation by constraint solving but then uniformly handles non-rigidity. The stiffness of the model depends on the number of iterations and the time step size. As explained previously, PBD is a technique for calculating the movement of a set of vertices through 3D space. The movement can be caused by external or internal forces on the vertices. In order to know the position and velocity of these vertices, we have to integrate the net force on them. As with Newton's second law as described in Eq. (13), we can get the acceleration, the second derivative of position.

$$\mathbf{M}\ddot{\mathbf{x}} = \mathbf{F}_{net} \tag{13}$$

$$\mathbf{F}_{net} = \mathbf{F}_{ext} + \mathbf{F}_{int} \tag{14}$$

In equations, $\mathbf{M}$ means mass vector, $\ddot{\mathbf{x}}$ means acceleration, $\mathbf{F}_{net}$ means net force exerted to object, $\mathbf{F}_{ext}$ means external force exerted to object, and $\mathbf{F}_{int}$ means internal force exerted to object.

The external forces are usually easy to apply, e.g. gravity, wind, drag, etc. The internal forces are hard to find and are different between every MPM methods. MD (Molecular Dynamics) uses potential for internal forces. DPD (Dissipative Particle Dynamics) uses conservative, dissipative and fluctuating for internal forces. SPH (Smoothed Particle Hydrodynamics) solves continuity equation and N-S equations. This method of obtaining the internal force is diverse and difficult, and involves many calculation processes. In order to reduce this process and improve stability, PBD is an efficient algorithm for eliminating instability by expressing it as a constraint condition for each particle without directly calculating the internal force [55].

The basic algorithm of PBD is shown in Figure 2-18. In the figure, $\mathbf{x}_i$ means the position of particle $i$, $\mathbf{v}_i$ means the velocity of particle $i$, $\mathbf{x}^*_i$ predicted the position of particle $i$, $\Delta t$ means time step, $N(\mathbf{x}^*_i)$ means neighboring particles of particle $i$, $n_i$ means accumulator of the particle, $\omega$ means user-defined parameter for over-relaxation.

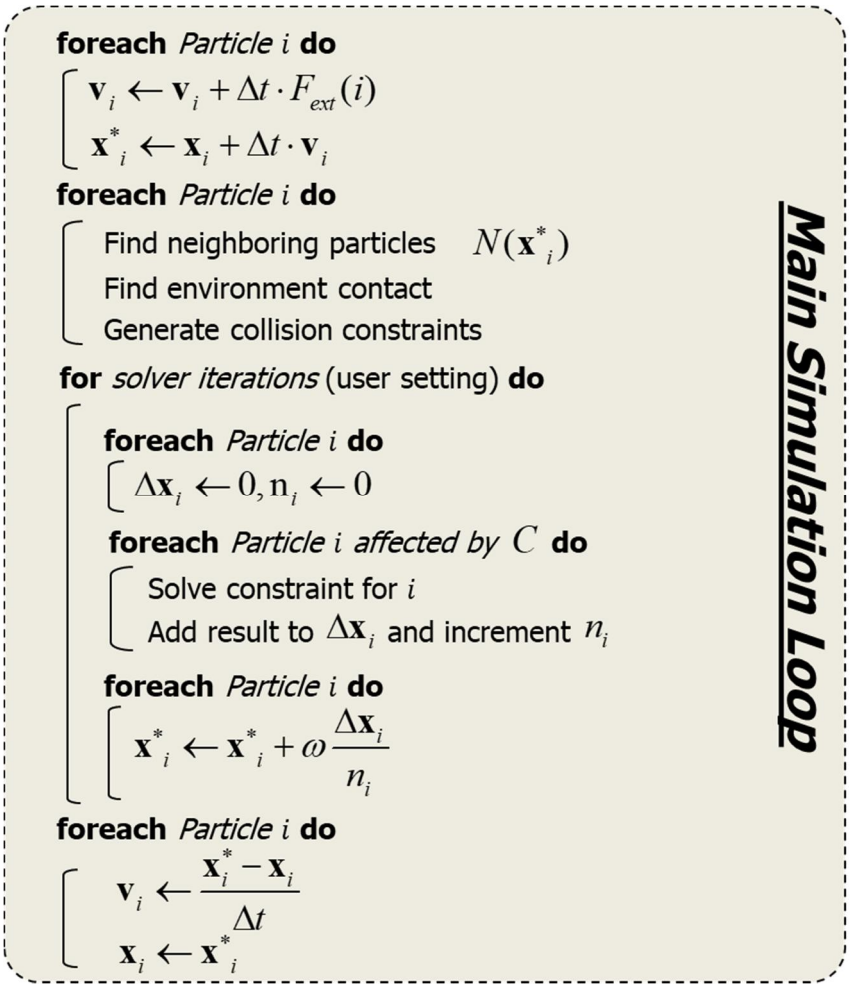


Figure 2-18. Main simulation loop of PBD

First, the velocity of each particle is obtained by integrating the external force, and the position is calculated by integrating the velocity. At this time, this position is not updated to the position of the next time directly to the predicted position but is temporarily stored in the memory for calculation. Then, we find nearby particles to find the constraint between each particle based on the calculated predicted position and set the constraint that each particle should satisfy. After that, the main iteration process is divided into

groups according to the types of constraints, and the constraints set for each group are calculated. We compute dx to satisfy the constraint, and we repeat the dx computed in each constraint several times through iteration to modify dx to satisfy all constraints. The predicted position is updated with the finally modified dx, the updated predicted position is updated with the position of the next time step, and the velocity is updated through the updated position.

Each process is described in detail as follows. The external forces on the particles are integrated with explicit Euler integration. Particle's position is not immediately updated. The resulting position is stored in a second variable called the predicted or proposed position. The particle's velocity is updated as well.

The particles are checked for collision with other particles and environment objects. Collision constraints are generated accordingly and temporarily added to the constraint groups. Find neighboring particles using sliced data structured and hash mapping method.

Hash-mapping method [56] has been applied to speed up neighboring particle searches performed every time unit with low construction cost and low memory usage. The hash mapping method generates a virtual grid with the same size as the support domain in the space where the particle exists, allocates memory only for the grid containing the particle among the generated grid, assigns the index of each particle to the grid memory. This is shown in Figure 2-19.

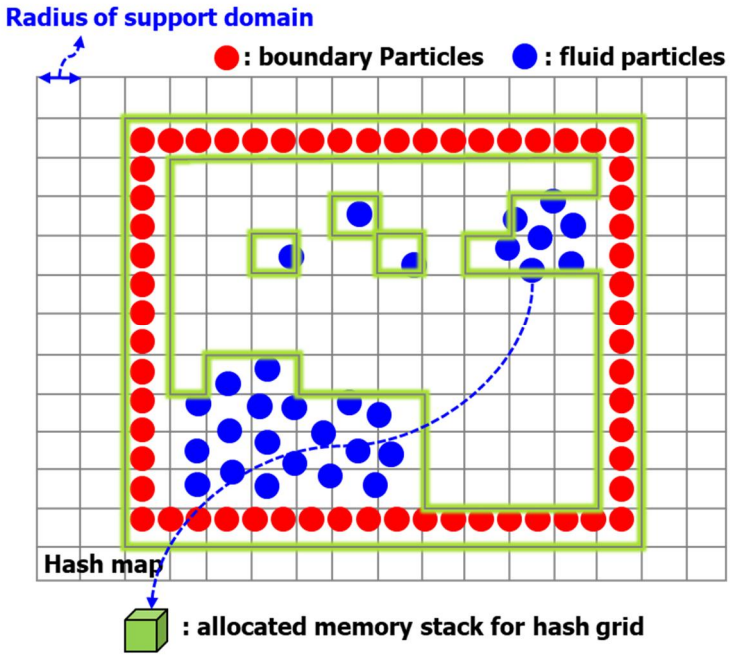


Figure 2-19. Allocation of memory using the hash-mapping method

The stored grids search for neighbor particles of each particle. In this process, each particle is searched for neighbor particles. First, find the hash grid containing the particle and find the hash grid around the hash grid. It is very easy to find the surrounding grid because the hash grid is an arbitrary set of the virtual grid. Only the particles in the found hash grid are searched for distances from the reference particle to find the surrounding particles to see if they fall within the real spherical support domain. The index of the found particle is stored separately in the memory allocated for each particle. By repeating this process for all particles, neighboring particles can be found. The finding sequence is shown in Figure 2-20.

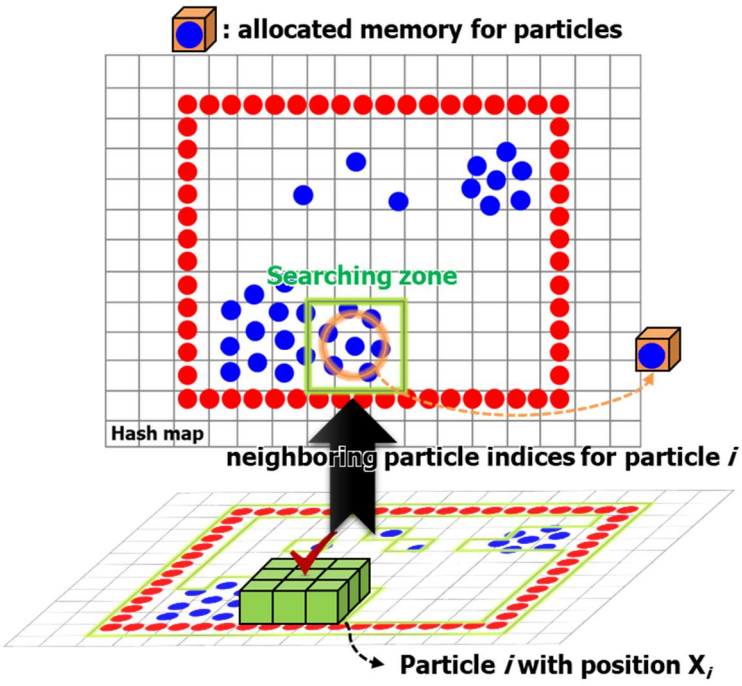


Figure 2-20. Find neighboring particle using the hash-mapping method

In general, there are various methods such as BVH (Bounding Volume Hierarchy; [57]), but we have confirmed that the hash mapping method is most suitable for searching neighboring particles of many particles.

The outer loop of the solver, where solveriterations is the amount of Jacobi iterations to perform. The ideal value depends on the simulation and should be user-settable. The constraints are grouped and the particles are fully processed per constraint group. The accumulators of the particles are set to zero. The constraints are solved and the results added to the accumulators. The particle's proposed position is updated with the averaged accumulated correction. Over-relaxation is applied as well. The particle's position and velocity are updated with the computed proposed position.

The most important thing in the above process is to obtain the constraint instead of the

internal force. When analyzing the motion of a particle in the conventional MPM method, we can consider the collision through the movement of the fluid or the external pressure through the governing equation. In PBD, however, all of these are replaced by constraints by the position of the particles. Constraint consists of equality constraints (Eq. (15)) and inequality constraints (Eq. (16)), which can be expressed in one expression (Eq. (17)). In general, however, the predicted position does not satisfy this constraint when only the external force is applied to obtain the predicted position. Therefore, it is necessary to recalculate the predicted position in order to satisfy the constraint. Therefore, it is necessary to make the preceding equation (Eq. (18)) linear. In order to satisfy the formula, it is in the direction of $\nabla C(\mathbf{p})$ which is the direction satisfying $C(\mathbf{p})$. Therefore, we can calculate $\Delta\mathbf{p}$ as Eq. (19) by calculating the Lagrange multiplier $\lambda$ about how to move in the $\nabla C(\mathbf{p})$ direction. In Eq. (17), '$\succ$' represents both equality constraint and inequality constraint.

$$C(\mathbf{x}_1, \mathbf{x}_2, ..., \mathbf{x}_n) = 0 \tag{15}$$

$$C(\mathbf{x}_1, \mathbf{x}_2, ..., \mathbf{x}_n) \geq 0 \tag{16}$$

$$C(\mathbf{p}) \succ 0 \tag{17}$$

$$C(\mathbf{p} + \Delta\mathbf{p}) \succ 0 \tag{18}$$

$$C(\mathbf{p} + \Delta\mathbf{p}) \approx C(\mathbf{p}) + \nabla C(\mathbf{p}) \cdot \Delta\mathbf{p} \succ 0 \tag{19}$$

$$\Delta\mathbf{p} = \lambda \nabla C(\mathbf{p}) \tag{20}$$

To compute $\lambda$, we substitute Eq. (20) into Eq. (19) and summarize it against $\lambda$, and $\lambda$ can be expressed as Eq. (22). If you substitute $\lambda$ for $\Delta\mathbf{p}$, we can get Eq. (23). Eq. (23) can be expressed by an expression for each particle as Eq. (24). In Eq. (24), $s$ can be expressed by a scaling factor as Eq. (25). We can express it by adding weight to inverse masses $w_i$, so $\Delta\mathbf{p}_i$ can be expressed as Eq. (26). In short, $\Delta\mathbf{p}_i$ can be expressed as Eq. (28). In Eq. (28), $\lambda$ is described as Eq. (29). Therefore, we can obtain the moving amount $\Delta\mathbf{p}_i$ of a particle satisfying a specific constraint through Eqs. (28) and (29), and $\lambda$ for each constraint can be obtained by obtaining a constraint for the position of the particle according to the type of constraints.

$$C(\mathbf{p}) + \nabla C(\mathbf{p}) \cdot \lambda \nabla C(\mathbf{p}) = 0 \tag{21}$$

$$\lambda = -\frac{C(\mathbf{p})}{\left|\nabla C(\mathbf{p})\right|^2} \tag{22}$$

$$\Delta\mathbf{p} = -\frac{C(\mathbf{p})}{\left|\nabla C(\mathbf{p})\right|^2} \nabla C(\mathbf{p}) \tag{23}$$

$$\Delta\mathbf{p}_i = -s\nabla_{\mathbf{p}_i} C(\mathbf{p}) \tag{24}$$

$$s = \frac{C(\mathbf{p})}{\sum_j \left|\nabla_{\mathbf{p}_j} C(\mathbf{p})\right|^2} \tag{25}$$

$$\Delta\mathbf{p}_i = -s\frac{w_i}{\sum_j w_j} \nabla_{\mathbf{p}_i} C(\mathbf{p}) \tag{26}$$

$$\Delta \mathbf{p}_i = -\frac{C(\mathbf{p})}{\sum_j w_j \left|\nabla_{\mathbf{p}_j} C(\mathbf{p})\right|^2} w_i \nabla_{x_i} C(\mathbf{p}) \tag{27}$$

$$\Delta \mathbf{p}_i = -\lambda w_i \nabla_{x_i} C(\mathbf{p}) \tag{28}$$

$$\lambda = \frac{C(\mathbf{p})}{\sum_j w_j \left|\nabla_{\mathbf{p}_j} C(\mathbf{p})\right|^2} \tag{29}$$

① Fixed position constraint

If the position of a particle must be fixed at a certain position, a fixed position constraint can be applied. The fixed position constraint is expressed mainly as a static rigid body, and the constraint can be expressed as Eq. (30). $\Delta \mathbf{p}_i$ can be obtained directly from Eq. (31). However, the expression for $\Delta \mathbf{p}_i$ and the $\lambda$ described above can be expressed by Eq. (32), and substituting the expression for $\lambda$. $\nabla C(\mathbf{p})$ for each position can be expressed as Eq. (33). Then, substituting the obtained Eqs. (32) and (33) for $\Delta \mathbf{p}_i$ into Eq. (34) can be expressed as Eq.(35).

$$\Delta \mathbf{x}_i = \mathbf{p} - \mathbf{x}_i \tag{30}$$

$$\mathbf{x}_i + \Delta \mathbf{x}_i = \mathbf{x}_i + \mathbf{p} - \mathbf{x}_i = \mathbf{p} \tag{31}$$

$$\lambda = -m_i \left\| \mathbf{p} - \mathbf{x}_i \right\| \tag{32}$$

$$\nabla_{x_i} C(\mathbf{p}) = \frac{\mathbf{p} - \mathbf{x}_i}{\left\| \mathbf{p} - \mathbf{x}_i \right\|} \tag{33}$$

$$\Delta \mathbf{x}_i = -\lambda w_i \nabla_{x_i} C(\mathbf{p}) \tag{34}$$

$$\Delta \mathbf{x}_i = m_i \left\| \mathbf{p} - \mathbf{x}_i \right\| w_i \frac{\mathbf{p} - \mathbf{x}_i}{\left\| \mathbf{p} - \mathbf{x}_i \right\|} = m_i \frac{1}{m_i} (\mathbf{p} - \mathbf{x}_i) = \mathbf{p} - \mathbf{x}_i \tag{35}$$

② Distance constraint

Distance constraint means that the particle and particle must be positioned at a certain distance. These constraints usually act between the particles that make up the moving rigid body. The distance constraints mimic a linear spring force in the classic mass-spring model. Therefore, a constraint expression can be expressed by Eq. (36). Then, we can express it by the expression Eq. (37) and the $\lambda$ for the constraint as Eq. (38). Applying this to the particles constituting the distance constraint, we can obtain the dpi for each particle by Eqs. (39) and (40).

$$C(\mathbf{x}_1, \mathbf{x}_2) = \left| \mathbf{x}_1 - \mathbf{x}_2 \right| - d \tag{36}$$

$$\nabla_{x_1} = \frac{\mathbf{x}_1 - \mathbf{x}_2}{\left| \mathbf{x}_1 - \mathbf{x}_2 \right|}, \ \nabla_{x_2} = -\nabla_{x_1} \tag{37}$$

$$\lambda = \frac{\left| \mathbf{x}_1 - \mathbf{x}_2 \right| - d}{w_1 + w_2} \tag{38}$$

$$\Delta \mathbf{x}_1 = -\frac{\left| \mathbf{x}_1 - \mathbf{x}_2 \right| - d}{w_1 + w_2} w_1 \frac{\mathbf{x}_1 - \mathbf{x}_2}{\left| \mathbf{x}_1 - \mathbf{x}_2 \right|} \tag{39}$$

$$\Delta \mathbf{x}_2 = \frac{\left| \mathbf{x}_1 - \mathbf{x}_2 \right| - d}{w_1 + w_2} w_2 \frac{\mathbf{x}_1 - \mathbf{x}_2}{\left| \mathbf{x}_1 - \mathbf{x}_2 \right|} \tag{40}$$

③ Collision constraint with the plane

In case of an infinite plane, the constraints aim to keep the particle on the same side of a plane throughout the time-step. Therefore, the same constraint as Eq. (41) can be applied. Where n is normal on the infinite plane, $d_{rest}$ is the distance between the plane and the origin, and $w_i$ is the inverse mass of particle $i$.

$$C(\mathbf{x}_1, \mathbf{x}_2) = |\mathbf{x}_1 - \mathbf{x}_2| - d \tag{41}$$

④ Fluid constraint

PBD analysis for rigid bodies and moving objects is possible for the constraints described above. However, in this study, we tried to apply PBD to flooding analysis, and it is necessary to simulate the fluid as PBD. The original fluid should be calculated to satisfy the N-S equation and the continuity equation. For a particle to behave like a liquid through PBD, the density constraint must be satisfied for an incompressible fluid. The density constraint can be expressed as Eq. (42), and the important thing here is to obtain the density $\rho_i$ of each particle. Monaghan [58] gives the SPH recipe for the particles on the particles. Applying this, the gradient of the constraint functions is given by. According to Monaghan [58], the density $\rho_i$ for each particle can be discretized as in Eq. (43), and the calculated $\nabla C(\mathbf{p})$ can be expressed as Eq. (44). Where $W$ is the kernel function. Mostly in PDB, Poly6 kernel is used for density estimation, and the Spiky

kernel is used for gradient calculation. The total position update including corrections from neighbor particles density constraint lambda is shown in Eq. (45).

$$C_i(\mathbf{p}) = \frac{\rho_i}{\rho_0} - 1 \tag{42}$$

$$\rho_i = \sum_j m_j W(\mathbf{p}_i - \mathbf{p}_j) \tag{43}$$

$$\nabla C(\mathbf{p}) = \frac{1}{\rho_0} \sum_j \nabla_{\mathbf{p}} W(\mathbf{p}_i - \mathbf{p}_j) \tag{44}$$

$$\Delta \mathbf{p}_i = \frac{1}{\rho_0} \sum_j (\lambda_i + \lambda_j) \nabla_{\mathbf{p}} W(\mathbf{p}_i - \mathbf{p}_j) \tag{45}$$

As described above, in this study, we used the PBD to calculate the flow rate through the vessel damage or vessel opening every hour and to calculate the weight and center of gravity considering the shape of the fluid in the filled compartments. This is shown in Figure 2-21. A fluid constraint and a collision constraint were used to analyze the fluid inside the vessel. Collision constraints and plane constraints were used between the hull and the fluid so that the fluid inside the vessel could interact with the hull.

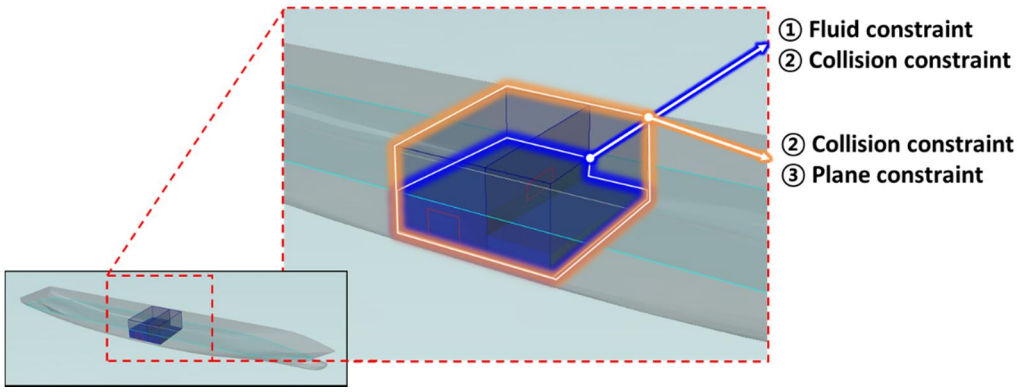


Figure 2-21. PBD constraints for intermediate flooding analysis

### (3) Equation of motion in the time domain (Cummins equation)

The PBD can express the flow rate and shape of the fluid flowing through the opening at every time step and can express the shape of the cold water inside the vessel. Therefore, the information about the ship's weight and center of gravity can be updated through the PBD. The updated information is reflected in the 6-DOF equation of motion.

The hydrodynamic force can be divided into two parts: the wave exciting force, which is exerted by the incident wave; and the radiation force from the wave due to the motion of the corresponding body in still water. The radiation force is composed of two terms, one is the force proportional to the acceleration of the motion, and the other one is the force proportional to the velocity of the motion. (Ham et al., [59])

$$\mathbf{F}_{hydrodynamic} = \mathbf{F}_{exciting} + \mathbf{F}_{radiation} \tag{46}$$

$\mathbf{F}_{exciting}$ is calculated by multiplying the force RAO (Response Amplitude Operator) with the sinusoidal function at a given frequency. The force RAO can be obtained from a

commercial solver, such as WADAM by DNV. The Cummins equation (Cummins, [60]) can be used to calculate $\mathbf{F}_{radiation}$ , which considers the impulse response of the floater in the time domain. The frequency-dependent added mass coefficient $a_{ij}(\omega)$ and the frequency-dependent damping coefficient $b_{ij}(\omega)$ at a given frequency $\omega$ can also be obtained from the commercial solver. Using the frequency-dependent coefficients $a_{ij}(\omega)$, and $b_{ij}(\omega)$, the added mass $\mathbf{A}$ and retardation function $\mathbf{B}(\tau)$ can be determined. The added mass at infinite motion frequency ($\mathbf{A}_\infty$), which is a constant matrix, is often used rather than calculating the integral because the equation is valid for any value of $\omega$, and thus also for $\omega = \infty$. Figure 2-22 summarizes the calculation procedure.

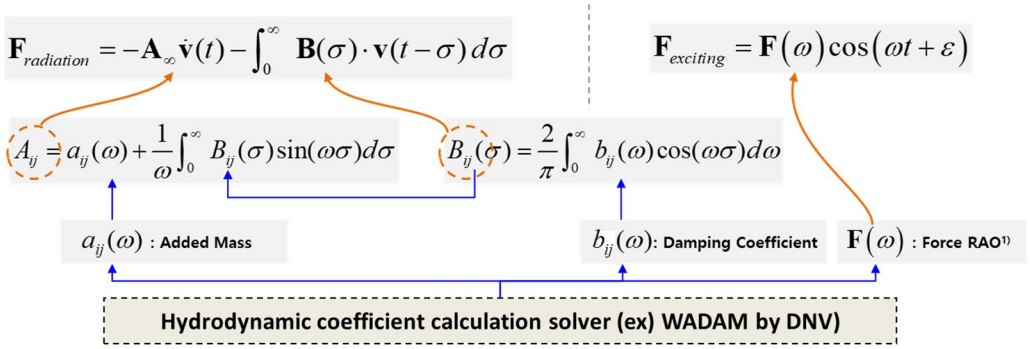

Figure 2-22. Calculation of the hydrodynamic force

In the case of a regular wave, one wave frequency ($\omega$) and one wave amplitude ($a$) are chosen. According to the wave frequency, only one force RAO ($\mathbf{F}(\omega)$) and a phase angle ($\varepsilon$) are also selected. However, in the case of an irregular wave, there are several $N$ wave frequencies and amplitudes according to the given wave spectrum. Therefore, $\mathbf{F}_{exciting}$ of the irregular wave is calculated as follows.

$$\mathbf{F}_{exciting} = \sum_{m=1}^{N} a_m \cdot \mathbf{F}\left(\omega_m\right)\cos\left(\omega_m t + \varepsilon_m\right) \tag{47}$$

where $a_{\mathrm{m}}$ is the wave amplitude at a given frequency, and $\varepsilon_{\mathrm{m}}$ is the phase angle.

Meanwhile, if the wave height, period, and direction are given stochastically, the analysis results such as motions and tensions can be regarded stochastically. As a result, the expected maximum value of the simulation results can be used to indicate the operation limit stochastically.

The calculated hydrodynamic force and the weight and center of gravity previously calculated by PBD can be expressed as a 6-DOF motion of the ship through Eq. (48), and the movement of the ship can be analyzed by calculating it at each time-step.

$$\left(\mathbf{M}+\mathbf{A}_{\infty}\right)\ddot{\mathbf{x}} + \int_0^{\infty} \mathbf{B}(\tau)\cdot\dot{\mathbf{x}}(t-\tau)\,d\tau + \mathbf{C}\mathbf{x} = \mathbf{F}\left(\omega\right)\cos\left(\omega t + \varepsilon\right) \tag{48}$$

## 2.4. Vulnerability evaluation

Before explaining the objective function the definition of the survivability and vulnerability of the ship have to be defined. According to Said [61], the survivability of the ship is defined as “the capability of a ship and its shipboard systems to avoid and withstand a weapons effects environment without sustaining impairment of their ability to accomplish designated missions”. And ship survivability has three major elements that express it well and they are susceptibility, vulnerability, and recoverability. After hit by an enemy, with vulnerability reduction and enhancement of recoverability, the system

capability can be recovered. The definitions of the susceptibility, vulnerability, and recoverability are as follows. The vulnerability refers to the inability of a ship to withstand damage from one or more attacks, its vincibility, and to its liability to serious damage or loss when attacked by weapons. The susceptibility refers to the inability of a ship to avoid being damaged in the pursuit of its mission and to its probability of being attacked. Lastly, the recoverability refers to the ability of a ship and its crew to prevent loss and restore mission-essential functions from an attack due to one or more weapons. From the viewpoint of the ship design, susceptibility is much related to the external shape of the ship. In order to reduce the susceptibility of a ship, designers adjust the RCS (Radar cross-section), IR (Infra-red), URN (Underwater radiated noise) by the external design change. If these performances are improved, the probability of the ship being detected by the enemy is reduced, so it can be said that the ship's susceptibility is low. But susceptibility has weak relation with arrangement design of the ship. Recoverability of the ship is related to the well trained ship crew and damage control system. So in the same point of view, it’s not rely on the ship design. But vulnerability has a strong relation with the arrangement design. Vulnerability can be reduced by adjusting the position of the partition wall and the position of the compartment. Among these, the vulnerability can be improved by adjusting the positions of the bulkheads and decks and the locations of rooms. Therefore, this study handles the vulnerability as a major component that represents the survivability of the ship. Regarding the arrangement design of a naval surface ship, two vulnerability scenarios for the bulkheads in the hull and for rooms in the superstructure are defined and evaluated as follows.

### 2.4.1. Bulkhead vulnerability

If an explosion due to an attack occurs within the compartment of a naval surface ship, the pressure of the explosion will act on adjacent bulkheads and decks, as shown in Figure 2-23. At this time, if the pressure due to the explosion can be minimized, we can say that the vulnerability of the ship may be reduced. In this sense, minimizing all explosion pressure of the bulkheads induced by all explosives may be a criterion to select a better alternative in the arrangement design in terms of the vulnerability. Thus, the bulkhead damage vulnerability (VBD) can be represented using Eq. (49).

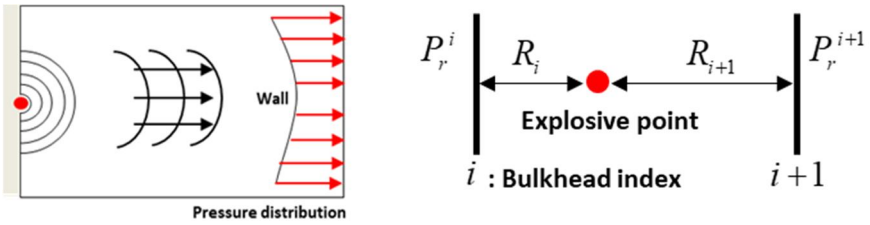


Figure 2-23. Bulkhead damage by attack

$$V_{BD} = \sum_{i=1}^{N_{B\&D}} P_r^i \tag{49}$$

In Eq. (49), the symbol $P^i_r$ is the explosion pressure of the $i$th bulkhead or deck due to an explosive, and the symbol $N_{B\&D}$ is the number of bulkheads and decks in the hull. The explosion pressure ($P^i_r$) of the bulkhead or deck due to an explosive can be calculated using Eq. (50) [62], [63]. This equation is an empirical fit equation for the reflected pressure according to the distance from the explosive point to the bulkhead or deck.

$$P_r^i = 2 \cdot P_0 \cdot \left\{ {P_{Snd}}^i + \frac{(\gamma+1) \cdot ({P_{Snd}}^i)^2}{(\gamma-1) \cdot {P_{Snd}}^i + 2\gamma} \right\} \tag{50}$$

In Eq. (50), the symbol $P_0$ is the ambient air pressure in Pa (101,300 Pa at sea level), the symbol $P_{Snd}$ is the non-dimensional side-on overpressure in Pa, defined as Eq. (51), and the symbol $\gamma$ is the specific heat ratio of $P_0$ and $P_{Snd}$, taken as 1.4.

$${P_{Snd}}^i = 0.55 \cdot \left\{ R_i \cdot \left( \frac{P_0}{E_W \cdot W} \right)^{1/3} \right\}^{-1.95} \tag{51}$$

In Eq. (51), the symbol $R_i$ is the distance from the center of the explosion to the $i$th bulkhead or deck in m, the symbol $E_W$ is the explosive energy per unit mass in $m^2/s^2$, and the symbol $W$ is the charge mass of an explosive in kg. In Eq. (50), $P^i_r$ is a function of the distance of bulkheads or decks from the explosive point. Therefore, to calculate the vulnerability of the ship, the positions of explosives corresponding to threats have to be defined. The types of threats also have to be selected. In this study, the anti-ship missile (ASMs), torpedoes, mines, collision, and grounding were considered as major threats to the ship. For each threat, the longitudinal damage distribution was assumed by referring to existing studies [64], [22]. We assumed that ASMs follow a piecewise linear distribution along the ship's length, torpedoes follow a normal distribution, and mines follow a linear distribution, as shown in Figure 2-24.

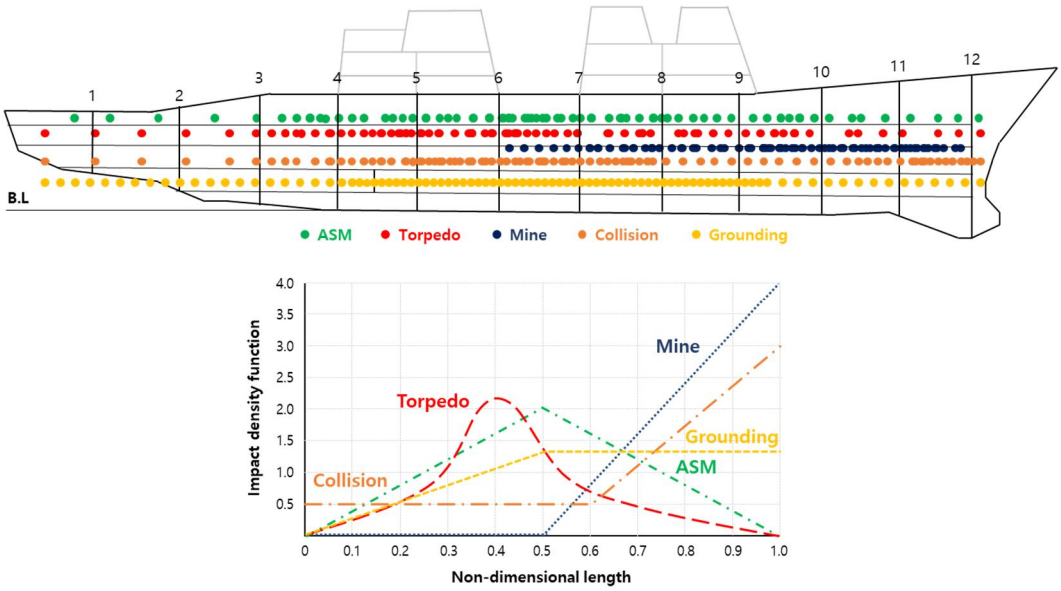


Figure 2-24. Distribution of attack points according attack type

As shown in Figure 2-24, the distribution of the ASMs has its peak point at midship because the midship part has the largest area being detected, and the remaining part shows a linear change. Due to the characteristics of torpedos, which target a ship by sensing the noise radiated underwater that is usually generated by an engine and propeller, the midpoint of the normal distribution slightly moved to the stern of the ship. In the case of mines, the probability of damage of the stern is zero, and the probability of damage to the bow side behaves linearly, as they will explode by the pressure over which the ship passes. In case of collision, There is a high probability that the ship will collide in the direction of the heading, and the probability of the center is the highest when it is collided by another ship. In case of grounding, the reef is likely to occur at the bow or center of the ship for future navigation. In this study, for all threats, the explosive energy per unit mass (EW) was assumed to be $4.184 \cdot 10^9$ $m^2/s^2$, and the charge mass (W) of the ASMs, torpedoes, mines, collision, and grounding was assumed to be 161 kg, 300 kg, 113.4 kg,

15 kg, and 20kg respectively, by referring to existing studies [64], [22] and analysis.

### 2.4.2. Room vulnerability

Similarly, the concept of vulnerability can be applied to rooms in the superstructure. In this study, the room damage vulnerability is defined as a summation of the multiplication of the probability being damaged and the important factor of each room, as shown in Eq. (52).

$$V_{RD} = \sum_{i=1}^{N_R} p_i \cdot e_i \tag{52}$$

In Eq. (52), the symbol $p_i$ and $e_i$ are the probability of damage and the important factor of the $i$th room, respectively, and the symbol $N_R$ is the number of rooms in the superstructure. A naval ship has a probability of being attacked along her length, breadth, and depth. If a certain room is placed in a certain position of the superstructure, the room has its own probability of damage according to its x-, y-, and z-positions, as shown in

Figure 2-25.

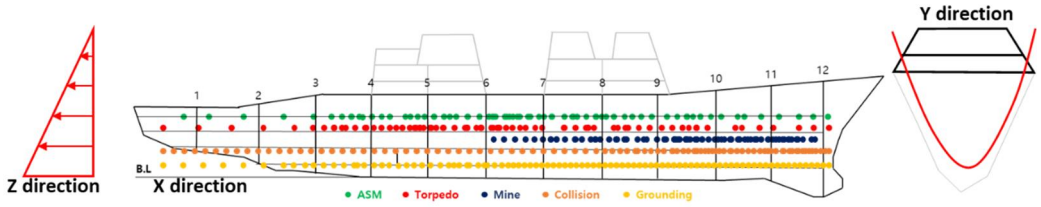


Figure 2-25. damage probability for room vulnerability evaluation

In this study, the probability of damage of the *i*th room is defined as the multiplication of the probability of damage length ($p_{DL}$) and the probability of impact ($p_{IP}$), as shown in Eq. (53) [65], [22].

$$p_i = {p_{DL}}^i \cdot {p_{IP}}^i \tag{53}$$

The probability of the damage length ($p_{DL}$) is again defined as Eq. (54). That is, $p_{DL}$ means the fraction of the target (e.g., room) that is assumed to have been damaged within a certain radius from the explosive point of an explosive.

$$\begin{aligned} {p_{DL}}^i &= \int_0^{a_i} Dam(a_i) \\ &= \int_0^{a_i} \frac{1}{\sqrt{2\pi}\cdot\left\{\frac{1}{2\sqrt{2}\cdot 1.45222}\ln(R_{SS}/R_{SK})\right\}\cdot a_i} \cdot \exp\left[-\frac{\ln^2(a_i/\sqrt{R_{SS}\cdot R_{SK}})}{2\cdot\left\{\frac{1}{2\sqrt{2}\cdot 1.45222}\ln(R_{SS}/R_{SK})\right\}^2}\right] \end{aligned} \tag{54}$$

In Eq. (54), the symbol $a_i$ is the longitudinal, transverse, or vertical distance between the centroid of the *i*th room and the explosive point which is normalized by the ship's

length, breadth, or depth, whichever is lesser. $R_{SK}$ is the sure kill radius that is assumed in this study as 0.02$L$ ($L$: ship's length), and $R_{SS}$ is sure save radius that is assumed as 0.15$L$ by referring to existing studies [22]. The probability of impact ($p_{IP}$)is defined as Eq. (55).

$$p_{IP}{}^{i} = \int_{x_1^i + a_i/2}^{x_2^i - a_i/2} \mathrm{Imp}_x(x)dx \cdot \int_{y_1^i + a_i/2}^{y_2^i - a_i/2} \mathrm{Imp}_y(y)dy \cdot \int_{z_1^i + a_i/2}^{z_2^i - a_i/2} \mathrm{Imp}_z(z)dz \tag{55}$$

In Eq. (55), the coordinates $x^i_1$ and $x^i_2$ are the x-coordinates aft and forward, which are normalized by the ship's length, of the $i$th room, respectively. The coordinates $y^i_1$ and $y^i_2$ are y-coordinates of the port and starboard, which are normalized by the ship's breadth, of the $i$th room, respectively. The coordinates $z^i_1$ and $z^i_2$ are the z-coordinates of the bottom and top of the $i$th room, respectively, and these are normalized by the ship's depth, including the superstructure. Function $\mathrm{Imp}_x(x)$ is the impact density function along the longitudinal direction for each threat. Considering that the ASMs follow a piecewise linear distribution along the ship's length, the torpedoes follow a normal distribution, and the mines follow a linear distribution, collision and grounding follows the special shape of the distribution. $\mathrm{Imp}_x(x)$ for each threat are assumed to follow Eqs. (56)-(60).

$$\mathrm{Imp}_x(x) = \begin{cases} 4x & if\ x \le 0.5 \\ -4x + 4 & if\ x > 0.5 \end{cases} \tag{56}$$

$$\mathrm{Imp}_x(x) = \frac{1}{\sqrt{2\pi} \cdot \sigma} \exp\left\{ -\frac{1}{2\sigma^2}(x - 0.4)^2 \right\} \tag{57}$$

$$\mathrm{Imp}_x(x) = \begin{cases} 0 & if\ x \le 0.5 \\ 8x - 4 & if\ x > 0.5 \end{cases} \tag{58}$$

$$\mathrm{Imp}_x(x) = \begin{cases} 0.5 & if\ x \le 0.6 \\ 6.25x - 3.25 & if\ x > 0.6 \end{cases} \tag{59}$$

$$\mathrm{Imp}_x(x) = \begin{cases} 2.67x & if\ x \le 0.5 \\ 1.33 & if\ x > 0.6 \end{cases} \tag{60}$$

In Eq. (57), the symbol $\sigma$ is the standard deviation of normal distribution.

Similarly, function $\mathrm{Imp}_y(y)$ is the impact density function along the transverse direction for each threat. In this study, we assume that this probability for all threats follows parabolic distribution along with the ship's breadth, as shown in Eq. (61).

$$\mathrm{Imp}_y(y) = 2\left\{(y-0.5)^2 + \frac{5}{12}\right\} \tag{61}$$

Finally, function $\mathrm{Imp}_z(z)$ is the impact density function along the vertical direction for each threat. In this study, we assume that this probability for all threats follows a linear distribution along with the ship's depth, including the superstructure, as shown in Eqs. (62)-(66).

$$\mathrm{Imp}_z(z) = 2 \tag{62}$$

$$\mathrm{Imp}_z(z) = -2z + 2 \tag{63}$$

$$\mathrm{Imp}_z(z) = -2z + 2 \tag{64}$$

$$\mathrm{Imp}_z(z) = 2 \tag{65}$$

$$\mathrm{Imp}_z(z) = -2z + 2 \tag{66}$$

When calculating the room damage vulnerability, the longitudinal damage distribution for each threat was assumed as the same as that of the bulkhead damage vulnerability in Figure 2-24.

If a specific room, including equipment, is damaged, such equipment can also have damage. In this sense, if a room has important equipment, the room should be more carefully considered during the arrangement design. Considering this fact, the importance factor ($e_i$) of each room can be defined by a summation of the multiplication of the importance co- efficient and the number of each piece of equipment in the room, as shown in Eq. (67).

$$e_i = \sum_{k=1}^{N_R{}^i} I_e{}^{ik} \cdot N_e{}^{ik} \tag{67}$$

In Eq. (67), the symbol $N^i_R$ is the number of all pieces of equipment in the $i$th room. The symbols $I^k_e$ and $N^{ik}_e$ are the importance factor (between 0 and 1) and the number of the kth equipment in the $i$th room, respectively. The importance factor ($I^{ik}_e$) for all equipment can be determined by a designer and are given as input data for the arrangement design.

## 2.5. Operability evaluation

A large amount of crew and cargo are put into operation in order to carry out smooth operation. Once a naval ship goes into operation, it is briefly carried out for several weeks to months, during which the movement of personnel and materials frequently occurs. In general operations, materials and crews for life and shift move, and in actual operation situations, movement of materials for arming is the main factor. Thus, a naval ship requires more efficient compartment and equipment placement than commercial ships. Therefore, in this study, operability was selected considering space efficiency, the proximity between compartments, and the relation between compartment and hull.

In this study, the operability was represented with the adjacency index (*AI*) that is calculated using the adjacency coefficient ($q_{ij}$) and the distance ($d_{ij}$) between the compartments *i* and *j*, as shown in Eq. (68) [20].

$$AI_R = \sum_{i=1}^{N_c-1} \sum_{j=i+1}^{N_c} q_{ij} \cdot d_{ij} \tag{68}$$

In Eq. (68), the symbol $N_c$ is the number of compartments.

### 2.5.1. Adjacency index between rooms

The adjacency coefficient is a constant that quantitatively represents the degree of closeness between compartments, and it can be calculated from the affinities and antagonism, as shown in Eq. (69) [38].

$$q_{ij} = Affinity_{ij} - Antagonism_{ij} \tag{69}$$

In Eq. (69), the affinity is the characteristic that makes it particularly advantageous to locate one compartment close to another specific compartment, and it is related to the movement of crews and supplies between compartments. A frequent movement of crews and supplies is anticipated between specific compartments; then it becomes advantageous to locate these compartments close to each other. The antagonism represents the characteristics that preclude a compartment from being separately and safely located near another specific compartment. As a consequence, the adjacency coefficient between each compartment can be calculated by subtracting the antagonism from the affinity. The adjacency coefficients ($q_{ij}$) between the compartments can then be determined by a designer and are given as one of the input data for the arrangement design.

### 2.5.2. Distance matrix between rooms

There are many rooms, including passages, in the superstructure. Thus, when we calculate the distance ($d_{ij}$) between the compartments (i.e., the room) $i$ and $j$, the passages between them should also be considered. In this study, Dijkstra's algorithm from graph theory was used to determine an accurate distance [7], [8]. For example, to find the shortest path between compartments 3 and 10, and its distance, all possible relationships among compartments 3, 10, and the passages can be represented in the adjacency graph, as shown in Figure 2-26.

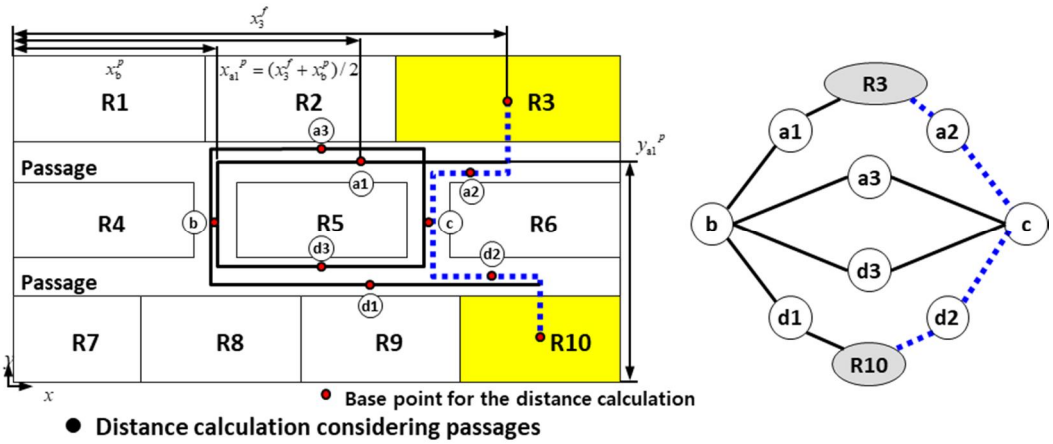


Figure 2-26. Distance calculation using Dijkstra's algorithm

In the adjacency graph of Figure 2-26, each node represents the compartment (3 and 10) or the passage (a, b, c, and d). Each edge represents the distance between the compartment and horizontal passage or between the horizontal and vertical passages. When using Dijkstra's algorithm, the length of each edge must be calculated to determine the shortest path, and its distance, between compartments *i* and *j*. To do this, two starting points for the distance calculation called "base points" should first be defined. In this study, a centroid (center of the area) of the compartment is used as the base point for the compartment. However, for the passage, it is difficult to define the base point. If the centroid of the passage is used as the base point, the redundant distances may be included in the resulting distance between the compartments. To avoid making this error, the base points for the vertical and horizontal passages are defined as follows. For the vertical passage (b and c), the centroid of the passage is used as the base point. For the horizontal passage (a and d), the y- and x-coordinates of the base point are assumed as the vertical centroid of the horizontal passage (for the y coordinate) horizontal centroids of the compartment and the vertical passage, and $(x^f + x^p)/2$ (for the x-coordinate). Here, $x^f$ and

$x^p$ represent the respectively. For example, the x-coordinate ($x^p_{a1}$ ) of the base point for the horizontal passage (a1) is assumed as the horizontal center point between compartment 3 and the vertical passage (b). The y-coordinate ($y^p_{a1}$ ) is assumed as the vertical center point of the horizontal passage (a1), as shown in Figure 2-26. An example defining the base points for the horizontal passages is shown in Figure 2-26, and the corresponding adjacency graph is shown in Figure 2-26.

In this study, not only the relation between the rooms but also the relation between the compartment in the hull and the room in the superstructure are considered. For example, galley should be close to the freshwater tank to use clean water, and the equipment room should be close to the engine room because there are much equipments associated with the main engine. In this study, this is considered as Eq. (70), and in Eq. (70), $d_k$ is assumed to be rectilinear distance. This is illustrated in Figure 2-27.

$$AI_{RC} = \sum_{k=1}^{N_k} d_k \tag{70}$$

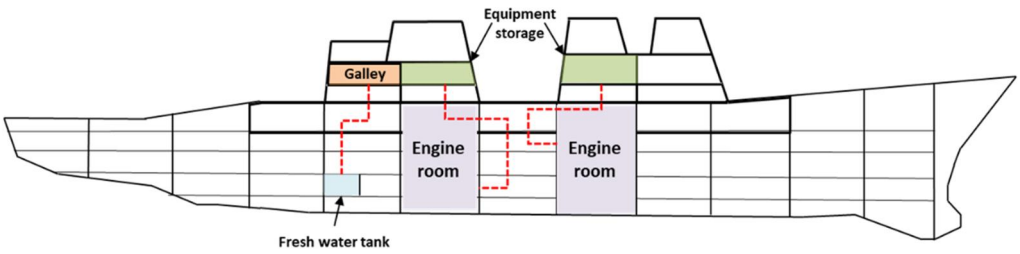


Figure 2-27. Interaction between rooms and compartments in the hull

## 2.6. Optimal arrangement for naval ships

This section describes an optimization method for the arrangement of a naval surface ship. As mentioned earlier, the arrangement method for the naval surface ship was formulated in one stage comparing with other studies. Simultaneously optimizing the hull and superstructure is difficult because there are so many design variables. Therefore, most studies have divided this into two or three and formulated the optimization problem as mentioned in Section 1.2.1. In this case, it is difficult to optimize considering the relationship between the divided parts (generally hull and superstructure), so in this study, the relationship between hull and superstructure can be additionally considered by optimizing the hull and superstructure at the same time. The optimization problem is the arrangement design of naval ship including hull and superstructure where the positions of the bulkheads and decks in the hull and the sequence of rooms and the positions of passages in the superstructure are determined by minimizing the maximum bending moment at the intact state, the space for liquid tanks, the bulkhead damage vulnerability due to the attack, maximizing initial GM value, minimizing the adjacency index between the rooms, the room damage vulnerability due to the attack, and the adjacency between hull and superstructure. It is very difficult to review the damage stability of all of them in reality because it takes a very long time to examine the damage stability (considering the intermediate flooding analysis) for many alternatives. Therefore, the intact stability is reviewed every alternatives, and finally, the damage stability is examined for the selected alternative. The configuration for the optimization procedure is shown in Figure 2-28.

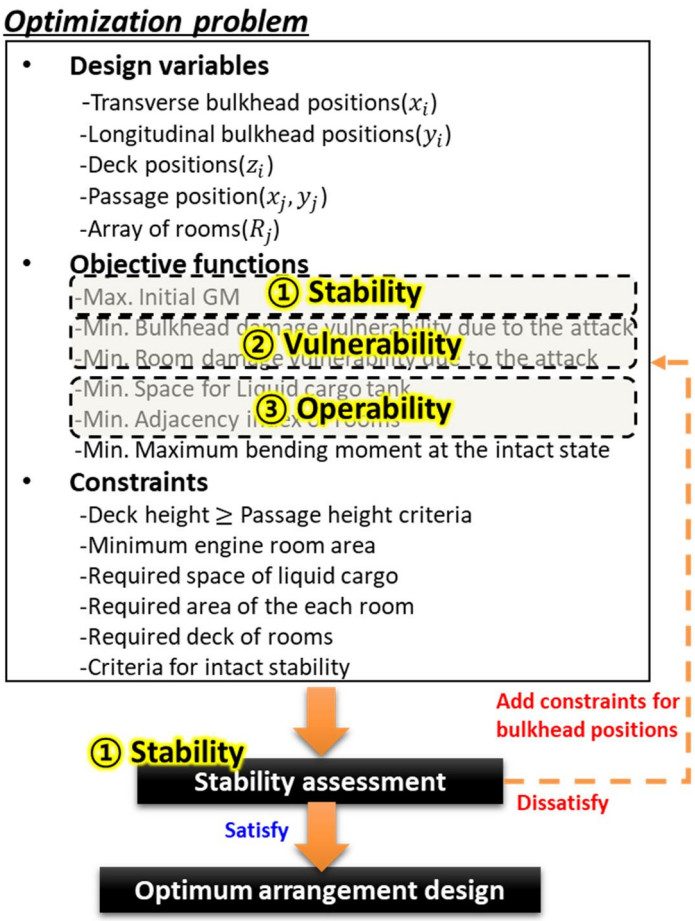


Figure 2-28. Configuration of the optimization problem for the arrangement design of a naval ship

For the optimization of the arrangement of a naval ship, the mathematical formulation of the optimization problems is described below.

Regarding the strength, combat performance, and survivability of a naval surface ship, the positions of the bulkheads and decks in the hull are important during the bulkhead arrangement. To ensure the structural strength, the maximum bending moment at the intact state should be minimized. In addition, to ensure the combat performance, the

space for the armament should be maximized, that is, the auxiliary space for the liquid tanks such as fuel oil tanks (FOTs), freshwater tanks (FWTs), water ballast tanks (WBTs), and lubrication oil tanks (LOTs) should be minimized. In order to maximize stability for a naval ship, the initial GM should be maximized. Finally, to ensure sufficient survivability of the ship, the bulkhead damage vulnerability due to an attack should be minimized. Regarding the operability and survivability of a naval surface ship, the sequence of rooms and the positions of the passages in the superstructure are important during the room arrangement. To ensure the operability, the adjacency index that represents the effectiveness of the flow of crews and supplies in the ship should be minimized. Also, to ensure sufficient survivability of the ship, the room damage vulnerability due to the attack should be minimized. Considering the relation between the hull and the superstructure, the adjacency considering the relationship between the existing compartments and rooms should be minimized as well as the adjacency satisfaction of the rooms inside the superstructure. For these reasons, the process for the arrangement of a naval ship was formulated as an optimization problem in this study.

### 2.6.1. Input information

For the bulkhead arrangement, a hull form and compartment model of the naval surface ship is required. Such information includes the number of bulkheads and decks, and the locations of the compartments, including the liquid tanks of the ship. Also, the information of the weight and the weight distribution at the loading conditions, such as minimum operating condition and full load condition, are also needed to assess the stability requirement. In this study, only two loading conditions that have a high

possibility to cause a severe state of a ship were considered. Here, the minimum operating condition means that a ship carries the minimum amount of cargo required for operation and it can cause a severe state in terms of the stability because the draft is relatively low. The full load condition means that a ship carries all cargo fully and it can cause a large amount of bending moment. Of course, if we consider more loading conditions, the optimal design will be more robust. The bending moment and the stability during the optimization of the bulkhead arrangement were considered as the objective function and the constraints, respectively. To prevent the space for liquid tanks from becoming too small during the optimization, the required volume for the liquid tanks (FOTs, FWTs, WBTs, and LOTs) should also be prepared. To evaluate the bulkhead damage vulnerability due to the attack, the longitudinal damage distribution, the explosive energy per unit mass, and the charge mass of the ASMs, torpedoes, mines, collision, and grounding are required. Finally, the minimum length for each of the engine rooms and the minimum deck height should be input to prevent those values from becoming too small during the optimization. These input data for the bulkhead arrangement can be summarized in Table 2-2.

Table 2-2. Input data for the bulkhead arrangement

| Input data | Notation |
|---|---|
| Hull form and compartment model | - |
| Number of bulkheads and decks | $N_{B\&D}$ |
| Locations of compartments in the hull, including liquid tanks | - |
| Weight and weight distribution at full load condition and minimum operating condition | - |
| Required volumes for liquid tanks (FOTs, FWTs, WBTs, and LOTs) | $V_{FOT}^{\min}$, $V_{FOT}^{\max}$, $V_{FWT}^{\min}$, $V_{FWT}^{\max}$, $V_{WBT}^{\min}$, $V_{WBT}^{\max}$, $V_{LOT}^{\min}$, $V_{LOT}^{\max}$ |
| Longitudinal damage distribution of all threats | - |

| | |
|---|---|
| Explosive energy per unit mass for all threats | $E_W$ |
| Charge mass of ASMs, torpedoes, and mines | $W_A$, $W_T$, $W_M$ |
| Minimum length for each of engine rooms | $l_{ER}^{\min}$ |
| Minimum deck height | $h_{deck}^{\min}$ |

For a room arrangement, a hull form and a compartment model of the naval surface ship are required, as in the bulkhead arrangement. Such information includes a number of bulkheads and decks. In addition, the number of rooms, the number of passages of each deck, and the locations of the entrance doors and inclined ladders in the superstructure should also be given, and the positions of the bulkheads and the decks in the hull that were obtained from the first stage are used as one of the input data in this stage. The locations of entrance doors of rooms and the locations of inclined ladders play a very important role in determining the distance ($d_{ij}$). Therefore, this study reflected them, and when calculating the distance between each room, we defined the distance ($d_{ij}$) so that it can only move through entrance doors and inclined ladders. The locations of entrance doors and inclined ladders used as input information in this study are shown in Figure 2-31. The locations of entrance doors and inclined ladders are not included in the design variables, but since the locations are dependent on the bulkheads and the passages, they are changed following the related bulkheads and passages during the optimization process. In the future, we will include them as design variables of the optimization problem. To evaluate the operability of the ship, the adjacency coefficients between rooms is needed. To evaluate the room damage vulnerability due to the attack, the longitudinal damage distribution of all threats, the number of all equipment in the rooms, and the importance factor and the number of each equipment in the rooms should also be given. The minimum area for each room should be input to prevent its value from becoming too small during the optimization. Finally, the number and the required locations of the

specific rooms (e.g., engine room, bridge, etc.) should be defined. These input data for the room arrangement are summarized in Table 2-3.

Table 2-3. Input data for the room arrangement

| Input data | Notation |
|---|---|
| Hull form and compartment model | - |
| Number of bulkheads and decks | $N_{B\&D}$ |
| Positions of bulkheads and decks from the first stage | $x_i, y_j, z_k$ |
| Number of rooms | $N_R$ |
| Number of passages in the deck $i$ | $N_P^i$ |
| Locations of entrance doors and inclined ladders | See Fig. 11 |
| Adjacency coefficients between the room $i$ and $j$ | $q_{ij}$ |
| Longitudinal damage distribution of all threats | - |
| Number of all equipment in the room $i$ | $N_R^i$ |
| Importance factor (between 0~1) of the equipment $k$ in the room $i$ | $I_e^{ik}$ |
| Number of the equipment $k$ in the room $i$ | $N_e^{ik}$ |
| Minimum area for each room | $a_i^{\min}$ |
| Number of specific rooms for the fixed location | $N_{Rfl}$ |
| Required locations of the specific room $i$ | $R_i^{\text{req}}$ |

### 2.6.2. Design variables

For the bulkhead arrangement, the design variables are the positions of the bulkheads and decks in the hull. Figure 2-29 and Table 2-4 show the design variables for the optimization of the bulkhead arrangement.

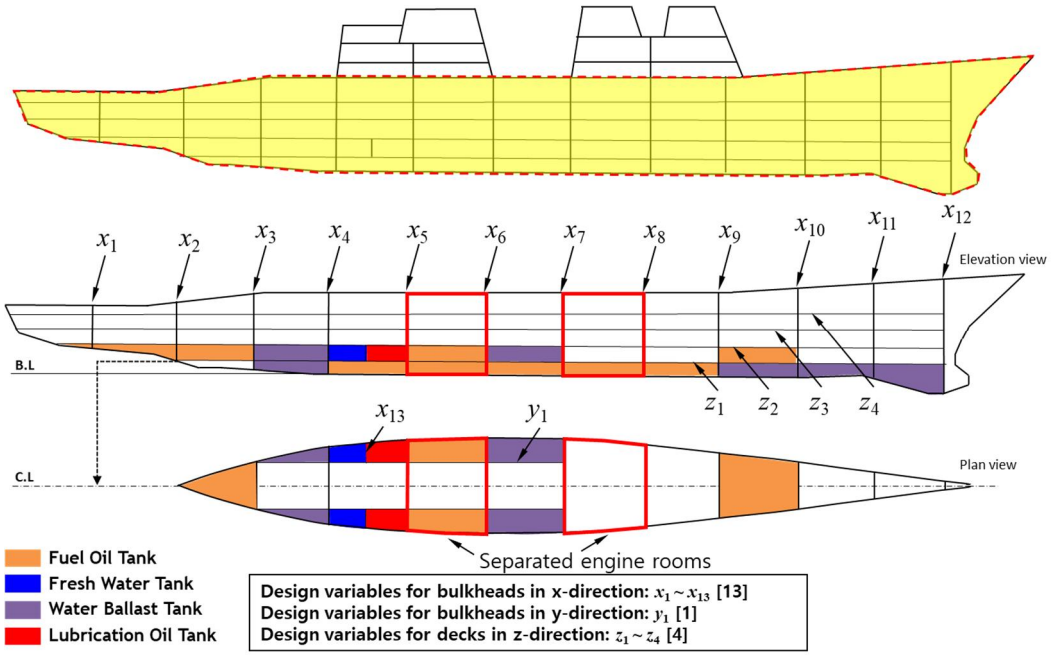


Figure 2-29. Design variables for the optimization of the bulkhead arrangement

Table 2-4. Design variables for the optimization of the bulkhead arrangement

| Design variables | Description |
|---|---|
| $x_i$ | x-coordinate of the bulkhead *i* (from the AP, positive forward) |
| $y_i$ | y-coordinate of the bulkhead *i* (from the center line, positive towards the port side) |
| $z_i$ | z-coordinate of the deck *i* (from baseline, positive upward) |

In this stage, the design variables are the sequence of rooms and positions of passages in the superstructure. Figure 2-30 and Table 2-5 shows the design variables for the optimization of the room arrangement. In this figure, the number in the square bracket ([ ]) means the region ID where each room is to be allocated. Thus, $R_1$ = {OR1}, $R_2$ = {SO1}, $R_3$ = {OR2}, $R_4$ = {SO2}, $R_5$ = {SO3}, …, $R_{33}$ = {CR10}. That is, the location of each room can be represented as an array of the room ID (e.g., OR1, CR1, etc.) through an

encoding process in a genetic algorithm (GA), and after optimization, the array can be converted into the room arrangement through the decoding process.

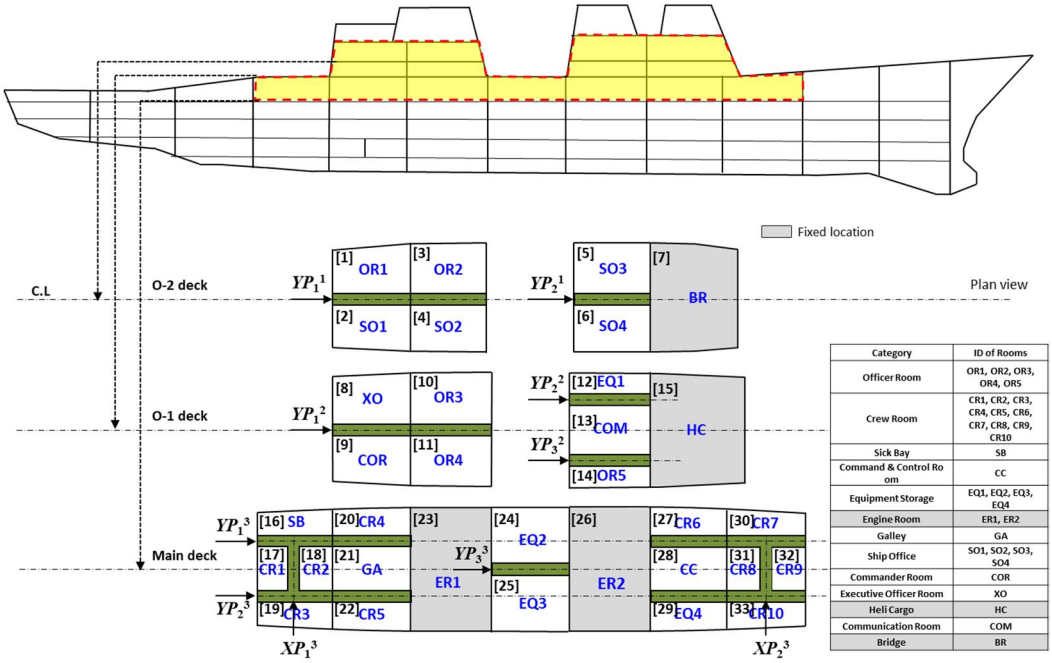


Figure 2-30. Design variables for the optimization of the rooms in the superstructure

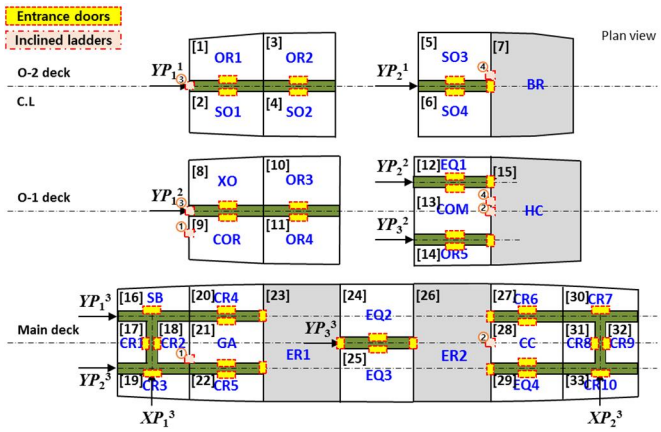


Figure 2-31. Locations of entrance doors and inclined ladders

Table 2-5. Design variables for the optimization of the rooms in the superstructure

| Design variables | Description |
|---|---|
| $R_i$ | Room to be allocated at the region $i$ ($i$ = 1, …, $N_R$) |
| $XP_k^i$ | x-coordinate of the passage $k$ in the deck $i$ (from AP, positive forward) |
| $YP_k^i$ | y-coordinate of the passage $k$ in the deck $i$ (from center line, positive towards port side) |

### 2.6.3. Objective functions

As previously mentioned, it is very important to ensure the structural strength, combat performance, and survivability of a ship in the bulkhead arrangement. Therefore, we introduced three objective functions to ensure these are obtained in the first stage of the optimization. The first objective function of this stage minimizes the maximum bending moment at the intact state. At this time, two loading conditions, such as the full load condition and minimum operating condition, were considered in this study. For each loading condition, the maximum bending moment can be obtained by calculating the buoyancy curve, the weight curve, the load curve, the sheer force curve, and the bending moment curve in the longitudinal direction of the ship. The bending moment can be obtained from the weight curve and the buoyancy curve of a ship under the given loading condition. Here, the weight curve represents the weight distribution of the ship in the longitudinal direction. Thus, if the positions of bulkheads change, the weight curve changes. The load curve is obtained by summing up two curves. If the load curve is integrated along the longitudinal direction, the sheer force curve can be obtained. If the shear force curve is integrated again along the longitudinal direction, the bending moment curve can be obtained. This objective function is intended to minimize the maximum value of the maximum bending moments for the two loading conditions. The second objective function minimizes the auxiliary space for the liquid tanks to maximize the

space for the armament. The auxiliary space for the liquid tanks can be obtained by summing up all volumes of the liquid tanks, including the FOTs, FWTs, WBTs, and LOTs. The third objective function minimizes the bulkhead damage vulnerability due to an attack. The bulkhead damage vulnerability ($V_{BD}$) can be calculated by using Eq. (49). The fourth objective function maximizes the initial GM. The GM can be calculated through applying ship calculation method as mentioned above. As previously mentioned, it is very important to ensure the operability and sufficient survivability of the ship in the room arrangement in the superstructure. Therefore, we introduced two objective functions to ensure these are obtained in the second stage of the optimization. The first objective function of this stage minimizes the adjacency index ($AI$) in Eq. (68) between the rooms. For this, the distance ($d_{ij}$) between the rooms should be calculated by using the method. The second objective function minimizes the room damage vulnerability due to an attack. The room damage vulnerability ($V_{RD}$) can be calculated by using Eq. (52). The objective functions for the optimization of the arrangement are summarized in Table 2-6.

Table 2-6. Objective functions for the optimization problem

| Objective functions | Type | Mathematical representation |
|---|---|---|
| The maximum bending moment at the intact state | Minimize | $F_1 = \max(BM_1, BM_2)$ (1: full load condition, 2: minimum operating condition) |
| Auxiliary space for liquid tanks | Minimize | $F_2 = V_{FOT} + V_{FWT} + V_{WBT} + V_{LOT}$ |
| Bulkhead damage vulnerability due to the attack | Minimize | $F_3 = V_{BD} = \sum_{i=1}^{N_{B\&D}} P_r^i$ |
| Initial GM | Maximize | $F_4 = GM = GZ / \sin\phi$ at small angle |
| Adjacency index between rooms | Minimize | $F_5 = AI = \sum_{i=1}^{N_R-1} \sum_{j=i+1}^{N_R} (q_{ij} \cdot d_{ij})$ |
| Adjacency index between rooms and compartments | Minimize | $F_6 = AI = \sum_{k=1}^{N_k} d_k$ |
| Room damage vulnerability due to the attack | Minimize | $F_7 = V_{RD} = \sum_{i=1}^{N_R} p_i \cdot e_i$ |

### 2.6.4. Constraints

When arranging the bulkheads and decks in the hull, some issues, including the stability, should be considered. Thus, the following constraints were formulated to consider such aspects.

#### (1) Constraints related to the criteria for intact stability

As mentioned in Section 2.3.1, a naval surface ship should satisfy the criteria for intact and damage stability. However, in case of damage stability considering intermediate flooding, there are many cases and it is difficult to evaluate them in every case. Thus, the stability of damage is only evaluated within the selected range after optimization. The criteria were used as constraints for the optimization in this stage, as shown in Eqs. (71)-(73).

$$g_1 = GZ_0 / GZ_{\max} - 0.6 \le 0 \quad \text{in the intact state} \tag{71}$$

$$g_2 = 1.4 - A_2 / A_1 \le 0 \quad \text{in the intact state} \tag{72}$$

$$g_3 = \phi_0 - 15 \le 0 \quad \text{in the intact state} \tag{73}$$

#### (2) Constraints related to the required volumes for liquid tanks

In general, the auxiliary space for the liquid tanks may have required a given volume for operation. Thus, there are constraints that bind the upper and lower limits for each liquid tank, as shown in Eqs. (74)-(81).

$$g_4 = V_{FOT}^{\min} - V_{FOT} \le 0 \tag{74}$$

$$g_5 = V_{FOT} - V_{FOT}^{\max} \le 0 \tag{75}$$

$$g_6 = V_{FWT}^{\min} - V_{FWT} \le 0 \tag{76}$$

$$g_7 = V_{FWT} - V_{FWT}^{\max} \le 0 \tag{77}$$

$$g_8 = V_{WBT}^{\min} - V_{WBT} \le 0 \tag{78}$$

$$g_9 = V_{WBT} - V_{WBT}^{\max} \le 0 \tag{79}$$

$$g_{10} = V_{LOT}^{\min} - V_{LOT} \le 0 \tag{80}$$

$$g_{11} = V_{LOT} - V_{LOT}^{\max} \le 0 \tag{81}$$

### (3) Constraints related to the required length for the engine rooms

If the length of each of the engine rooms should have a minimum length, such requirements can be formulated as constraints, as shown in Eqs. (82), (83).

$$g_{12} = l_{ER}^{\min} - \left| x_5 - x_6 \right| \le 0 \tag{82}$$

$$g_{13} = l_{ER}^{\min} - \left| x_7 - x_8 \right| \le 0 \tag{83}$$

In Eqs. (82), (83), the values $|x_5 - x_6|$ and $|x_7 - x_8|$ are the length of each of the engine rooms, as shown in Figure 2-29

.

### (4) Constraints related to the required deck height

If the height between the adjacent decks should have the minimum distance, such requirements can be formulated as constraints, as shown in Eqs. (84)-(88).

$$g_{14} = h_{deck}^{\min} - |z_1 - 0| \le 0 \tag{84}$$

$$g_{15} = h_{deck}^{\min} - |z_2 - z_1| \le 0 \tag{85}$$

$$g_{16} = h_{deck}^{\min} - |z_3 - z_2| \le 0 \tag{86}$$

$$g_{17} = h_{deck}^{\min} - |z_4 - z_3| \le 0 \tag{87}$$

$$g_{18} = h_{deck}^{\min} - |D - z_4| \le 0 \tag{88}$$

### (5) Constraints related to the required area for rooms

If the area of each room should have the minimum area according to the ship owner's requirements, such requirements can be formulated as constraints, as shown in Eq. (89).

$$g_{18+i} = a_i^{\min} - a_i \le 0 \quad (i = 1, \ldots, N_R) \tag{89}$$

### (6) Constraints related to the required locations of the specific rooms

If specific rooms, such as the engine room (ER1, ER2), bridge (BR), and heli cargo (HC), should have fixed locations, such requirements can be formulated as constraints, as shown in Eq. (90).

$$g_{18+N_R+i} = R_i - R_i^{\text{req}} = 0 \quad (i = 1, \ldots, N_{Rfl}) \tag{90}$$

### 2.6.5. Optimization algorithm

Optimization algorithms are divided into global and local optimization algorithms, and several types of algorithms are available for global optimization, including GA (Goldberg, 1989; Davis, 1991). Global optimization algorithms may be suitable for large-scale problems that have many local optima, but they require more iterations to obtain an acceptable optimum in comparison with local optimization algorithms. Several classes of local optimization algorithms also exist, including sequential linear programming (SLP) (Arora, 2012), sequential quadratic programming (SQP) (Arora, [66]), and a method for feasible directions (MFD) (Vanderplaats, [67]). Each of these local optimization algorithms can be used to effectively find the optimum. However, in some cases, these local optimization algorithms find an optimum that is relatively close to the starting point. In addition, the objective functions and constraints presented in this study include nonlinear equations which are difficult to be solved with general optimization algorithms. Also, since the permutation is used in the second stage as design variables, the algorithm which can handle the permutation should be used. In this study, NSGA-II (Deb et al., [68]) which is a kind of multiobjective GA was used to solve multi-objective nonlinear optimization problems of this study. Of course, SPEA-II (Zitzler et al., [69]) and SMPSO (Nebro et al., [70]) can be used. Through comparative tests among them by us, NSGA-II that had shown the best performance was finally selected and used to solve the optimization problems of this study. For efficient use of NSGA-II, the seed is used to improve the convergence speed of the solution by basically selecting the solution

satisfying the constraint as the initial solution. In addition, in order to increase the computing time, To GPU through parallelization using GPU.

# 3. Verifications

In this study, three evaluation factors: stability, vulnerability, and operability were considered for the arrangement design of a naval ship. Therefore, for each evaluation factor, basic verification of the contents suggested in Section 2 is necessary. In this section, the verification of each background theory is carried out by comparing the experimental results and the simulation results in various related studies and verified the applicability of using the proposed method in this study.

## 3.1. Verifications of intermediate flooding analysis

In this chapter, we have confirmed that the proposed intermediate flood analysis method is actually applicable. As described above, PBD was used to calculate the flow of fluid and the shape of the fluid contained in the vessel, and the calculated weight and center of gravity were assigned to the 6-degree-of-freedom Cummins equation And analyzed the behavior of the ship. Therefore, verification of PBD and flood analysis using 6-DoF equations of motion should be verified for the intermediate flooding analysis.

### 3.1.1. Verification of PBD

To evaluate whether the PBD method proposed in this study is suitable for calculating the actual flow rate, Kleefsman et al. [71] dam breaking experiment.

### (1) Verification model

Kleefsman et al. [71] were filled with water of 1.228 m in height, and 0.5 m in width in a water tank of about 3 meters for the experiment, and the length, breadth, and height for breaking in front of 1.248 m were 0.161 m, 0.403 m and 0.161 m box was installed. Kleefman et al. [71] detailed specifications for the dam breaking experiment are shown in Figure 3-1.

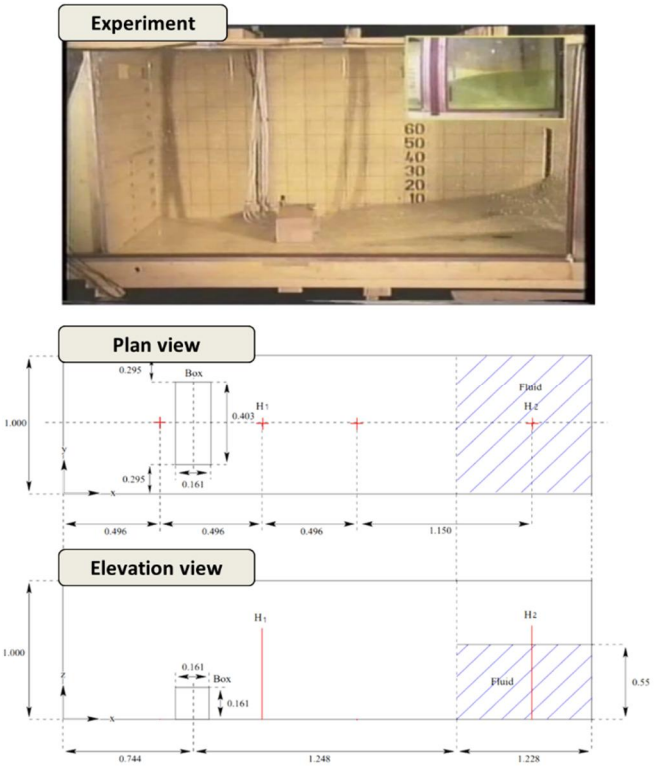


Figure 3-1. Dam breaking experiment of Kleefsman et al. [71]

In this study, it was simulated with PBD and the fluid dam was described as 108,540 particles. The modeled results are shown in Figure 3-2. The simulation time was about 6

seconds, and the fluid dam hit the opposite wall again and returned to the original wall. Then, the time to the opposite wall was set again.

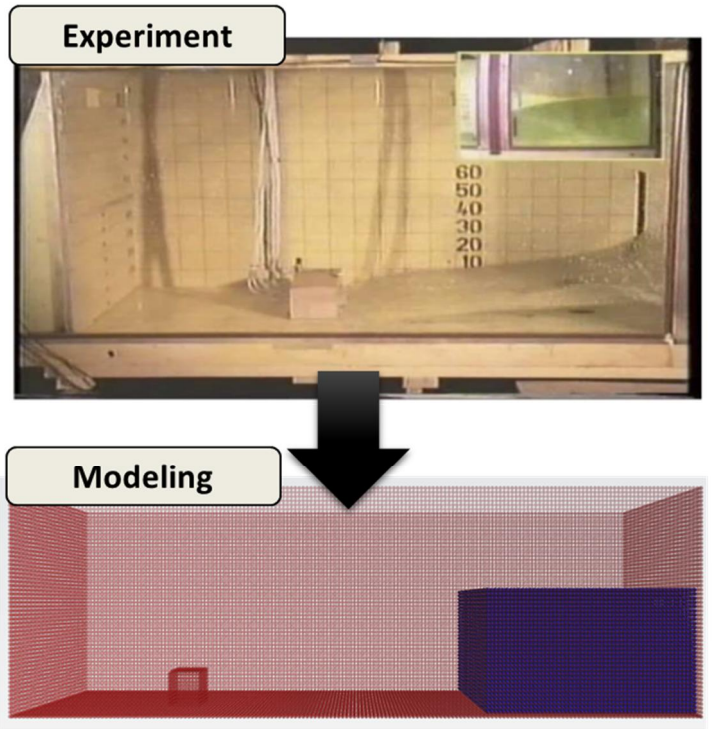


**Environment discretization**

| | |
|---|---|
| Particle initial spacing [mm] | 0.1833 |
| Fluid particles (x, y, z) | 67×54×30 = 108,540 |

Figure 3-2. Modeling for dam breaking

### (2) Verification results

In this study, Kleefsman et al. [71], the PBD simulation were carried out by simulating the same situation, and the heights at 'H1' and 'H2' positions were compared with time in Fig. The pressure on the right side 'P1' of the breaking box and the pressure on the upper side 'P2' were compared.

Figure 3-3 is the result of the simulation conducted in this study. As shown in Figure 3-3, you can see that the fluid is poured into the box over time and back again.

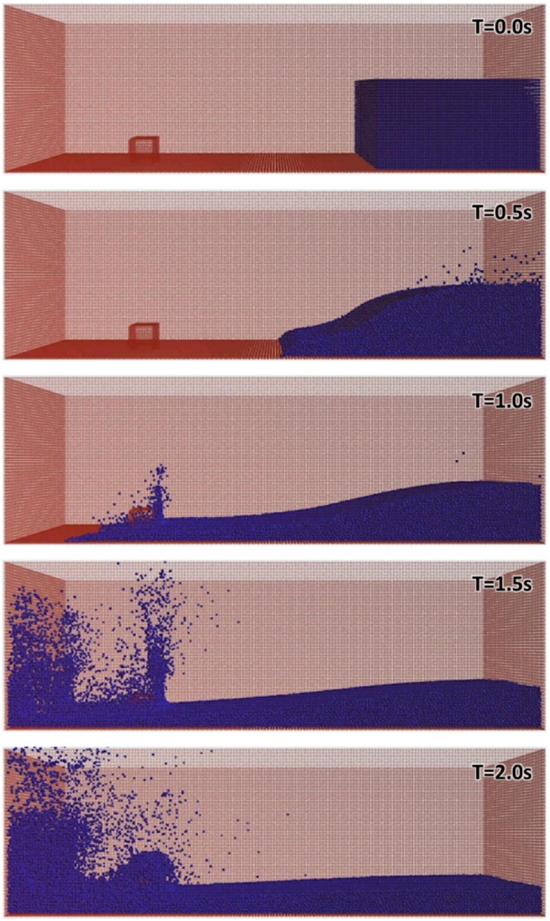


Figure 3-3. Screen shot of dam breaking simulation

First, the height comparison results are shown in Figure 3-4. In Figure 3-4, the red dotted line and the blue dotted line are Kleefsman et al. [71] and the CFD results. And the solid green line is Wang et al. [72], Kleefsman et al. [71] are simulated through the Explicit Moving Particle Semi-Implicit (EMPS) method, one of the MPM methods. Finally, the solid blue line shows the results of the PBD simulation conducted in this study.

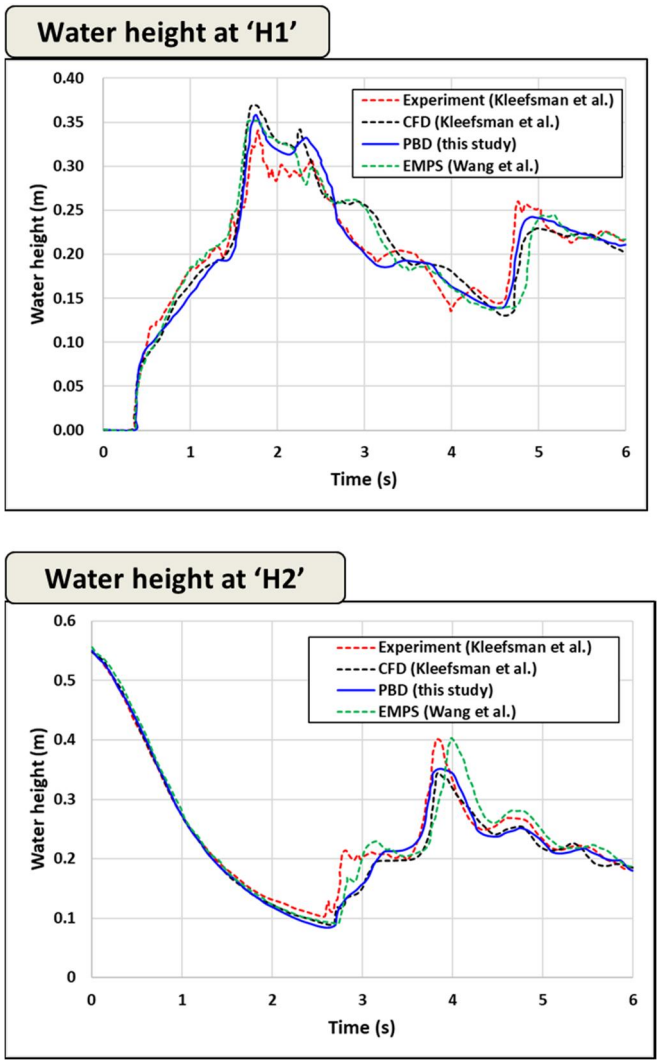


Figure 3-4. Water height results at 'H1' and 'H2'

As can be seen in Figure 3-4, the results of this study are very good compared with the experimental results. And the results of other studies are somewhat similar to the experimental results. Therefore, it is expected that the flow calculation through the PBD proposed in this study will be accurate.

The following is a comparison of the pressure results at 'P1' and 'P2' on the right side

and top side of the breaking box shown in Figure 3-5. The red dotted line shows the experimental results of Kleefsman et al. [71], and the black dotted line indicates the results of CFD analysis results of Kleefsman et al. [71]. Finally, the solid blue line shows the results of the PBD simulation conducted in this study.

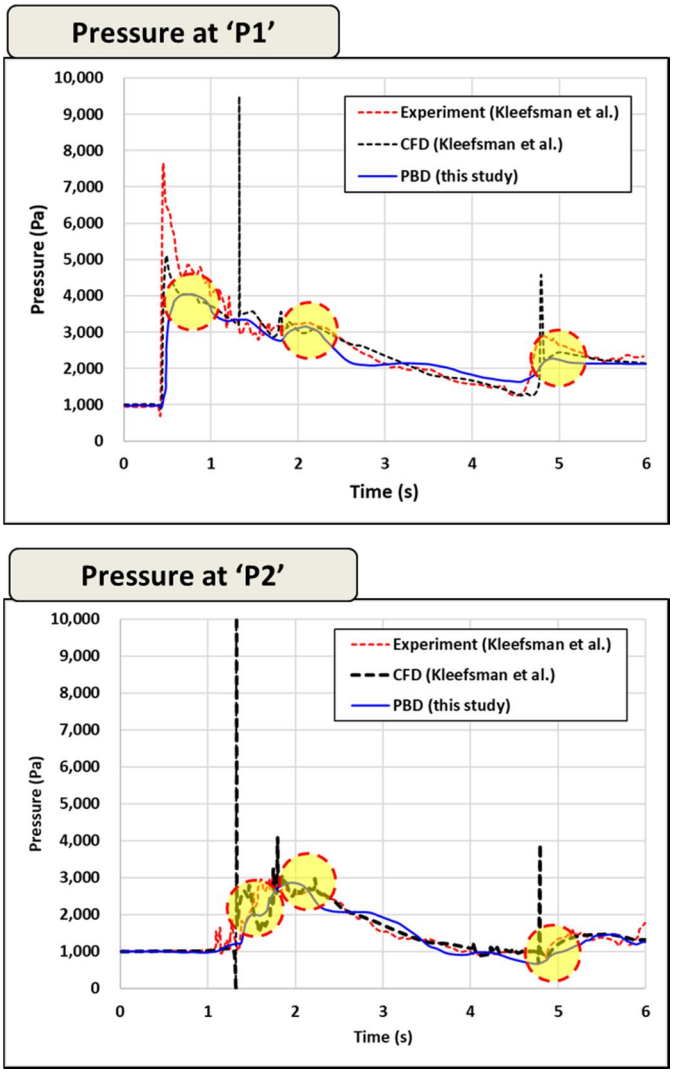


Figure 3-5. Pressure results at 'P1' and 'P2'

In Figure 3-5, the breaking point is represented by a yellow circle. In the case of the

pressure calculated by the PBD at that position, the phenomenon of crumbling can be found. When calculating the pressure with the PBD, the constraint is calculated through the iteration as much as the user set, and it is expected that the result can be obtained because the iteration cannot be set infinitely.

However, as described above, the advantage of PBD is that it makes it easier to parallelize algorithms and computes the constraints through the position, resulting in less computing time than other methods. As a result, we confirmed that the simulation time in this study is the shortest. Simulation time is 6 sec. In this study, when PBD simulation is performed on the computer of Table 3-1, it is confirmed that it can be calculated at about 5 seconds or more in real-time. Kleefsman et al. [71], the CFD results show that the analysis takes about 6 hours. Therefore, the flow rate calculation method using the PBD method proposed in this study is excellent in terms of speed and is suitable for the flow rate calculation. Comparison of computing time is summarized in Table 3-2.

Table 3-1. Specification of simulation computer of this study

| Category | Specification |
|---|---|
| CPU | Intel Core i7-7700K 4.2GHz |
| GPU | NVIDIA GeForce GTX 1080Ti |
| RAM | 32GB |

Table 3-2. Comparison of computation time

| Studies | Time |
|---|---|
| Simulation time | 6 sec |
| Computing time of this study | 5 sec |
| Computing time of CFD (Kleefsman et al.) | 6 hours |
| Computing time of EMPS (Wang et al.) | N/A |

### 3.1.2. Verification of dynamic flooding analysis

In this study, flow calculation through PBD and fluid shape inside the hull are calculated. We then update the weight and center of gravity of the vessel every hour. Calculate the six degrees of freedom movement of the ship by releasing the Cummins equation reflecting the updated weight and center of gravity. In order to verify that the 6-DOF kinematics calculation is accurate, this study applied it to flooding analysis of the oil tanker and confirmed its accuracy by comparison with the quasi-static analysis result.

### (1) Verification model

The model used for verification is an oil tanker about 180 m in size, and the tanker has a double hull. It was assumed that the water ballast tank on the starboard in the full loading condition suffered damage of 2 m in length and 2 m in length. The model used for the verification is shown in Figure 3-6, and damaging information is summarized in Table 3-3.

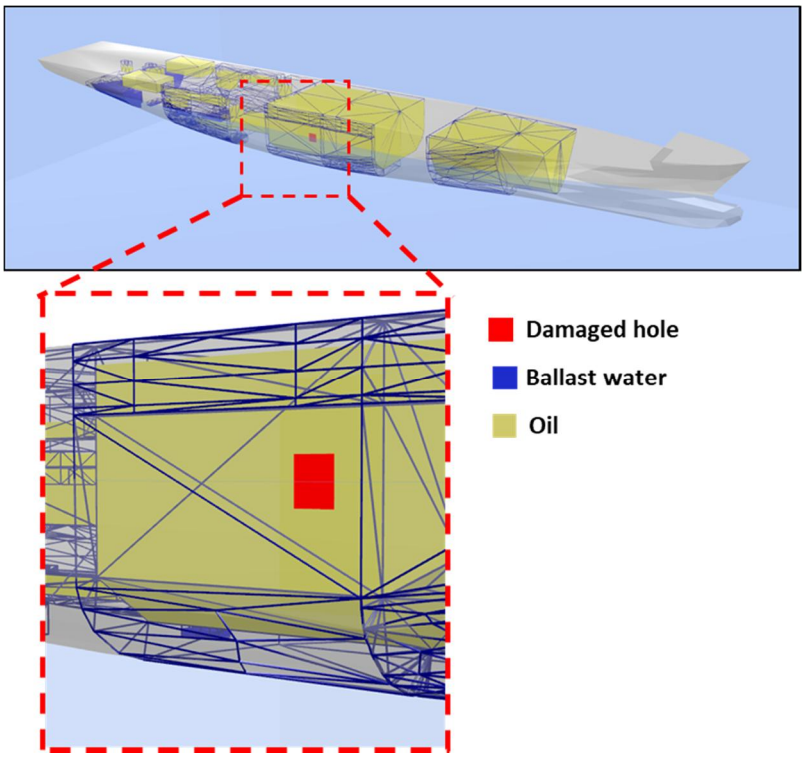


Figure 3-6. Model for verification of dynamic flooding analysis

Table 3-3. Damaged scenario for verification of dynamic flooding analysis

| Analyzing method | Damaged compartments | Damage size | Environmental condition |
|---|---|---|---|
| Quasi-static<br>Dynamic | One ballast tank in the starboard | 2 × 2 m | Calm water |

### (2) Verification results

In order to compare the quasi-static and dynamic analysis results, we compared the roll and heave values of the ship and the amount of water in the damaged ballast tank. The results are shown in Figure 3-7.

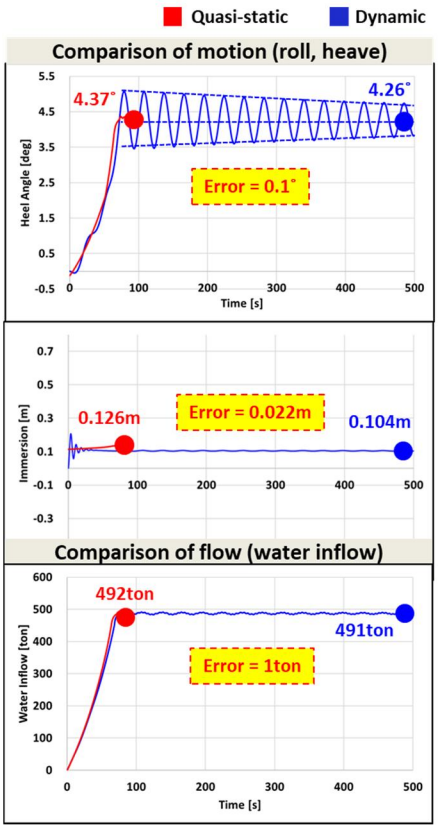


Figure 3-7. Results of motion and flow comparison

As shown in Figure 3-7, the motion calculated through the Cummins equation showed oscillatory motion, but as time went by, it became close to the result of the quasi-static analysis, and the behavior was very similar, we can see the same thing. Therefore, it is confirmed that the proposed intermediate flood analysis method is suitable for practical flood analysis.

### 3.1.3. Verification with the experiment by Ruponen [24]

We compared the experimental results of Ruponen [27] to verify that the proposed mid-level flood analysis method is similar to the actual one. Ruponen [27] produced a

barge type model and simulated the progressive flooding process by creating simple compartments inside and compared it with experimental results through quasi-static analysis. On the other hand, Strasser et al. [34] simulated Ruponen [27] experiments through CFD analysis and compared the results. In this study, two case studies of Ruponen [27] were simulated in the same way, and the results were compared and verified.

### (1) Verification model

Ruponen [27] constructed several compartments inside a 4 m barge type vessel to verify his quasi-static flooding analysis method and compared it with his analysis results. The model produced by Ruponen [27] is shown in Figure 3-8, and the detailed specification is shown in Table 3-4. Figure 3-8 also includes a description of the two cases.

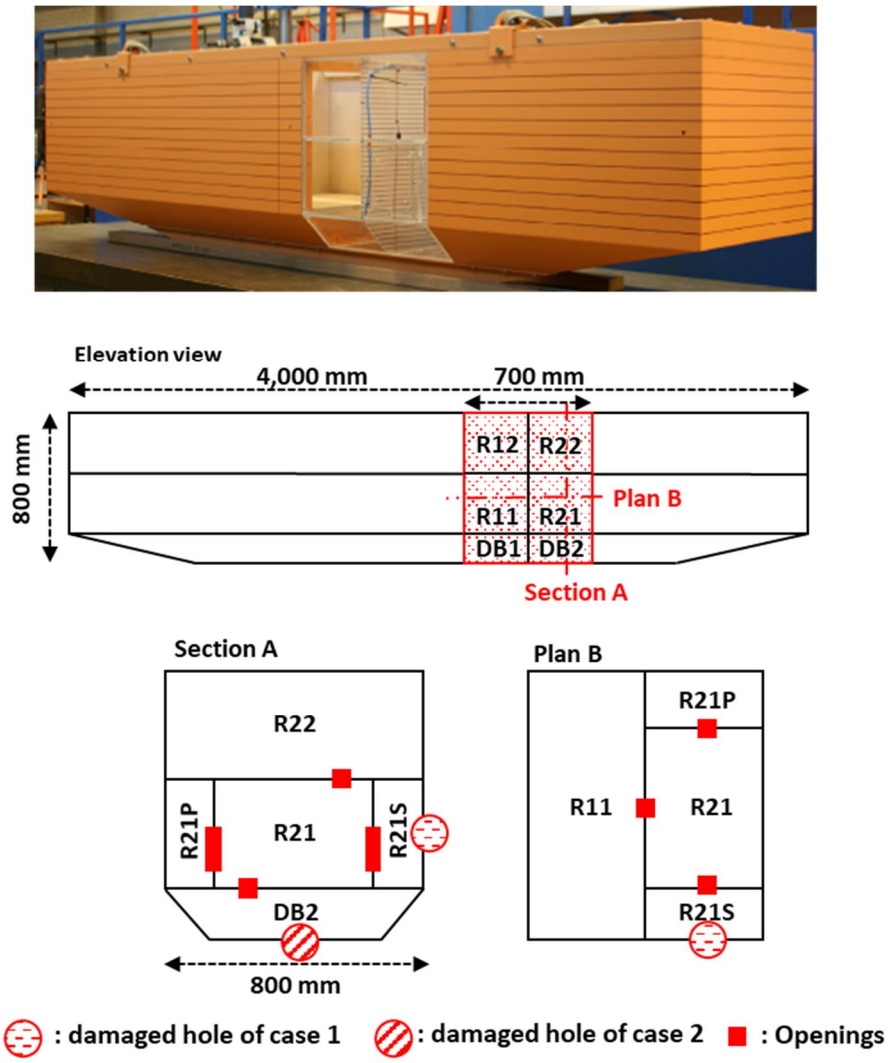


Figure 3-8. Barge type model of Ruponen [27]

Table 3-4. Main dimensions of barge type model

| Main dimension | Value |
|---|---|
| Length | 4.000 m |
| Breadth | 0.800 m |
| Depth | 0.800 m |
| Draft | 0.500 m |
| KG | 0.278 m |
| Displacement | 1.450 $m^3$ |

As shown in Figure 3-8, flooding experiment was conducted through two cases. Case 1 is damaged when the port is damaged, and Case 2 is damaged when the bottom of the hull is damaged. The detailed location and size of the damage are shown in Figure 3-8.

In this study, the dynamic flooding analysis method using PBD under the same conditions was simulated and the results were analyzed by Ruponen [27] and Strasser et al. [34] compared with CFD results.

### (2) Verification results

① Case1 – damaged hole at starboard

When the ship starboard was damaged, the pitch and heave motion results of the ship were compared. Figure 3-9 shows the variation of the pitch and heave of the ship over time. In Figure 3-9, the solid orange line and the black solid line represent the experimental results and quasi-static analysis results of Ruponen [27], respectively, and the green solid line is Strasser et al. [34]. The results of this study are as follows. Finally, the solid blue line shows the results of this study.

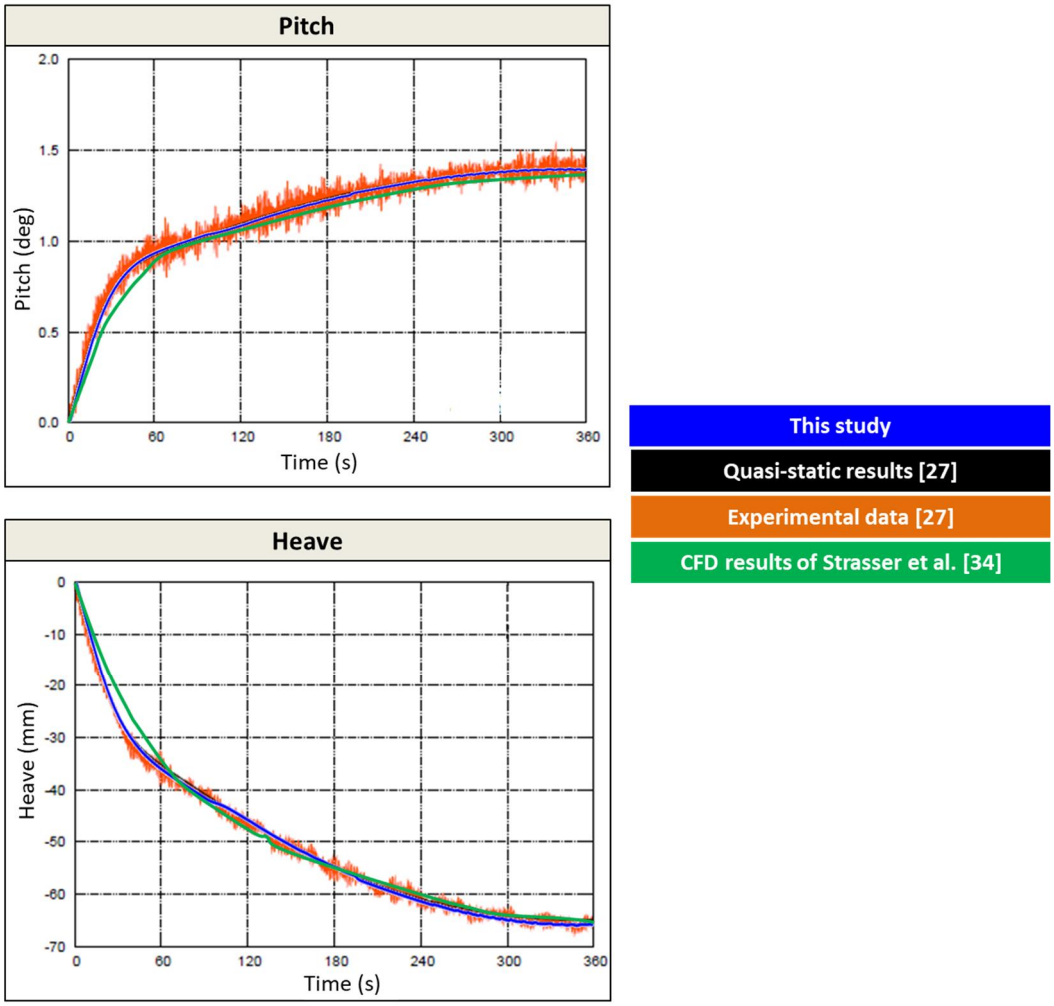


Figure 3-9. Pitch and heave motion of Case 1

As can be seen in Figure 3-9, the results of this study are very similar to the experimental results, and it can be seen that oscillatory motion hardly occurs in this experiment because the size of the damage is very small compared to the size of the model. So the transit motion is rarely occurs

② Case2 – damaged hole at the bottom

When the bottom of the ship was damaged, the pitch and heave motion results of the ship were compared. Figure 3-10 shows the variation of the pitch and heave of the ship over time. In the graph, the solid orange line and the black solid line show the experimental results and quasi-static analysis results of Ruponen [27], respectively, and the blue solid line shows the results of this study.

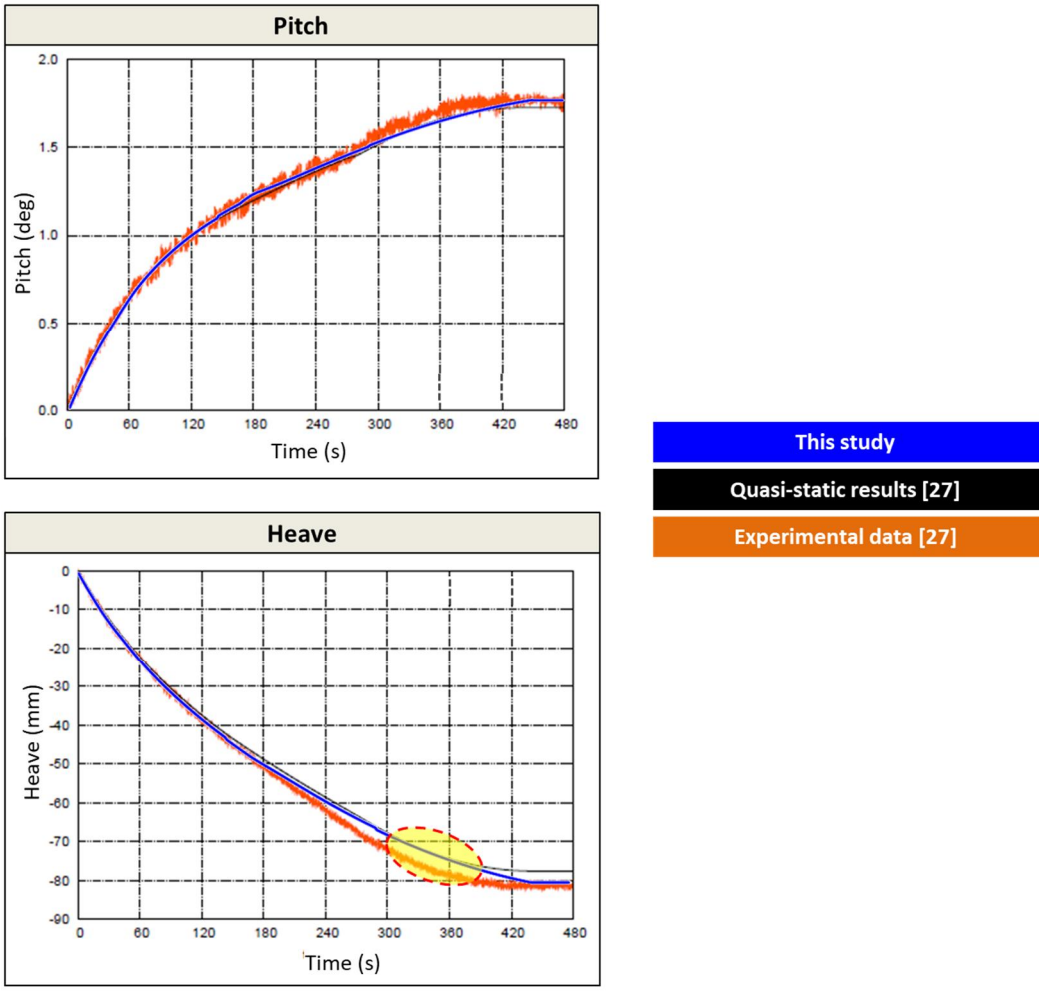


Figure 3-10. Pitch and heave motion of Case 2

As shown in Figure 3-10, the results of this study are very similar to the experimental results, and it can be seen that oscillatory motion hardly occurs in this experiment because the size of the damage is very small compared to the size of the model, Is hardly generated. In addition, we can see that the heave is slightly slower than the real part in the yellow circles. This is because the viscosity is not considered when calculating the flow rate in this study. But the difference is very slight.

### 3.1.4. Verification with the experiment by Hosseini et al. [32]

Previously, Ruponen [27]tested barge type linearity with very small transit motion because the damage size is very small compared to the hull. Therefore, quasi-static analysis is appropriate. However, if the damage is large and the ship has a linear shape similar to that of the actual ship, the dynamic effect is larger, and the oscillatory motion is more frequent. Hosseini et al. [35] were compared with the experimental results.

#### (1) Verification model

Hosseini et al. [35] made a model using the ship's linearity of the cruise ship released by SSRC (Ship Stability Research Center) and made a compartment for flood analysis itself. The shape of the hull is as shown in Figure 3-11, and the main dimension of the ship is shown in Table 3-5.

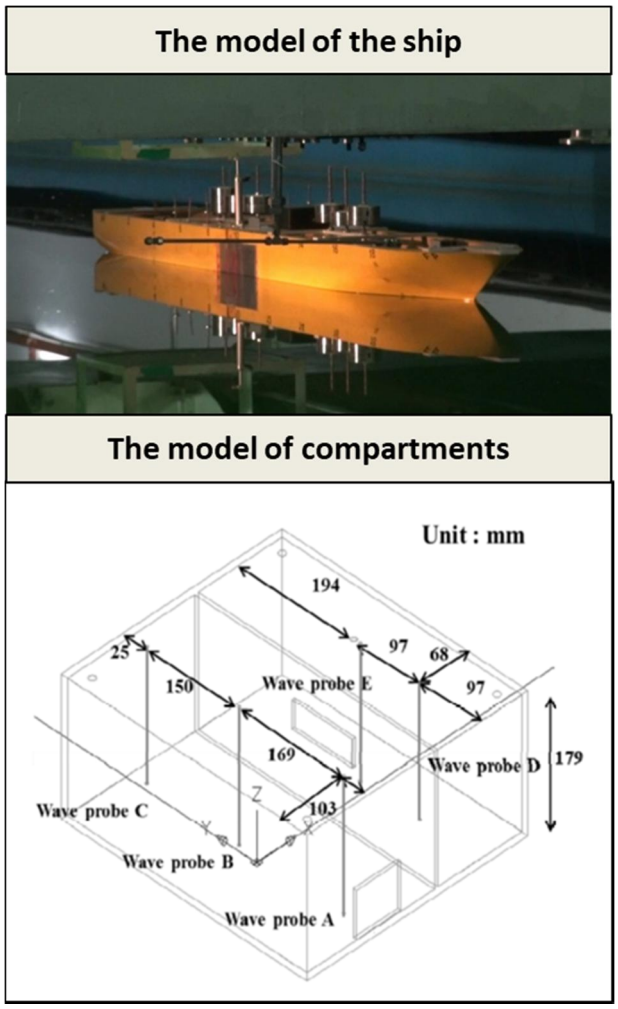


Figure 3-11. Cruise ship model of SSRC and compartments for flooding

Table 3-5. Main dimensions of Cruise ship model of SSRC

| Main dimension | Value |
|---|---|
| Length | 3.000 m |
| Breadth | 0.430 m |
| Draft | 0.100 m |
| KG | 0.199 m |
| Displacement | 0.100 ton |

In addition, the compartment model inside the hull is composed of two compartments in total, and it has experimented that the inside is opened and the flooding progresses from the damage to the outside and spread out from the inside compartment. Detailed figures and shapes of compartments are shown in Figure 3-11.

In this study, it is simulated and modeled as shown in Figure 3-12 and compared with experimental results using an intermediate flooding analysis.

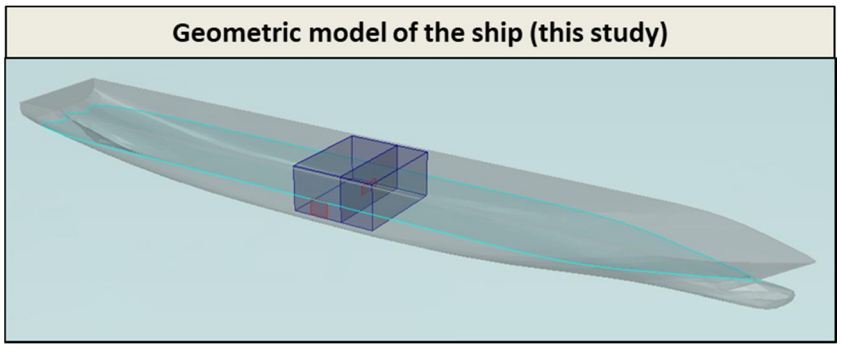


Figure 3-12. Geometric model of SSRC in this study

### (2) Verification results

External damage is introduced into the ship through damage to the ship's starboard, and the incoming fluid is propagated to other compartments. This situation was simulated through an intermediate flooding analysis, and Figure 3-13 shows the damage situation.

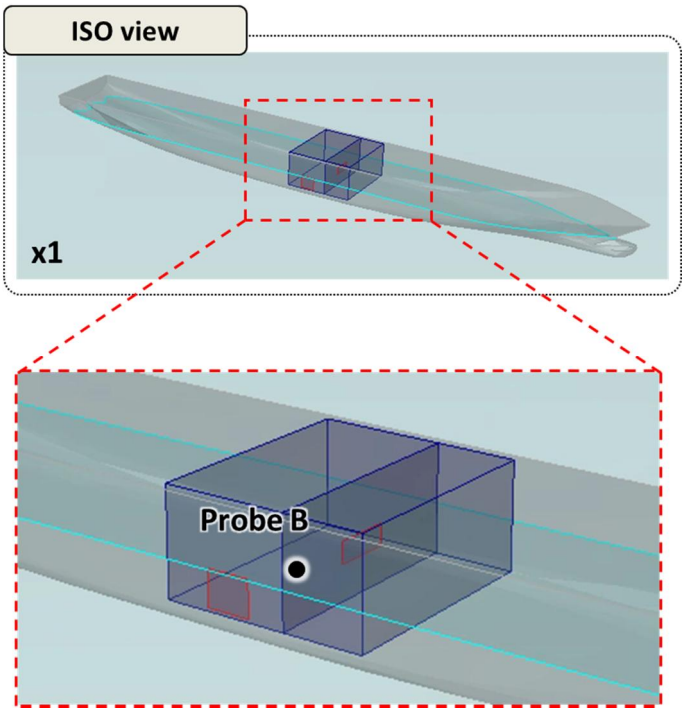

Figure 3-13. Damage location and position of ‘Probe B’

The rolling motion of the ship and the water level at 'Probe B' are shown in Hosseini et al. [35], and compared with CFD results. Figure 3-14 shows roll motion and water height at 'Probe B'. The red dotted line and the black dotted line in the graph are shown in Hosseini et al. [35] and CFD analysis results, and the blue solid line shows the results of this study. Both results are similar to the experimental results. However, for the first result, we can see that the rolling cycle is slightly different. This is due to the difference between the added mass and the damping coefficient due to the inconsistency of the model line. In this way, the proposed method is similar to the steady-state flooding analysis, and it is confirmed that dynamic analysis can be performed.

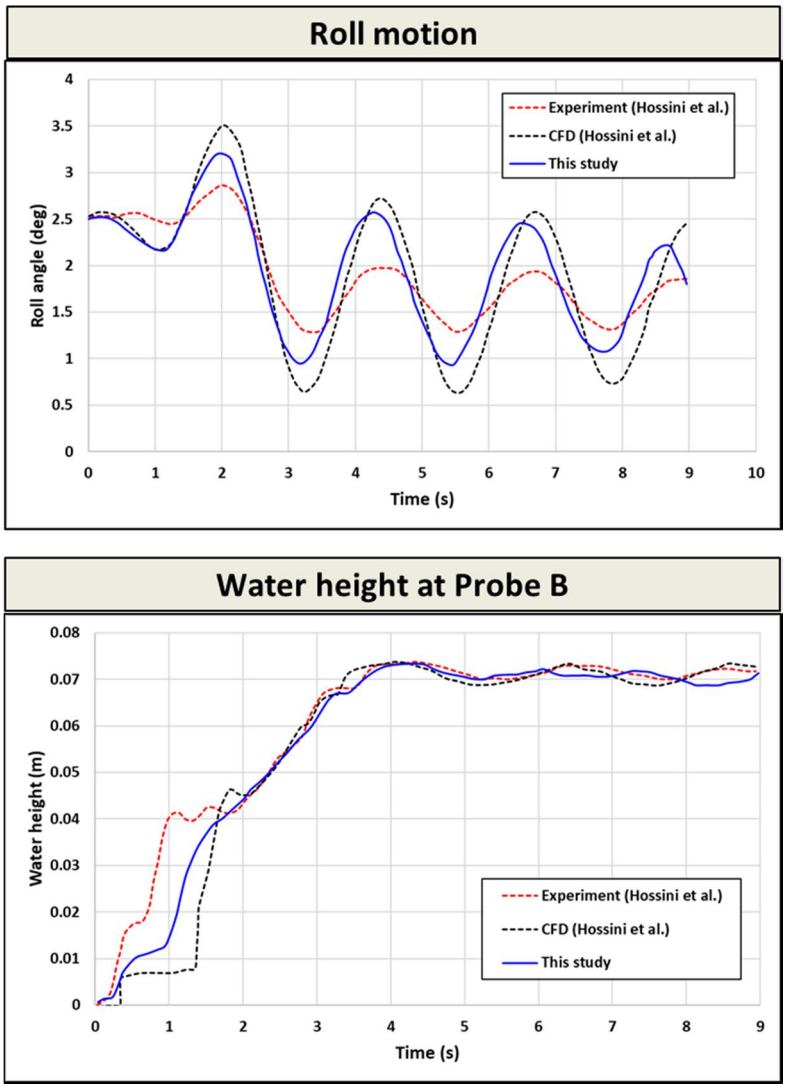


Figure 3-14. Results of roll motion and water height at 'Probe B'

### 3.1.5. Verification with the experiment by Debra et al. [42]

To verify flooding analysis methods considering oil leakage, the results of this study were compared with the two sets of experimental results in Debra et al. [42], where an oil leakage experiment was conducted using a box filled with oil.

### (1) Verification model

Figure 3-15 shows the geometry and the main dimensions of the oil box. In Case 1, the box was set on the ground and the oil level was tracked. In Case 2, the box was set in a water pool and the oil level as well the water level were tracked. Figure 3-16 shows the two cases of oil leakage.

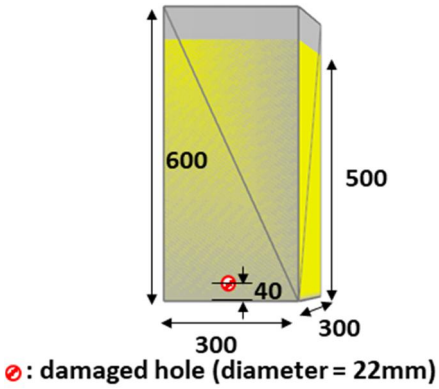


Figure 3-15. Geometry and main dimensions of oil box

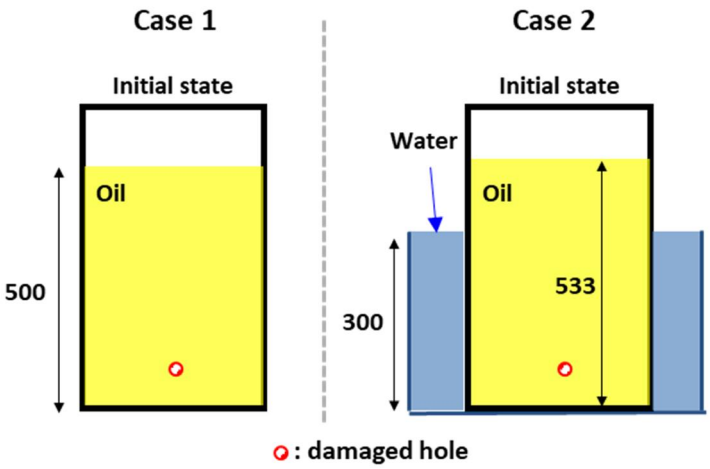


Figure 3-16. Illustration of two cases of oil leakage

The simulation results in this study and the experimental results in Debra et al. [42] were compared. Figure 3-17 shows the oil height inside the box for Case 1. It can be seen that the two results are quite similar, and the final error is 1 mm.

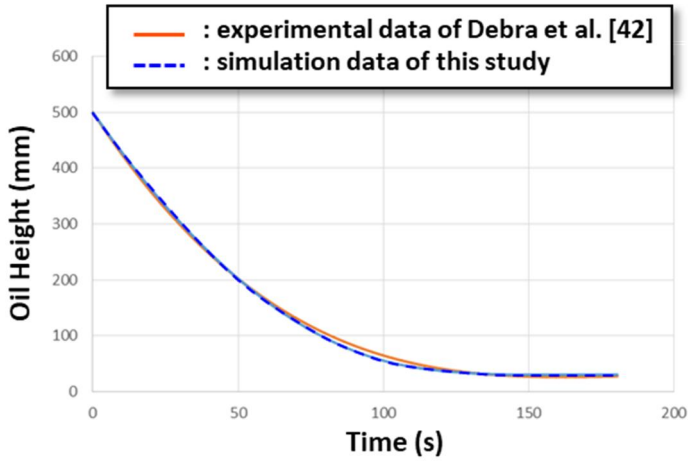


Figure 3-17. Case 1 – comparison of oil height in the box

Figure 3-18 shows the comparison of oil and water height in Case 2. It can be seen that oil flows out until the water reaches the top of the opening. The final error is 1 mm. The water flows in the box until the water reaches the top of the opening, and the final error of final is 2 mm.

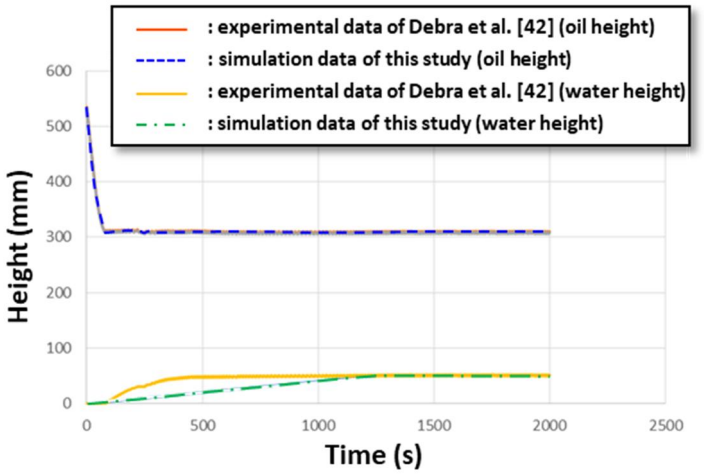


Figure 3-18. Case 2 – comparison of oil and water height in the box

As shown in the results, the oil flow rate in the simulation is slightly higher than in the experiment in Case 1, and the water flow rate in the simulation is slightly lower than in the experiment in Case 2. In this study, the viscosity was neglected, and only oil density was considered, accounting for the aforementioned errors.

## 3.2. Verifications of stability

In this study, static restoration and damage restoration were evaluated according to the criteria described in Section 2.3. In order to calculate intact damage stability, it is necessary to calculate the GZ curve and HA curve according to the heeling angle of the ship, which is calculated mainly by the commercial program NAPA in the fieldwork. However, in this study, it is implemented to calculate it automatically in the optimization process, and accordingly, the GZ curve and the HA curve calculation function are naturally implemented and included. Therefore, it is confirmed that the stability result

calculated by the calculation module of this study agrees with the commercial program. First, we used the barge type ship with a simple box shape to verify the GZ curve calculation function by comparing the result of this study with that calculated by NAPA. After that, we compared the results of this study with the results of NAPA for the actual Navy oiler to evaluate the damage stability evaluation function.

### 3.2.1. Stability evaluation for barge type ship

The barge type ship of the box shape was used to verify the GZ curve calculation function which is the most basic function of the stability evaluation. The GZ curve can be calculated as described in Section 2.3.3, and is calculated assuming only free-heave for comparison with NAPA, and calculated in the fixed trim state. The main dimensions of the barge type ship are as shown in Table 3-6, and the shape is as shown in Figure 3-19.

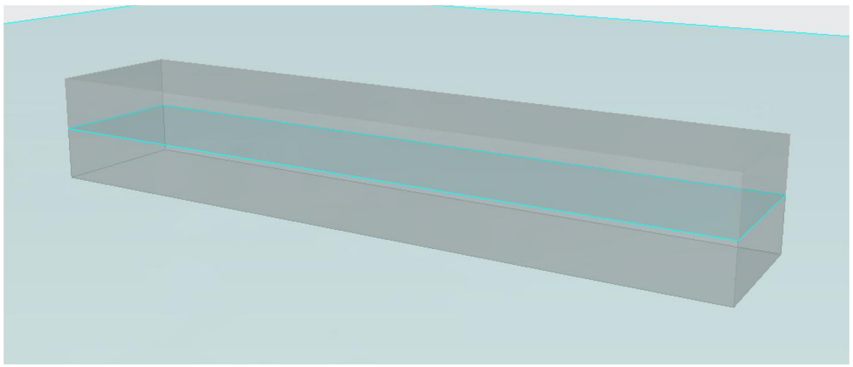

Figure 3-19. Barge type ship for verification of stability

Table 3-6. Main dimensions of barge type ship for verification of stability

| Main dimension | Value |
|---|---|
| Length | 50.000 m |
| Breadth | 10.000 m |
| Depth | 7.500 m |
| Draft | 3.75 m |
| KG | 3.75 m |
| Displacement | 1,921.875 ton |

We modeled the same vessel through NAPA and calculated the GZ curve through NAPA's calculation function. The results of NAPA is shown in Figure 3-20. And the results of the GZ curve calculated in this study is shown in Figure 3-21.

STABILITY CURVE

| ANGLE | (deg.) | 5.0 | 10.0 | 15.0 | 20.0 | 30.0 | 40.0 | 50.0 | 60.0 | 75.0 |
|---|---|---|---|---|---|---|---|---|---|---|
| KN | (m) | 0.358 | 0.717 | 1.081 | 1.452 | 2.234 | 3.097 | 3.665 | 3.951 | 4.018 |
| KG*SINFI | (m) | 0.327 | 0.651 | 0.971 | 1.283 | 1.875 | 2.410 | 2.873 | 3.248 | 3.622 |
| DGZ | (m) | 0.000 | 0.000 | 0.000 | 0.000 | 0.000 | 0.000 | 0.000 | 0.000 | 0.000 |
| GZ | (m) | 0.031 | 0.066 | 0.111 | 0.169 | 0.359 | 0.687 | 0.792 | 0.703 | 0.396 |
| AREA | (mrad) | 0.001 | 0.006 | 0.013 | 0.025 | 0.069 | 0.161 | 0.293 | 0.426 | 0.573 |

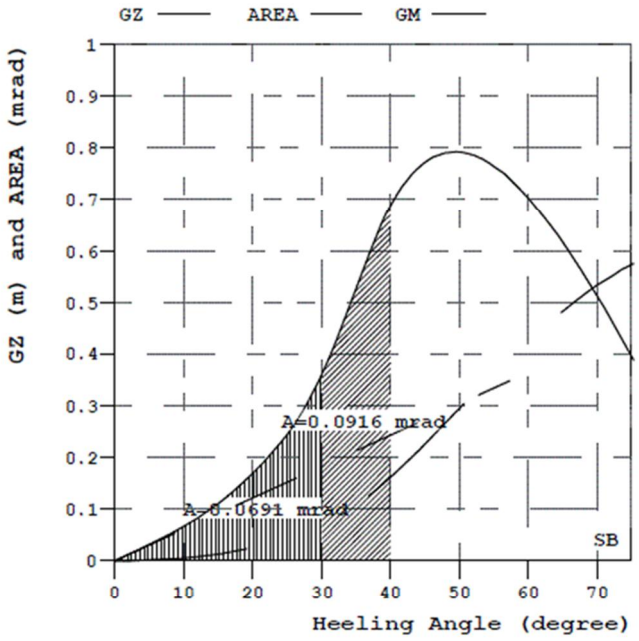


ATTAINED STABILITY VERSUS IMO CRITERIA

- IS Code Ch.2.2

| STABILITY CRITERIA | | UNIT | ACTUAL | REQ. | STATUS |
|---|---|---|---|---|---|
| GM | | m | 0.347 | 0.150 | OK |
| Area under GZ curve up to 30 deg. | *) | mrad | 0.069 | 0.055 | OK |
| Area under GZ curve up to 40 deg. | *),**) | mrad | 0.161 | 0.090 | OK |
| Area under GZ curve between 30 and 40 deg. | **) | mrad | 0.092 | 0.030 | OK |
| Max.GZ in angle of heel >= 30 deg. | | m | 0.793 | 0.200 | OK |
| Max.GZ occurs at | | deg. | 49.396 | 25.000 | OK |

*) From 0 deg. or the angle of steady equilibrium
**) To 40 deg. or the angle of flooding

Figure 3-20. GZ curve calculated in NAPA for barge type ship

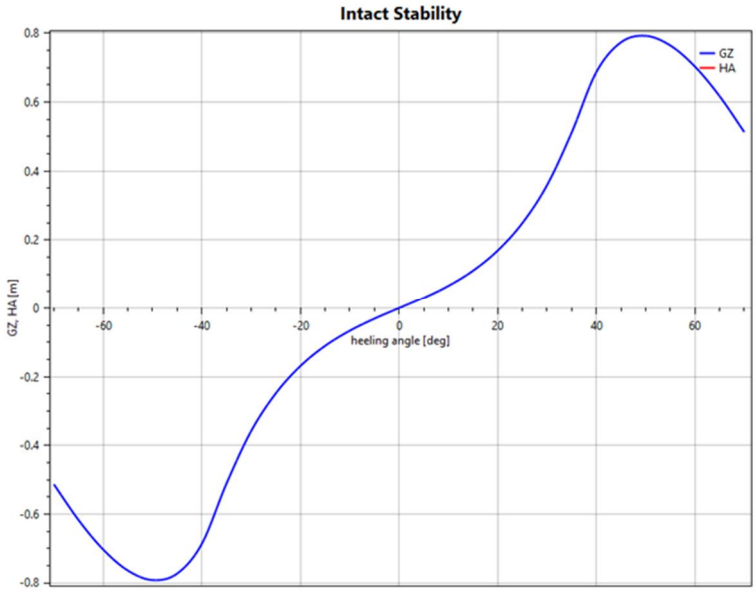


Figure 3-21. GZ curve calculated in this study for barge type ship

The results of NAPA were compared with those of this study. And the results show exactly the same as NAPA's results. Therefore, it is confirmed that the calculation module implemented in this study was applicable.

### 3.2.2. Stability evaluation for Navy oiler

Above, we confirmed that the GZ curve calculation function is correct for the barge type ship. In order to confirm whether it is possible to apply it accurately in real shipshape, we compared the results of five criteria for damage stability by using Navy oiler. Navy oiler used the same as described in the previous Section 3.1.2(1). First, GZ curve calculation results are compared with each other as shown in Figure 3-22.

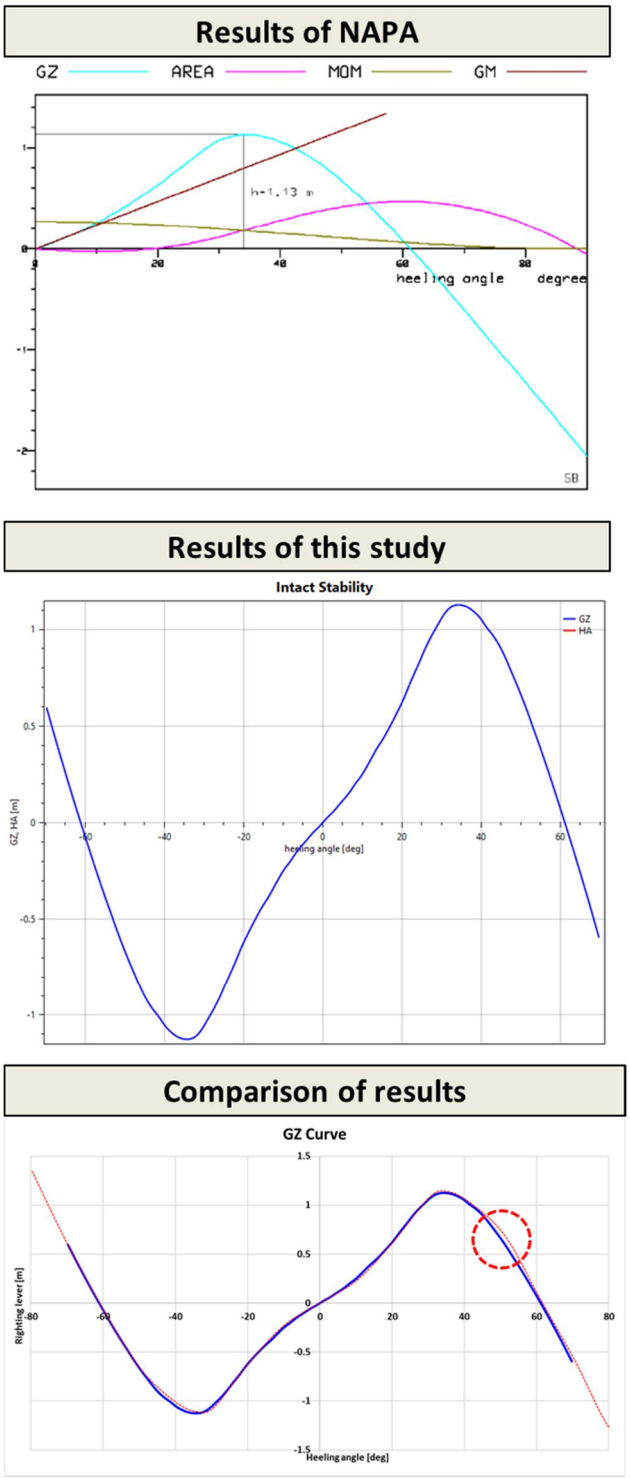


Figure 3-22. Results of stability evaluation for Navy oiler

In Figure 3-22, but we can see that there is a slight error in the vicinity of 50 deg. This is not the exact linear shape used in this study, but the linear shape is converted to mesh for flooding analysis, I expect it to be a little different. However, it is confirmed that the error is within the limit of 1%.

In addition, for the comparison of the damage stability results, assuming that all three cases (aft body, midship, forebody) are damaged, the values for five damage stability criteria are compared and the results are shown in Table 3-7.

Table 3-7. Results of damage stability evaluation of Navy oiler

| Criteria | Criteria 1 | | Criteria 2 | | Criteria 3 | |
|---|---|---|---|---|---|---|
| | Initial heel < 15.0 | | $A_2/A_1 \geq 1.4$ | | $A_2 \geq 0.012$ | |
| | NAPA | This study | NAPA | This study | NAPA | This study |
| Fore body | 0.000 | 0.000 | 36.888 | 36.913 | 0.524 | 0.531 |
| Midship | 0.825 | 0.825 | 28.596 | 28.602 | 0.286 | 0.288 |
| Aft body | 1.987 | 1.987 | 12.782 | 12.801 | 0.113 | 0.119 |
| Criteria | Criteria 4 | | Criteria 5 | | Difference average | |
| | $GZ_{max} - HA \geq 0.075$ | | Distance $_{margin\ line} > 0.0$ | | | |
| | NAPA | This study | NAPA | This study | | |
| Fore body | 1.131 | 1.131 | 4.807 | 4.815 | 1.03% | |
| Midship | 0.780 | 0.782 | 4.001 | 4.021 | 2.11% | |
| Aft body | 0.426 | 0.424 | 1.533 | 1.536 | 1.07% | |

As can be seen from the table, it is very similar to the calculation result of NAPA by 1 ~ 2% difference. Therefore, it can be said that the intact stability and damage stability evaluation method implemented in this study can be applicable and verified.

## 3.3. Verification of vulnerability

The vulnerabilities proposed in this study can be classified into the vulnerability of the

bulkhead and the vulnerability of the compartment, as described in Section 2.4. However, two vulnerabilities are very difficult to verify through experiments or research results. Therefore, this study confirms whether the vulnerability assessment method proposed in Section 2.4 can be applied to the arrangement optimization of a naval ship by applying it to a simple model.

To verify the survivability module, the simple compartment which has five compartments and four bulkheads as shown in Figure 3-23 are considered.

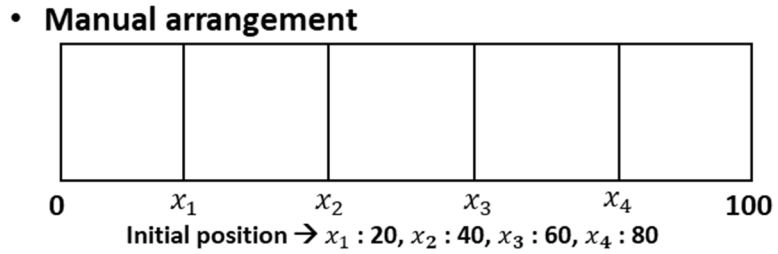


Figure 3-23. Manual arrangement of bulkheads for verification

Also, two impact point distributions as shown in Figure 3-24 are assumed and investigated the change of the bulkhead position. In the first case, impact points are distributed concentrating on the center part. And the second case, impact points are distributed concentration on the slightly left part from the center. The number of impact points was set to fifty which is same in the two cases.

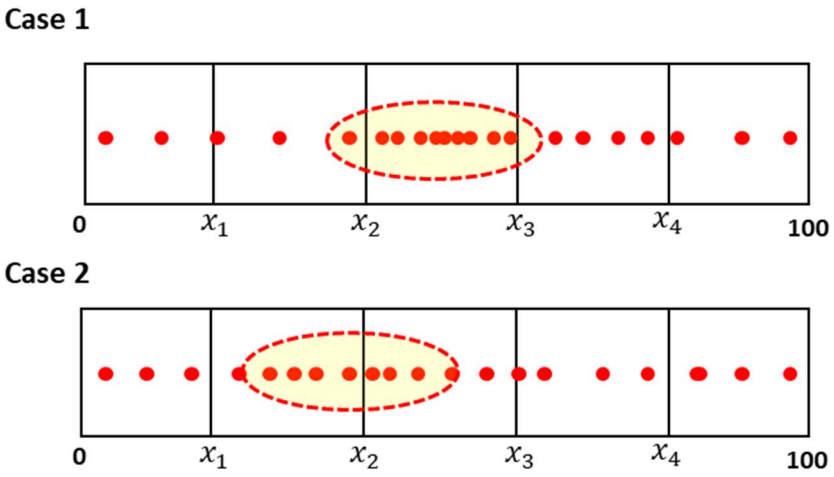


Figure 3-24. Damage distribution for two cases of verification

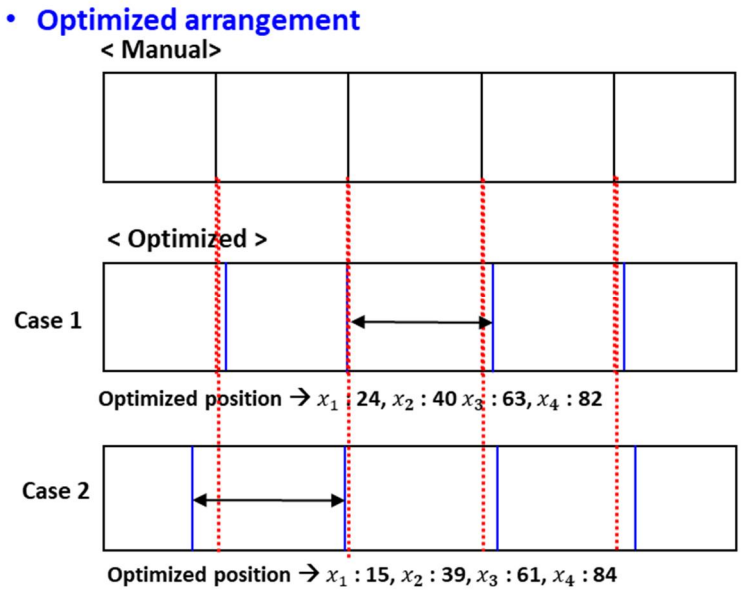


Figure 3-25. Results of optimized bulkhead arrangement for two cases

Table 3-8. Optimized results of bulkhead vulnerability

| | | Vulnerability | Difference |
|---|---|---|---|
| Case 1 | Manual | 4,608.5 MPa | -3,289.5 (71% improved) |
| | Optimized | 1,319.0 MPa | |
| Case 2 | Manual | 1,884.0 MPa | -801.7 (42% improved) |
| | Optimized | 1,081.3 MPa | |

Verification result is as shown in Figure 3-25. And the values for the vulnerability of bulkheads are summarized in Table 3-8. In the first case, the positions of the bulkhead have changed so that the center part is wider than the initial arrangement. In the second case, the positions of the bulkhead have also changed and the second room became wider. As described in the previous chapter, the explosive pressure acting on the wall is a function proportional to the distance. Therefore, the result can be considered reasonable that the interval of bulkheads between the dense explosive points becomes wider.

## 3.4. Verification of operability

Similar to vulnerability, operability evaluation is hard to compare with experiment or real world. Therefore, after setting a brief example, we verified that operability can be applied in the arrangement optimization process through adjacency and distance matrix.

To verify operability module, adopted the algorithm to the simple example. Six rooms are considered to be arranged: Engine room (ER), Equipment room (EQ), Officers room (OR), Galley (GA), Crew room (CR), Sickbay (SB). And the initial arrangement is as shown in Figure 3-26.

- **Initial arrangement**

| | | |
|---|---|---|
| EQ | ER | OR |
| GA | CR | SB |

Figure 3-26. Manual arrangement of rooms for verification

The adjacency matrix of these rooms is as shown in Figure 3-27. As represented in this figure, adjacency between ER and CR has the lowest value, and that of CR and SB has the highest value. In other words, ER and CR have to be placed further away, and CR and SB have to be placed pretty close.

- **Adjacency matrix**

| | ER | EQ | OR | CR | GA | SB |
|---|---|---|---|---|---|---|
| ER | - | | | | | |
| EQ | 0 | - | | | | |
| OR | 0 | 1 | - | | | |
| CR | -3 | 1 | 1 | - | | |
| GA | -2 | 0 | 1 | 0 | - | |
| SB | -1 | 0 | 0 | 2 | 1 | - |

Figure 3-27. Adjacency matrix for the arrangement of rooms for verification

Distance between the rooms was calculated as shown in Figure 3-28. The midpoint of the room was set as a node, adopted Dijkstra's algorithm for finding the shortest path. In the operability module, inclined ladder, room entrances, path node were all considered,

but in this simple example, only the node was considered.

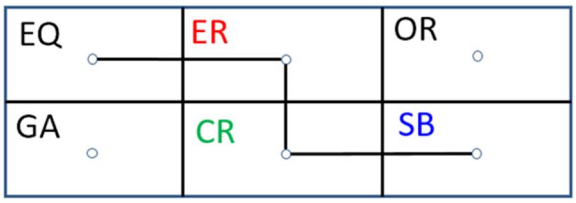


Figure 3-28. Distance calculation for verification

Verification result is shown in Figure 3-29. As compared to the initial arrangement, the arrangement was changed. We can confirm that CR and SB, which has the highest adjacency value were located closest, conversely, ER and CR, which has the lowest adjacency value were located further away. And such an arrangement is consistent with what we intended. Also, adjacency index has decreased as shown in Table 3-9.

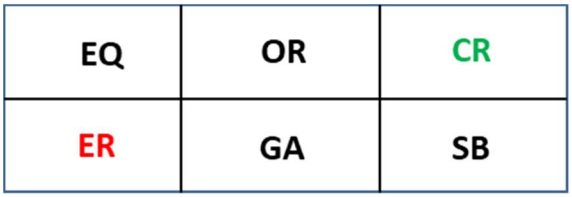


Figure 3-29. Optimization results for verification

Table 3-9. Optimized results of room adjacency

| | Adjacency | Difference |
|---|---|---|
| Manual | 4 | -9 (200% improved) |
| Optimized | -5 | |

# 4. Application

In this study, three factors were considered for the optimal placement of the traps. First, we conducted a stability assessment to determine whether the ship had sufficient stability as a naval ship during the operation and whether it was operating or not sinking despite various damages. Secondly, the vulnerability of the naval ship was taken into account in order to prevent the bulkhead or compartment from losing its function due to various damages, or to minimize damage. Finally, in order to facilitate the smooth movement of the crew and materials during the various operations of the naval ship, operational considerations were considered. In order to apply this method, we developed the program itself in this study. And U.S. Navy Destroyer to confirm its effectiveness.

## 4.1. Overview of SyFAP and SyLOP

In this study, we developed a dynamic flooding analysis method in addition to the PBD method described above and developed SyFAP (SyDLab's Flooding Analysis Program) for this purpose. For application in batch design, SyLOP (SyDLab's Layout Optimization Program) was developed, and the module was interfaced with SyFAP so that the damage stability evaluation can be performed automatically after the optimal placement of the ship.

### 4.1.1. SyFAP (SyDLab. Flooding Analysis Program)

SyFAP was implemented to be able to perform both quasi-static analysis using the

orifice equation described in Appendices A and dynamic analysis using PBD described in (chapter). PBD requires computation of many particles, and parallelization using GPU is indispensable for this. In this study, we implement PBD solver in C ++ with relatively fast speed and parallelization using CUDA to implement dynamic flooding analysis as soon as possible. We also implemented the GUI using C # language and Windows Presentation Foundation (WPF) to make it easy for users to use. The GUI configuration of SyFAP is shown in Figure 4-1.

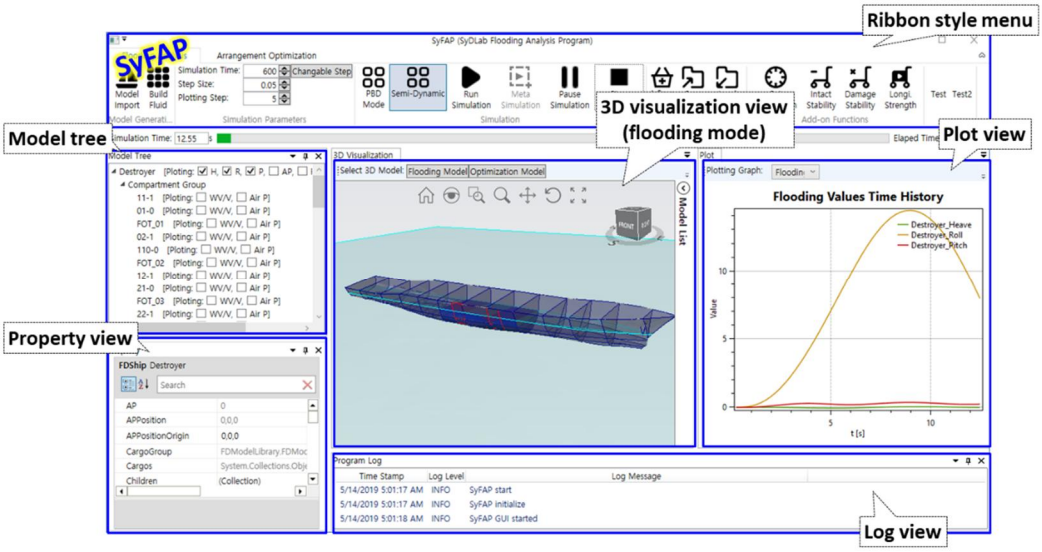


Figure 4-1. Screenshot of SyFAP

Figure 4-1 is a screenshot of SyFAP. It is composed of ribbon-style menu for user's convenience and can easily utilize the functions. In addition, through the model tree and property view, the property of the ship subject to flood analysis can be seen in detail. In 3D visualization view, it is possible to check the behavior of ship in three dimensions and the amount of fluid contained in the vessel in real-time during submergence, plotting

view in real-time and the amount of water in compartments.

### 4.1.2. SyLOP (SyDLab. Layout Optimization Program)

SyLOP was developed for the optimal layout design of traps and can be used in conjunction with SyFAP described above. SyFAP has various optimization algorithms such as NSGA-II, SMPSO, and SPEA-II optimization algorithms, and it can be parallelized for each generation. Speed. And for the convenience of user's GUI, we used C # and WPF like SyFAP mentioned above. The screen composition of SyLOP is shown in Figure 4-2.

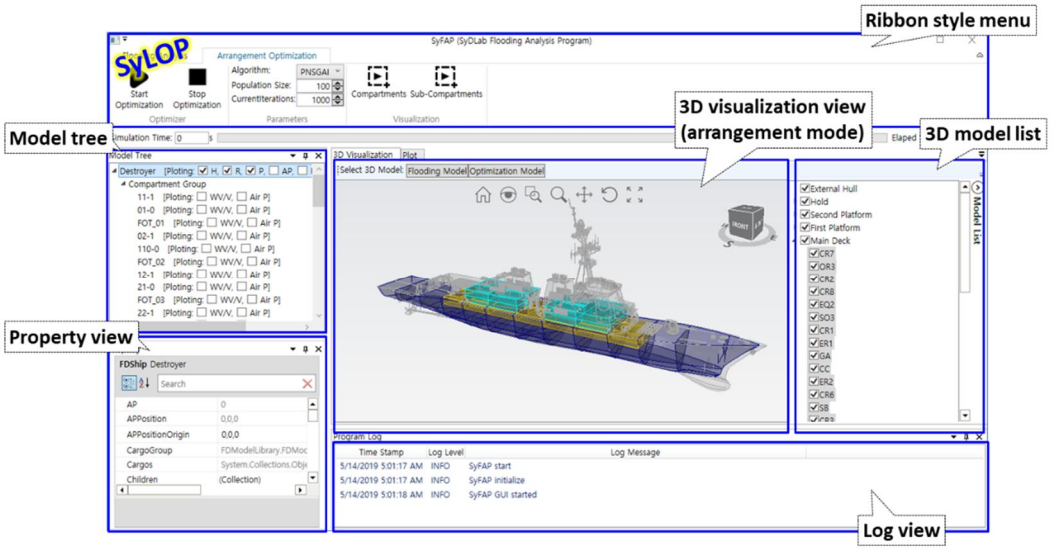


Figure 4-2. Screenshot of SyLOP

As shown in Figure 4-2, SyLOP is configured so that users can easily use various functions through the ribbon style menu. Also, the constraint and objective function are improved during optimization through 3D visualization and plot view. Can be confirmed.

In addition, it has a function to visualize not only three-dimensional visualization but also a compartment or a compartment desired by the user, or a specific deck only by placing a 3D model list.

## 4.2. Target for application

As mentioned earlier, the proposed method focuses on the arrangement design of the naval surface ship. The bulkhead arrangement was optimized in the first stage of optimization, and in the second stage, the room arrangement was optimized. A 10,000-ton class missile destroyer was selected as an example in this study [3]. The length, breadth, and draft of the ship are 154 m, 20 m, and 9.4 m, respectively. The bulkhead arrangement in the hull, including tanks, is shown in Figure 4-3 and the room arrangement in the superstructure is shown in Figure 4-4. In this study, we optimized the arrangement of 14 bulkheads and 4 decks during the first stage. After optimizing the bulkhead arrangement, we have optimized the arrangement of 33 rooms and 12 passages, and we then present each result of the arrangement. More details of the input data are summarized in Table 4-1. Table 4-2 shows the adjacency coefficients ($q_{ij}$) between the rooms of the example.

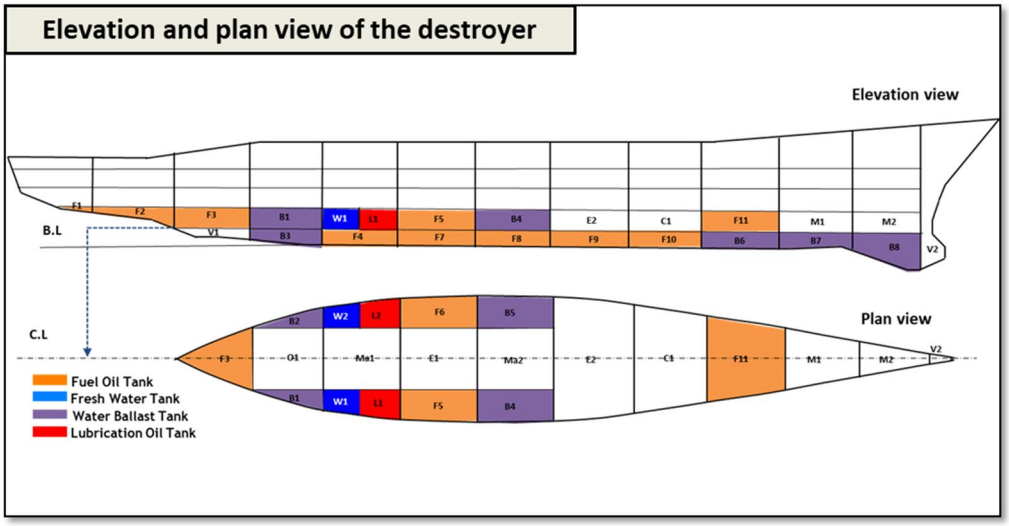


**Index**

- F1 : Fuel oil tank #1
- F2 : Fuel oil tank #2
- F3 : Fuel oil tank #3
- V1 : Void tank #1
- B1 : Water ballast tank #1
- Ma1 : Machinery control room
- B2 : Water ballast tank #2
- B3 : Water ballast tank #3
- W1 : Fresh water tank #1
- E1 : Engine room #1
- W2 : Fresh water tank #2
- L1 : Lubrication oil tank #1
- L2 : Lubrication oil tank #2
- F5 : Fuel oil tank #5
- Ma2 : Machinery and equipment room
- F6 : Fuel oil tank #6
- F7 : Fuel oil tank #7
- B4 : Water ballast tank #4
- E2 : Engine room #2
- B5 : Water ballast tank #5
- F8 : Fuel oil tank #8
- C1 : Crew living space #1
- F9 : Fuel oil tank #9
- O1 : Offices space #1
- F10 : Fuel oil tank #10
- F11 : Fuel oil tank #11
- B6 : Water ballast tank #6
- M1 : Magazines #1
- M2 : Magazines #2
- V2 : Void tank #2

Figure 4-3. Application target for bulkhead arrangement

| Category | ID of Rooms |
|---|---|
| Officer Room | OR1, OR2, OR3, OR4, OR5 |
| Crew Room | CR1, CR2, CR3, CR4, CR5, CR6, CR7, CR8, CR9, CR10 |
| Sick Bay | SB |
| Command & Control Room | CC |
| Equipment Storage | EQ1, EQ2, EQ3, EQ4 |
| Engine Room | ER1, ER2 |
| Galley | GA |
| Ship Office | SO1, SO2, SO3, SO4 |
| Commander Room | COR |
| Executive Officer Room | XO |
| Heli Cargo | HC |
| Communication Room | COM |
| Bridge | BR |

Figure 4-4. Application target for room arrangement

Table 4-1. Input data for the optimization of the example

| Bulkhead arrangement | | |
|---|---|---|
| Input data | Notation | Value |
| Hull form and compartment model | - | See Fig. 10 |
| Number of bulkheads and decks | $N_{B\&D}$ | 18 (= 14 + 4) |
| Locations of compartments in the hull, including liquid tanks | - | See Fig. 9 |
| Required volumes for liquid tanks (FOTs, FWTs, WBTs, and LOTs) | $V_{FOT}^{\min}$, $V_{FOT}^{\max}$, $V_{FWT}^{\min}$, $V_{FWT}^{\max}$, $V_{WBT}^{\min}$, $V_{WBT}^{\max}$, $V_{LOT}^{\min}$, $V_{LOT}^{\max}$ | 2,500 $m^3$, 3,000 $m^3$, 80 $m^3$, 110 $m^3$, 800 $m^3$, 1,100 $m^3$, 85 $m^3$, 110 $m^3$ |
| Longitudinal damage distribution of all threats | - | See Fig. 6 |
| Explosive energy per unit mass for all threats | $E_W$ | $4.184 \cdot 10^9$ $m^2/s^2$ |
| Charge mass of ASMs, torpedoes, and mines | $W_A$, $W_T$, $W_M$ | 161 kg, 300 kg, 113.4 kg |
| Minimum length for each of engine rooms | $l_{ER}^{\min}$ | 11.5 m |
| Minimum deck height | $h_{deck}^{\min}$ | 1.95 m |
| Room arrangement | | |
| Input data | Notation | Value |
| Positions of bulkheads and decks from the first stage | $x_1$~$x_{13}$, $y_1$, $z_1$~$z_4$ | Determined from the first stage |
| Number of rooms | $N_R$ | 33 |
| Number of passages in the deck $i$ | $N_P^i$ | 2, 3, 7 |
| Adjacency coefficients between the room $i$ and $j$ | $q_{ij}$ | See Table 11 |
| Locations of entrance doors and inclined ladders | - | See Fig. 11 |
| Longitudinal damage distribution of all threats | - | See Fig. 6 |
| Number of all equipment in the room $i$ | $N_R^i$ | Different from each room |
| Importance factor (between 0~1) of the equipment $k$ in the room $i$ | $I_e^{ik}$ | |
| Number of the equipment $k$ in the room $i$ | $N_e^{ik}$ | |
| Minimum area for each room | $a_i^{\min}$ | |
| Number of specific rooms for the fixed location | $N_{Rfl}$ | 4 |
| Required locations of the specific room $i$ | $R_i^{\text{req}}$ | $R_7^{\text{req}}$ = {BR}, $R_{15}^{\text{req}}$ = {HC}, $R_{23}^{\text{req}}$ = {ER1}, $R_{26}^{\text{req}}$ = {ER2} |

Table 4-2. Adjacency coefficients between rooms of the example

| Category | - | OR | CR | SB | CC | EQ | ER | GA | SO | COR | XO | HC | COM | BR |
|---|---|---|---|---|---|---|---|---|---|---|---|---|---|---|
| Officer Room | OR | 2 | - | - | - | - | - | - | - | - | - | - | - | - |
| Crew Room | CR | 1 | 2 | - | - | - | - | - | - | - | - | - | - | - |
| Sick Bay | SB | 0 | 2 | 0 | - | - | - | - | - | - | - | - | - | - |
| Command & Control Room | CC | 2 | 0 | 0 | 0 | - | - | - | - | - | - | - | - | - |
| Equipment Storage | EQ | -1 | 2 | 0 | 2 | 2 | - | - | - | - | - | - | - | - |
| Engine Room | ER | -1 | 0 | -1 | 0 | 2 | 2 | - | - | - | - | - | - | - |
| Galley | GA | 0 | 3 | 2 | 0 | -1 | -2 | 0 | - | - | - | - | - | - |
| Ship Office | SO | 0 | 2 | 0 | 0 | 0 | 0 | 0 | 2 | - | - | - | - | - |
| Commander Room | COR | 2 | 0 | 0 | 3 | 0 | -2 | 0 | 0 | 0 | - | - | - | - |
| Executive Office Room | XO | 2 | 0 | 0 | 3 | 0 | -2 | 0 | 0 | 3 | 0 | - | - | - |
| Heli Cargo | HC | -1 | 2 | 0 | 0 | 0 | 0 | 0 | 0 | 0 | 0 | 0 | - | - |
| Communication Room | COM | 2 | 0 | 0 | 0 | 0 | 0 | 0 | 0 | 0 | 0 | 0 | 0 | - |
| Bridge | BR | 2 | 0 | 0 | 0 | 1 | 0 | 0 | 0 | 0 | 0 | 0 | 1 | 0 |

## 4.3. Optimization results and discussions

The arrangement of the 14 bulkheads and 4 decks was optimized, as mentioned earlier. the positions of the bulkheads and the decks were optimized to minimize the maximum bending moment at the intact state, to minimize the auxiliary space for liquid tanks, to maximize the initial GM value as mentioned in Section 2.3, and to minimize the bulkhead damage vulnerability due to the attack, as mentioned in Section 2.4. Next, the arrangement of 33 rooms and 12 passages was optimized. the sequence of rooms and the positions of the passages were optimized to minimize the adjacency index between the rooms and between rooms and compartments and to minimize the room damage vulnerability due to the attack, as mentioned in Section 2.4.1.

Seven objective functions were used to optimize the bulkhead arrangement. Therefore, the seven-dimensional Pareto-optimal set can be obtained as a result of optimization. In this section, we compared the initial design and optimal designs. The design alternative evenly considering all the effects of the objective functions was selected through the

normalization of seven objective functions. Table 4-3 shows a comparison of the objective function values for the arrangement between the initial design and the optimal design. When performing the optimization, the adjacency information for the room arrangement was extracted through consultation with experts of naval surface ships. In the case of the initial design, the values of the objective functions were calculated to be the same as the optimal design. That is, they were calculated according to the formulation mentioned in 2.6.3.

Table 4-3. Comparison of the objective function values

| Objective functions | Type | Initial (A) | Optimization (B) | Ratio (B/A-1) |
|---|---|---|---|---|
| Maximum bending moment at the intact state | Minimize | 362,261 kN·m | 294,980 kN·m | -19.8% |
| Auxiliary space for liquid tanks | Minimize | 4,390 $m^3$ | 3,799 $m^3$ | -14.4% |
| Bulkhead damage vulnerability due to the attack | Minimize | 12.58 GPa | 9.01 GPa | -29.1% |
| Initial GM | Maximize | 1.26 m | 1.34 m | +5.5% |
| Adjacency index between rooms | Minimize | 17,794 | 15,438 | -14.6% |
| Adjacency index between rooms and compartments | Minimize | 246 | 236 | -4.2% |
| Room damage vulnerability due to the attack | Minimize | 0.0212 | 0.170 | -20.3% |

As shown in Table 4-3, the maximum bending moment in the intact state decreased from 362,262 kN·m (initial design) to 294,908 kN·m (optimal design) by 19.8%. Also, the auxiliary space for the liquid tanks decreased from 4,390 $m^3$ (initial design) to 3,799 $m^3$ (optimal design) by 14.4%. The initial GM for stability is increased from 1.26 m to 1.34 m by 5.5%. The bulkhead damage vulnerability improved significantly from 12.58 GPa (initial design) to 9.01 GPa (optimal design) by 29.1%. Further comparisons between the initial design and the optimal design for the bulkhead arrangement are shown in Table 4-4 and Figure 4-5.

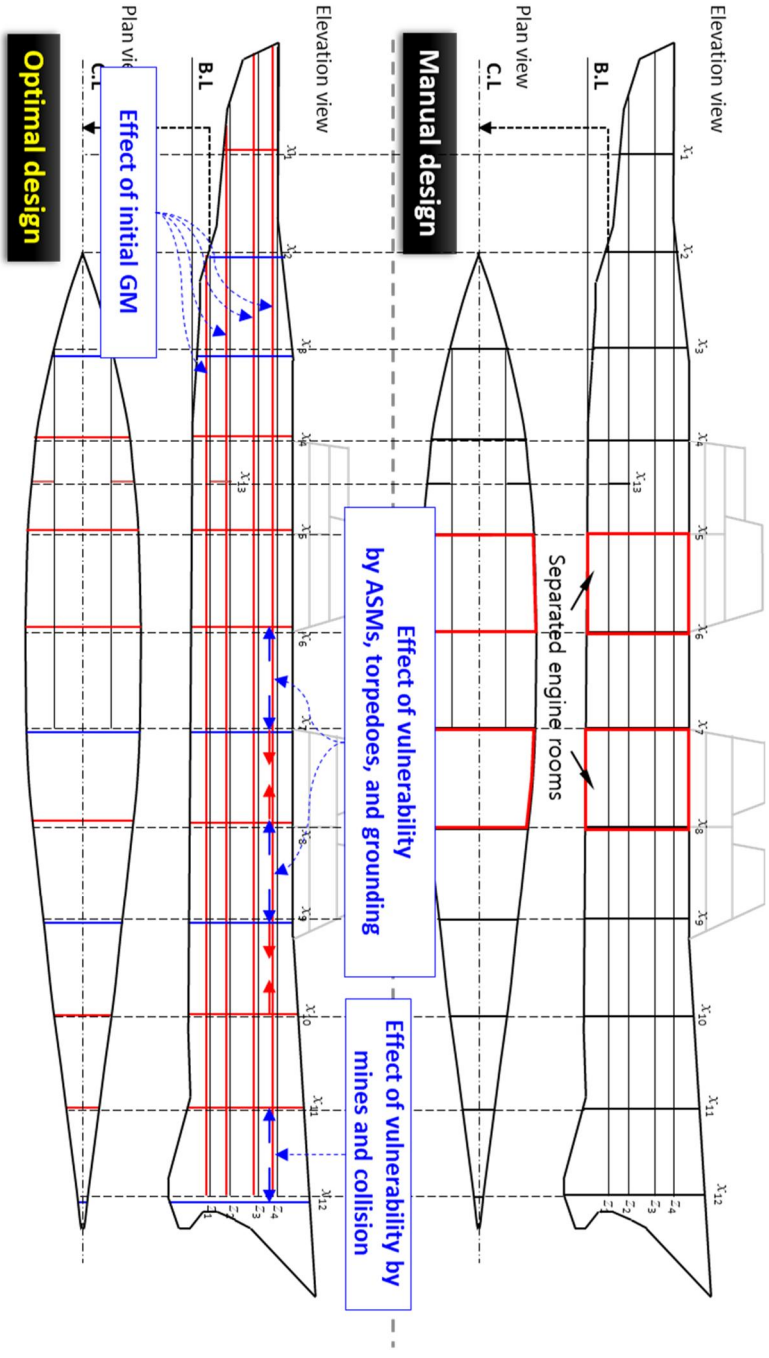


Figure 4-5. Comparison of the bulkhead arrangement between initial and optimal design

Table 4-4. Comparison of the values of design variables for the bulkhead arrangement

| Design variables | Initial (A) | Optimization (B) | Difference (B-A) | Design variables | Initial (A) | Optimization (B) | Difference (B-A) |
|---|---|---|---|---|---|---|---|
| $x_1$ | 10.2 | 9.6 | -0.5 | $x_{10}$ | 116.8 | 116.8 | 0.5 |
| $x_2$ | 23.0 | 23.3 | -0.3 | $x_{11}$ | 128.6 | 128.6 | 0.0 |
| $x_3$ | 33.6 | 35.2 | 1.6 | $x_{12}$ | 140.9 | 140.9 | 1.0 |
| $x_4$ | 46.5 | 46.0 | -0.5 | $x_{13}$ | 52.4 | 52.4 | 0.7 |
| $x_5$ | 57.8 | 57.0 | -0.8 | $y_1$ | 4.7 | 4.8 | 0.1 |
| $x_6$ | 70.2 | 69.6 | -0.5 | $z_1$ | 3.1 | 2.9 | -0.3 |
| $x_7$ | 80.8 | 81.7 | 0.9 | $z_2$ | 5.3 | 5.1 | -0.2 |
| $x_8$ | 93.9 | 93.8 | -0.1 | $z_3$ | 9.3 | 9.1 | -0.2 |
| $x_9$ | 104.4 | 106.3 | 1.8 | $z_4$ | 12.2 | 11.9 | -0.3 |

The bulkhead damage vulnerability depends on the summation of the explosion pressures ($P^i_r$) of the bulkheads and decks due to explosives such as ASMs, torpedoes, mines, collision, and grounding as shown in Eq. (50). From Eq. (50) and Eq. (51), we can see that the explosion pressure of the bulkhead or deck is inversely proportional to its distance from the explosion point. Meanwhile, the distribution of the explosion points by the ASMs and torpedoes has its peak point near the midship, as shown in Figure 2-24. The distribution by the mines has its peak point near forebody. Therefore, to minimize the bulkhead damage vulnerability, the distances between the bulkheads near the midship and forebody were changed during the optimization. That is, in the case of the midship, the distances between $x_6$ and $x_7$ and between $x_8$ and $x_9$ increased. As a result, the distances between $x_5$ and $x_6$ (1st engine room) and between $x_7$ and $x_8$ (2nd engine room) decreased. In the case of the forebody, the distance between $x_{11}$ and $x_{12}$ increased. However, the distance between $x_{10}$ and $x_{11}$ decreased.

As shown in Table 4-3, the adjacency index between rooms of the optimal design decreased from 17,794 (initial design) to 15,438 (optimal design) by 14.6%, the adjacency index between rooms and compartments of the optimal design decreased from

246 (initial design) to 236 (optimal design) by 4.2%, and the room damage vulnerability improved from 0.0212 (initial design) to 0.0170 (optimal design) by 20.3%. More comparisons between the initial design and the optimal design for the room arrangement are shown in Table 4-5 and Figure 4-6.

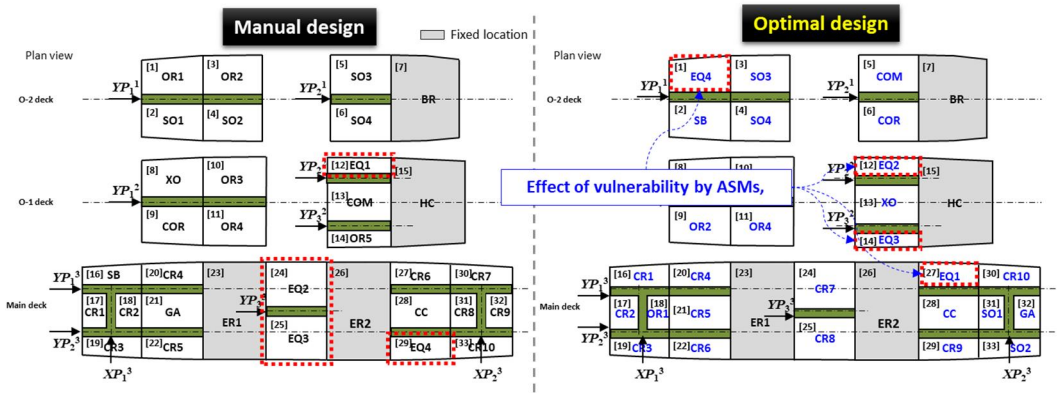


Figure 4-6. Comparison of the room arrangement between the initial and optimal design

Table 4-5. Comparison of the values of design variables for the room arrangement

| Design variables | Initial (A) | Optimization (B) | Difference (B-A) | Design variables | Initial (A) | Optimization (B) | Difference (B-A) |
|---|---|---|---|---|---|---|---|
| $YP_1^1$ | 0.0 | -0.2 | -0.2 | $YP_2^3$ | -5.0 | -5.5 | -0.5 |
| $YP_2^1$ | 0.0 | -0.5 | -0.5 | $YP_3^3$ | 0.0 | -0.8 | -0.8 |
| $YP_1^2$ | 0.0 | -0.3 | -0.3 | $YP_4^3$ | 5.0 | 4.2 | -0.8 |
| $YP_2^2$ | 3.0 | 3.4 | 0.4 | $YP_5^3$ | -5.0 | -5.6 | -0.6 |
| $YP_3^2$ | -3.0 | -2.3 | 0.7 | $XP_1^3$ | 41.0 | 41.8 | 0.8 |
| $YP_1^3$ | 5.0 | 4.5 | -0.5 | $XP_2^3$ | 110.0 | 110.6 | 0.6 |

According to the adjacency coefficients between rooms in Table 4-2, the galley (GA) and the crew rooms (CR1~CR10), the commander room (COR) and the command & control room (CC), the executive office room adjacency coefficient between them. The GA and the ER, the COR and the (XO) and the CC, and the XO and the COR have a high

value (= 3) of the ER, and the XO and the ER have a low value (= -2) of the adjacency coefficient between them. To minimize the adjacency index, the rooms with a high value of the adjacency coefficient should be arranged close to each other and the rooms with a low value should be arranged apart from each other. In Figure 4-6, we can see that the optimal design satisfied these requirements well, relative to the initial design. The room damage vulnerability depends on the summation of the multiplication of the probability of damage ($p_i$) due to explosives and the importance factor ($e_i$) of rooms, as shown in Eq. (52). The probability of damage of the rooms is proportional to the multiplication of the probability of damage length ($p_{DL}$) and the probability of impact ($p_{IP}$), as shown in (53). To minimize the room damage vulnerability, the rooms (e.g., command & control room, equipment storages) with a high importance factor should be arranged apart from the explosive points as far as possible. Since most of the explosive points are located at midship and at the forebody, such rooms should be arranged away from the points. As shown in Figure 4-6, in the case of the initial design, some of the equipment storage (EQ2 and EQ3) is located midship. However, we can see that such rooms were arranged aft and forward in the optimal design. In addition, the CC was also located in the forebody but after optimization, we can see that it moved to after body. As a result, the room damage vulnerability of the optimal design was lower than that of the initial design.

### 4.3.1. Damage stability evaluation for optimization results

Damage stability analysis is assumed to be 15% in the longitudinal direction, half breadth, and total deck damage, as described in Section 2.3.2. However, this is only used to select flooded compartments, and in actual flooding analysis, the damage size and location of the compartment is needed. The size of the damage to the compartment needs

realistic assumptions. In this study, the dynamic flooding analysis is carried out on the assumption that the entire outer shell of the compartment is damaged. However, since this is a very harsh assumption which cannot be realistic, the dynamic flooding analysis is carried out assuming the damage size as 3 cases (1 × 1m damage, 3×3 m damage, and entire outer shell). Figure 4-7 shows damage size and position of 3 cases.

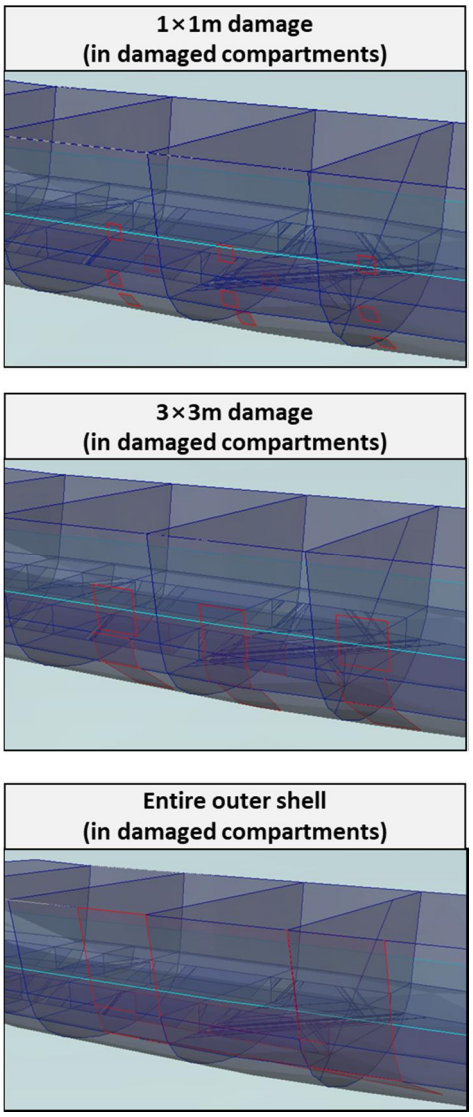


Figure 4-7. Screenshot of damage size and position

As seen in Figure 4-7, we compared 3 cases of damage size, and the damaged area is midship because the severity of flooding is high when the ship damaged in midship.

Figure 4-8 shows a comparison of motion of ship when damaged in midship as mentioned previously. The results contain heave, roll, and pitch motion over time. The

graph above in Figure 4-8 shows the motion of the entire time to reach static position. And the graph below in Figure 4-8 shows the motion to 100s to see the effects of the size of the damage. As shown in Figure 4-8, the dynamic motion is shown when damage size is over 3×3 m. If damage size is small compared with the ship size, the dynamic motion is rarely occurring. So it is very similar to the results of the quasi-static analysis. However, it is important to apply dynamic flooding analysis when we want to analyze the dynamic motion of the ship when flooding starts.

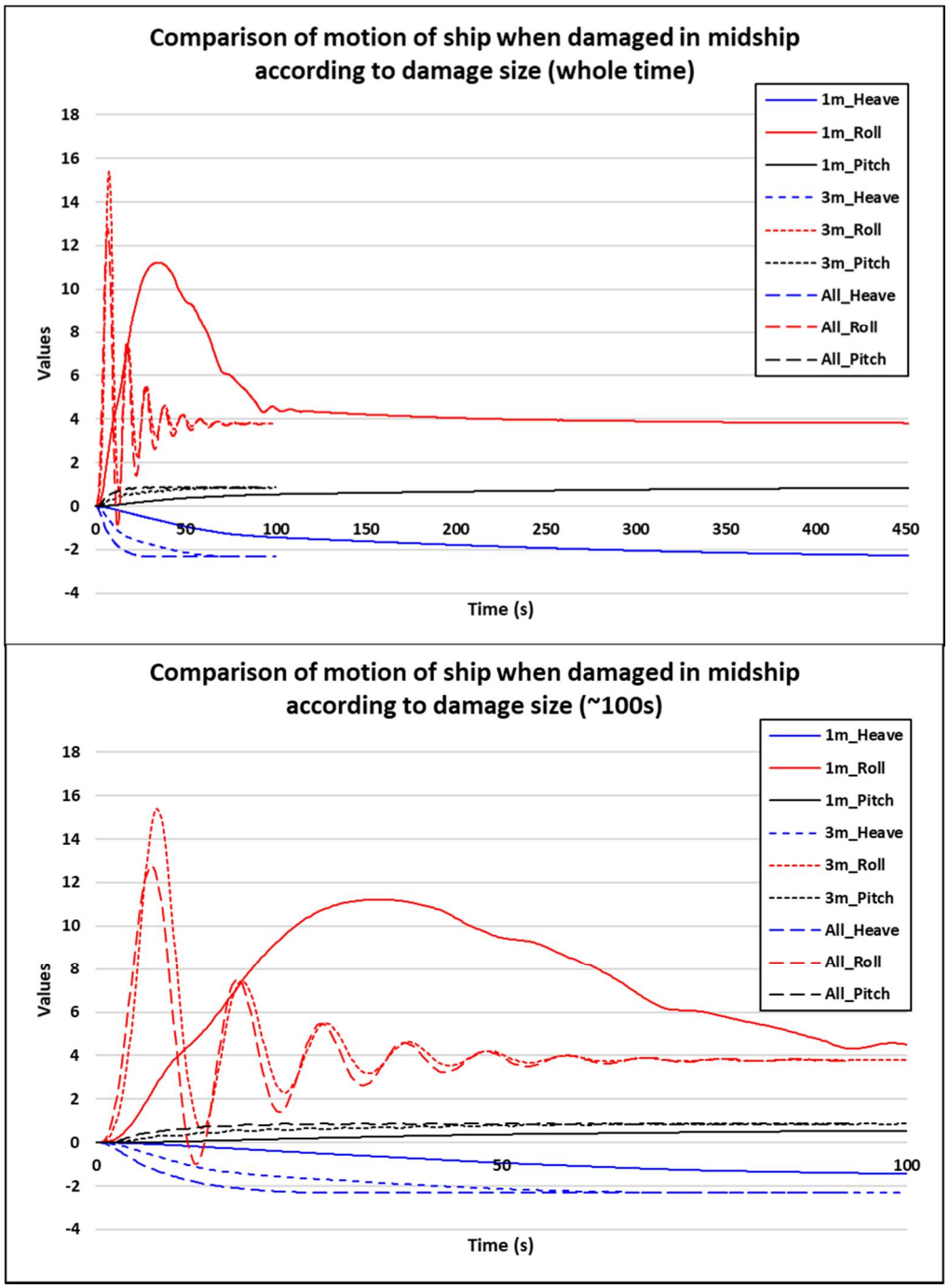


Figure 4-8. Comparison of motion of ship when damaged in midship according to damage size

As described in Section 4.3, the position of bulkheads and compartments is optimized for seven objective functions through the proposed optimization of arrangement design for naval ship method proposed in this study. Intact stability and initial GM were considered in the optimization process as constraints, but damage stability was not evaluated. Therefore, we evaluated the damage stability of the three cases (after body, midship, and forebody) as mentioned in Section 2.3.2, and as shown in Figure 4-9.

Table 4-6 shows five values of damage stability evaluation criteria within three. In addition to calculating 5 values in the final state after damage, 5 values were continuously evaluated during the damage progress, and 5 damage stability criteria were evaluated at each moment of flooding.

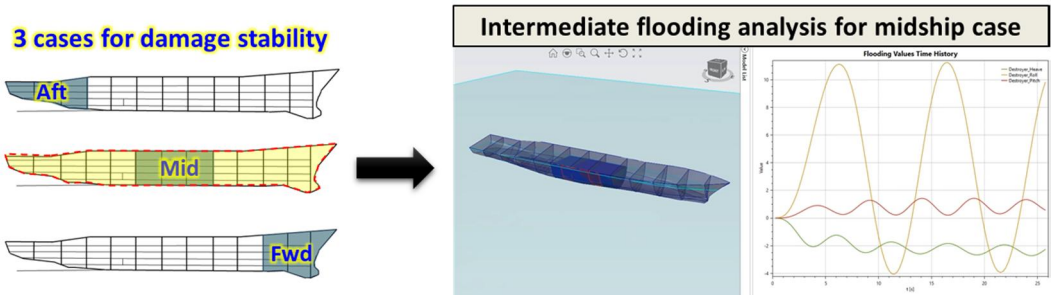


Figure 4-9. Three cases for damage stability evaluation and results of intermediate flooding analysis for midship case

Table 4-6. Results of damage stability evaluation for three cases (after body, midship, forebody)

| Criteria | Criteria 1 | | Criteria 2 | | Criteria 3 | |
|---|---|---|---|---|---|---|
| | Initial heel < 15.0 | | $A_2/A_1 \geq 1.4$ | | $A_2 \geq 0.012$ | |
| | Optimized | Intermediate | Optimized | Intermediate | Optimized | Intermediate |
| Fore body | 0.000 | Satisfied | 6.701 | Satisfied | 0.382 | Satisfied |
| Midship | 3.821 | Satisfied | 2.184 | Satisfied | 0.132 | Satisfied |
| Aft body | 0.593 | Satisfied | 9.878 | Satisfied | 0.415 | Satisfied |
| Criteria | Criteria 4 | | Criteria 5 | | | |
| | $GZ_{max} - HA \geq 0.075$ | | Distance $_{margin\ line} > 0.0$ | | | |
| | Optimized | Intermediate | Optimized | Intermediate | | |
| Fore body | 0.336 | Satisfied | 2.105 | Satisfied | | |
| Midship | 0.175 | Satisfied | 0.513 | Satisfied | | |
| Aft body | 0.419 | Satisfied | 2.643 | Satisfied | | |

As shown in Table 4-6, when the midship was damaged, the most severe heel appeared. However, all of the five criteria for damage stability were satisfied, and it was found that all of them were satisfactory even during flooding. Therefore, it was confirmed that the optimal solution selected by the optimal arrangement for the naval ship has no problem in terms of damage stability.

### 4.3.2. Applying wave loads for optimization results

In this study, it is assumed that the flooding process has occurred in a steady sea state without any external forces of the ship during damage. Therefore, in the above Section 4.3.1, only the flooding analysis in the static state was carried out according to this assumption.

However, the hydrodynamic coefficient and the six degrees of freedom equations allow the wave to be considered. Therefore, we analyze the effect of waves when in the flooding situation through three cases as described in Table 4-7.

Table 4-7. Case description for dynamic flooding analysis in waves

| Case description | Case 1 | Case 2 | | Case 3 | |
|---|---|---|---|---|---|
| Damaged position | Midship | Midship | | Midship | |
| Wave angle | No waves | 90 deg | Regular waves | 90 deg | Regular waves |
| Wave height | | 1 m | | 2 m | |
| Wave period | | 4 sec | | 6 sec | |

The only difference between the three cases was wave height and period. Damaged position for cases was midship, and damage size is $1 \times 1$ m quadrangle for each compartment in midship.

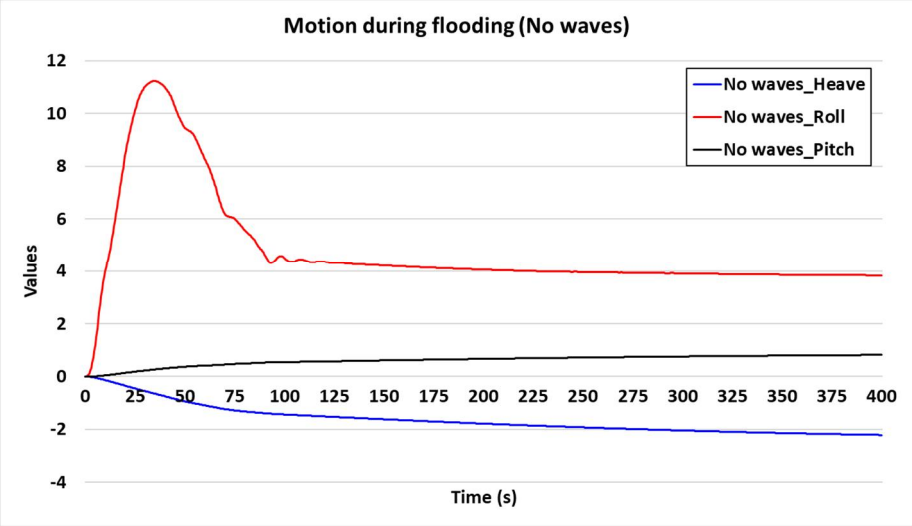


Figure 4-10. Ship motion during flooding – Case 1

Figure 4-10 shows the results of case 1 with three ship motions. Case 1 is in a state where the wave does not work. It can be seen that the damage size is smaller than the size of the ship and the dynamic behavior rarely occurs. However, it can be seen that rolling

occurs at about 11 degrees due to the asymmetry of the compartments and converges to the final state.

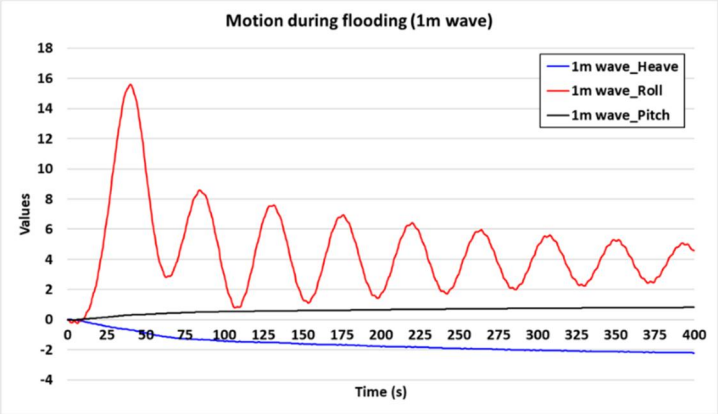


Figure 4-11. Ship motion during flooding – Case 2

Figure 4-11 shows the results of case 2 as three-ship movements. In Case 2, the ship is flooded with a 1m regular wave. Even if the magnitude of the damage is small, dynamic motion is generated by the influence of waves. It can be seen that the rolling angle occurs up to about 15 degrees due to the interaction with the flooding and waves.

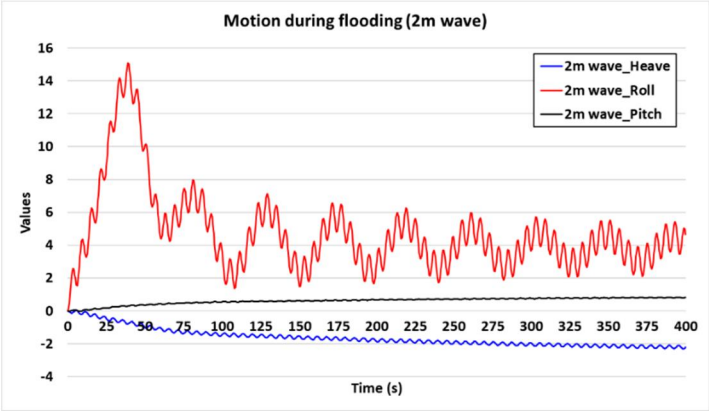


Figure 4-12. Ship motion during flooding – Case 3

Figure 4-12 shows the results of Case 3 as three-ship movements. In Case 3, the ship is flooded with a 2m regular wave. As shown in Case 2, even if the magnitude of the damage is small, it can be seen that the dynamic motion is generated due to the influence of the wave, and the influence of the wave is strong, so that fluctuation occurs in the rolling. In addition, as in Case 2, rolling angles up to about 15 degrees are observed due to the interaction with the flooding and waves.

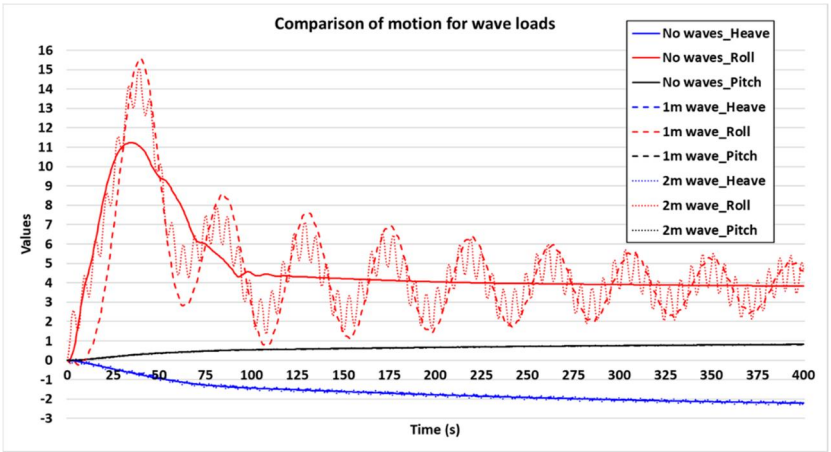


Figure 4-13. Comparison of ship motion in waves

Figure 4-13 compares the motions of the three cases. In the absence of waves, moderate flooding behavior becomes very severe when waves are applied. Therefore, dynamic flooding analysis can be carried out under various environmental conditions to confirm that flooding occurs under more severe conditions.

# 5. Conclusion and future works

## 5.1. Summary

This study investigated the assessment method of the fitness of the initial arrangement design of a naval ship considering ship flooding. Three evaluation items were considered for suitability evaluation of arrangement design. The first is to evaluate whether the ship meets the stability of the operation in the course of the operation, and also evaluates whether the damage satisfies the damage stability. The second is a vulnerability, which attempts to calculate and minimize damage to the bulkhead and compartment for various damage to the trap. Third, the operability was to minimize the proximity of the vessel to facilitate the movement of crew and goods in the operation of the vessel. Using three evaluation items, we formulated an optimization problem for the arrangement design of naval ships. In addition, we developed own program for the application. Each will be described in detail as follows.

In this study, the analysis of the flooding behavior of a ship using the PBD based flow calculation and the 6-DOF equation of motion and the damage stability of the ship were evaluated by the flooding behavior.

The vulnerability of the vessel considering the damage of the bulkhead and the compartment was evaluated. The probability of damage to the bulkheads and compartments (ASMs, torpedos, mines, collisions, and grounding) was calculated and multiplied by the explosion pressure to evaluate the vulnerability of the bulkheads and the vulnerability of the compartments respectively.

The operability considering the relation between the room and the compartments in the hull was evaluated. The shortest distance was calculated considering the corridor and the movement route, and the adjacency matrix between the compartments was created considering the affinity and antagonism. Finally, we calculated the adjacency coefficient through the shortest distance and nearest neighbor.

We proposed the optimization problem for the arrangement design of naval ship considering the stability, vulnerability, and operability described above. The optimum arrangement method was formulated as one problem considering the hull and superstructure at the same time. Finally, we propose a batch optimal method considering stability, vulnerability, and operability.

A program for initial arrangement design and intermediate flooding analysis were developed. To do this, we propose a framework for flood analysis and optimal layout design based on as mentioned items in above and developed a program with rapid analysis and convenience.

## 5.2. Contributions

This study has several contributions distinguished from the other work.

### 5.2.1. Theoretical contributions

In this study, we propose a rapid dynamic flooding analysis method that takes into account the dynamic effects of fluids and ships, but also the dynamic flood analysis method of other studies, by proposing the intermediate flood analysis method using 6-

DOF motion equation and PBD.

Therefore, when combined with the PBD and 6 DOF motion equations, it is possible to perform accurate flooding analysis including the dynamic behavior of the ship fluid in addition to the dynamic behavior of the ship. This is necessary for flood analysis in case of large damage of ship or movement of the ship.

More precisely, using the dynamic flooding analysis proposed in this study, we can calculate flow rate through the opening, considering dynamic motion and the center of gravity considering the dynamic behavior of the fluid. In addition, we can calculate the center of gravity of the fluid contained in the compartment considering the dynamic motion of the ship.

Figure 5-1 shows a comparison of quasi-static analysis and dynamic analysis method proposed in this study. If the damage is smaller than the size of the ship, the dynamic behavior due to flooding is not large and there is no difference between the quasi-static analysis and the dynamic analysis result (in the case of 1m damage). However, as the damage increases (sudden flooding progresses), the influence of the dynamic behavior of the fluid or vessel inside the vessel increases, and dynamic analysis through dynamic analysis method is required. Dynamic analysis method can detect the fatal damage behavior which cannot be found by quasi-static analysis (in case of 3m damage).

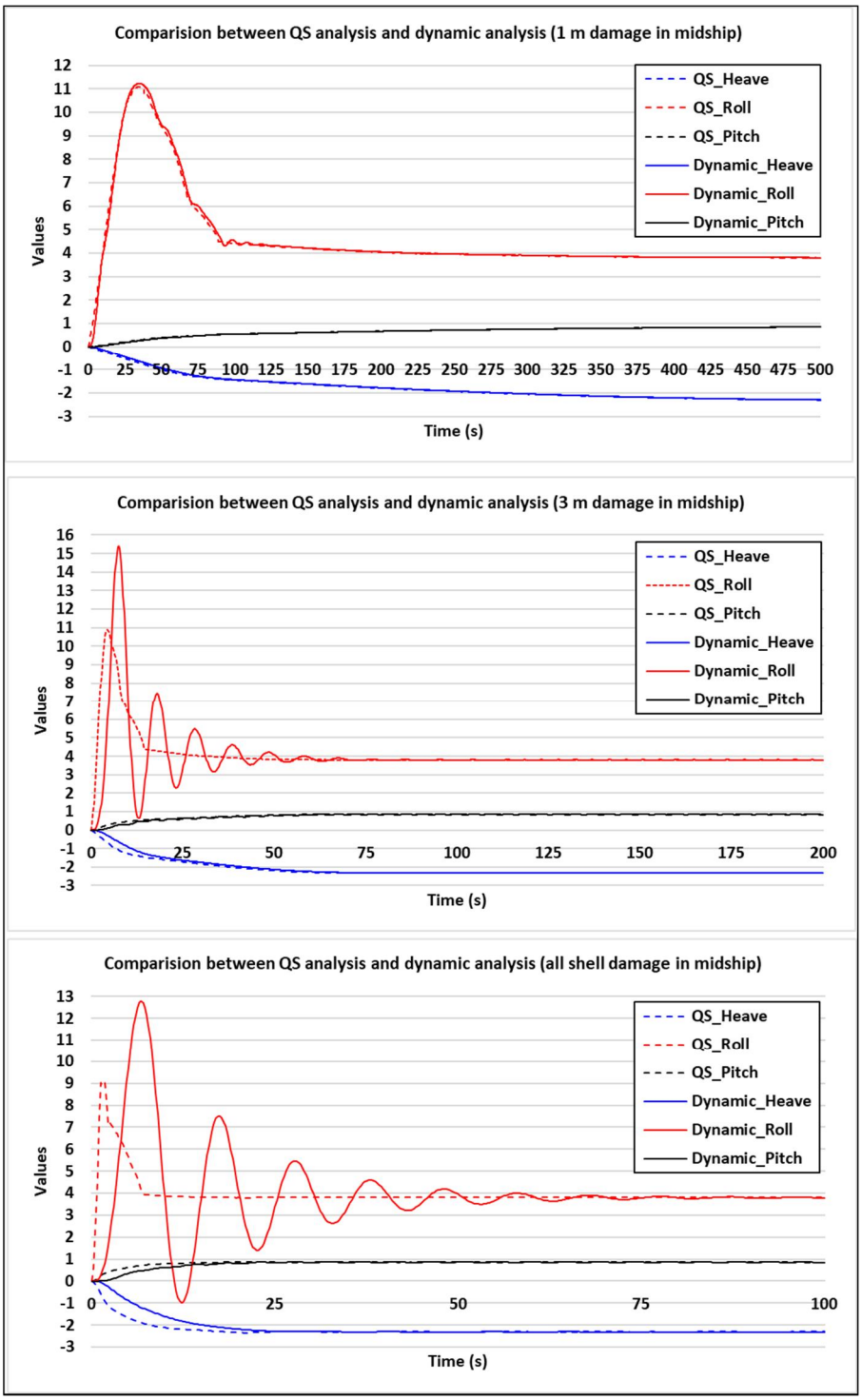


Figure 5-1. Comparison of QS and dynamic flooding analysis

When we use dynamic flooding analysis, we can calculate the CoG of fluid in compartments using two methods; dynamic/hydraulic orifice equation and PBD as shown in Figure 5-2. As mentioned above, the dynamic motion of fluid in compartments can be applied by using PBD.

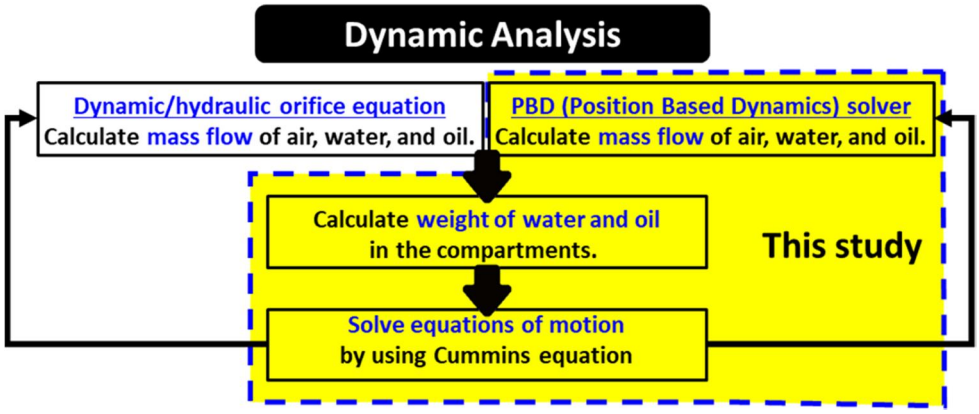


Figure 5-2. Process of dynamic flooding analysis

Figure 5-3 shows the motion of flooded ship with two methods for CoG update; orifice equation and PBD. Comparison of flow calculation and fluid shape calculation method for internal compartment during dynamic flooding analysis (difference of orifice equation and PBD method). When calculating the flow rate and the fluid shape in the compartment using the orifice equation, we cannot consider the dynamic effect to calculate the weight and center of gravity. When the damage is small compared to the size of the ship, the results of flooding analysis using the orifice equation and the results of flooding analysis using PBD are almost the same. When the damage is large, there is a difference between the results of flooding analysis using the orifice equation and the results of flooding analysis using PBD. In particular, when the damage is assumed to be 3

m at midship, and PBD is used to analyze it, the center of gravity is different due to the shape of the internal fluid, and thus the first criterion of damage stability is not satisfied. Based on these results, dynamic flooding analysis using PBD proposed in this study is indispensable.

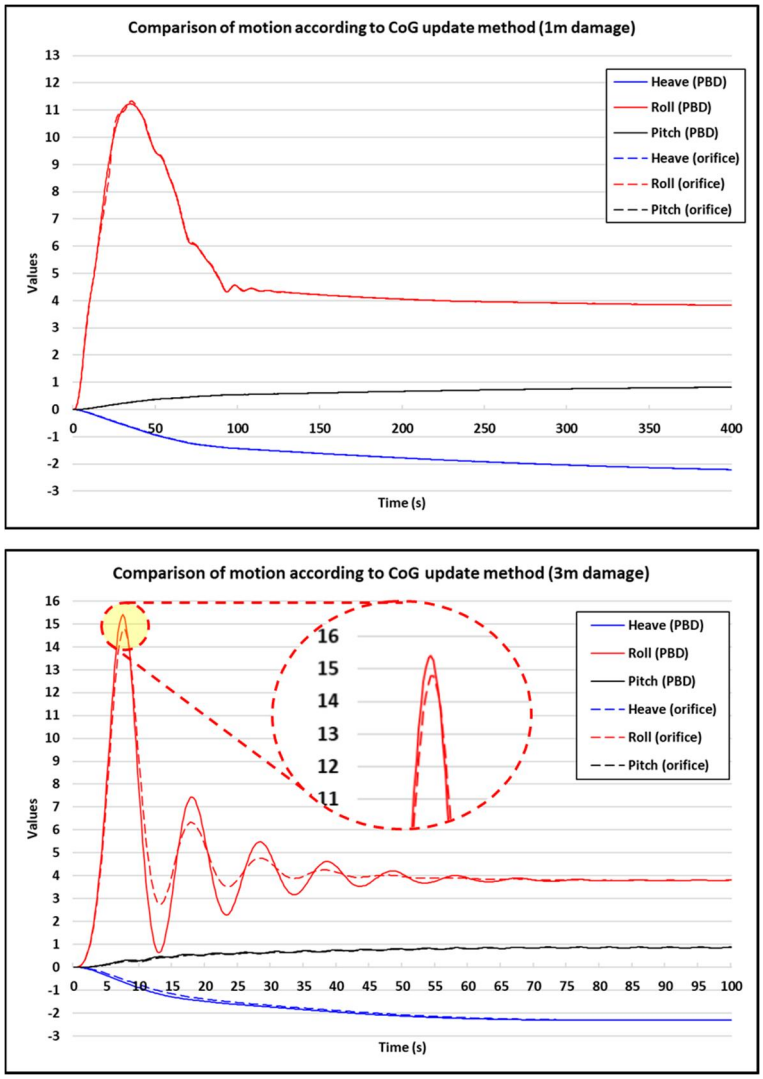


Figure 5-3. Comparison of motion according to CoG update method

And, free-trim was considered in the evaluation of damage stability. This makes it possible to consider the longitudinal shape that was not previously considered and also to evaluate the damage stability in consideration of the free water surface of the longitudinal compartment according to the lateral inclination.

In this study, we propose an optimal layout method considering both hull and superstructure. In this paper, we formulate the optimization problem to consider the influence between hull and superstructure in the optimization process.

### 5.2.2. Contributions for applications

We confirmed that the proposed methods in this study are applicable by applying it to optimize the initial design of U.S. Navy Destroyer. In addition, the method proposed in this study can be implemented through simple modeling and input information, and it is expected to be applicable to various ships and ship types using the method proposed in this study.

### 5.2.3. Other contributions

In this paper, we propose a rapid analysis method for the proposed method, which dramatically improves the analysis speed, which is an obstacle in the dynamic flooding analysis. By developing a program considering user convenience, and accessibility.

## 5.3. Future works

In order to improve the flooding analysis method proposed in this study, the vulnerability assessment considering the escape of passengers after flooding will be carried out and the improvement and upgrading of the operability evaluation will be carried out faithfully reflecting the expert system and designer requirements. In addition, the accuracy of flooding analysis method will be improved through computation and interpolation of the hydrodynamic coefficient by the attitude of a ship.

Although the method proposed in this study has been verified by various methods, actual flooding data will be acquired through collaboration with each shipyard for actual validation and the reliability of the program will be improved.

# References


[1] L. C. A. Whitcomb, D. Ph, and L. T. J. J. Szatkowski, “Concept Level Naval Surface Combatant Design in the Axiomatic Approach To Design Framework,” *Design*, pp. 300–308, 2000.

[2] M. I. Roh and K. Y. Lee, *Computational Ship Design*. Springer, 2017.

[3] S. K. Jung, M. I. Roh, and K. S. Kim, “Arrangement method of a naval surface ship considering stability, operability, and survivability,” *Ocean Eng.*, vol. 152, no. August 2017, pp. 316–333, 2018.

[4] R. of K. Navy, “Criteria for stability, 조함(수)-기-0-007(1),” 2014.

[5] Y. C. Byun, “A Study on Determination of Ship Main Dimension and Compartments Arrangement Supporting Expert System,” Seoul National University, Republic of Korea, 1998.

[6] S.-C. Shin, S.-Y. Kim, and J.-K. Park, “Evaluation of Engine room Machinery Arrangement using Fuzzy Modeling,” *J. Korean Inst. Intell. Syst.*, vol. 12, no. 2, pp. 157–163, 2002.

[7] K. Y. Lee, S. N. Han, and M. I. Roh, “An improved genetic algorithm for facility layout problems having inner structure walls and passages,” *Comput. Oper. Res.*, vol. 30, no. 1, pp. 157–163, 2003.

[8] K. Y. Lee, M. I. Roh, and H. S. Jeong, “An improved genetic algorithm for multi-floor facility layout problems having inner structure walls and passages,” *Comput. Oper. Res.*, vol. 32, no. 4, pp. 879–899, 2005.

[9] A. Papanikolaou and E. Boulougouris, “Design aspects of survivability of surface naval and merchant ships,” *Contemp. Ideas Sh. Stab.*, no. 2, pp. 553–564, 2007.

[10] S. Helvacioglu and M. Insel, “A reasoning method for a ship design expert system,” *Expert Syst.*, vol. 22, no. 2, pp. 72–77, 2005.

[11] D. J. Andrews, “Simulation and the design building block approach in the design of ships and other complex systems,” in *Proceedings of the Royal Society A: Mathematical, Physical and Engineering Sciences*, 2006, pp. 462, 3407–3433.

[12] E. K. Nick, “Fuzzy optimal allocation and arrangement of spaces in vanal surface ship design,” the University of Michigan, 2008.

[13] B. van Oers, D. Stapersma, and H. Hopman, “Issues when selecting naval ship configurations from a Pareto-optimal set,” in *12th AIAA/ISSMO Multidisciplinary Analysis and Optimization Conference*, 2008, pp. 1–19.

[14] M. G. Parsons, H. Chung, E. Nick, A. Daniels, S. Liu, and J. Patel, “Intelligent ship arrangements: A new approach to general arrangement,” *Nav. Eng. J.*, vol.

120, no. 3, pp. 51–65, 2008.

[15] M. I. Roh, S. U. Lee, and K. Y. Lee, "Development of an Optimal Compartment Design System of Naval Ships Using Compartment Modeling and Ship Calculation Modules," *J. Soc. Nav. Archit. Korea*, vol. 46, no. 4, pp. 424–434, 2009.

[16] B. Y. Chung, S. Y. Kim, S. C. Shin, Y. H. Koo, and A. Kraus, "Optimization of compartments arrangement of submarine pressure hull with knowledge based system," *Int. J. Nav. Archit. Ocean Eng.*, vol. 3, no. 4, pp. 254–262, 2011.

[17] J. H. Shin, "A study on spatial arrangement of naval ships considering survivability," Seoul National University, 2013.

[18] S. H. Ju, Y. M. Kim, Y. K. Jeong, and J. G. Shin, "Compartment arrangement algorithm and application based on the survivability of naval vessel," in *Proceedings of the Society of CAD/CAM Conference*, 2014, pp. 1167–1170.

[19] K. S. Kim, M. I. Roh, and S. Ha, "Expert system based on the arrangement evaluation model for the arrangement design of a submarine," *Expert Syst. Appl.*, vol. 42, no. 22, pp. 8731–8744, 2015.

[20] K. S. Kim and M. I. Roh, "A submarine arrangement design program based on the expert system and the multistage optimization," *Adv. Eng. Softw.*, vol. 98, pp. 97–111, 2016.

[21] J. Jung, "Optimization of spatial arrangement at an early design stage of naval ship through layer-based integrated survivability evaluation," Seoul National University, Republic of Korea, 2016.

[22] E. K. Boulougouris and A. D. Papanikolaou, "Optimisation of the survivability of naval ships by genetic algorithms," in *Proceedings of the International Conference on Computer and IT Application and in the Maritime Industries*, 2004.

[23] D. J. Andrews, "Simulation and the design building block approach in the design of ships and other complex systems," *Proc. R. Soc. A Math. Phys. Eng. Sci.*, vol. 462, no. 2075, pp. 3407–3433, 2006.

[24] B. van Oers, D. Stapersma, and H. Hopman, "Issues When Selecting Naval Ship Configurations from a Pareto-Optimal Set," *12th AIAA/ISSMO Multidiscip. Anal. Optim. Conf.*, no. September 2008, 2008.

[25] P. Ruponen, "Model tests for the progressive flooding of a box-shaped barge, HUT Ship Laboratory Report M-292," 2006.

[26] P. Ruponen, "Adaptive time step in simulation of progressive flooding," *Ocean Eng.*, vol. 78, pp. 35–44, 2014.

[27] P. Ruponen, *PROGRESSIVE FLOODING OF A DAMAGED PROGRESSIVE FLOODING OF A DAMAGED Doctoral Dissertation*. 2007.

[28] P. Ruponen, P. Kurvinen, I. Saisto, and J. Harras, "Air compression in a flooded

tank of a damaged ship," *Ocean Eng.*, vol. 57, pp. 64–71, 2013.

[29] P. Ruponen, P. Kurvinen, I. Saisto, and J. Harras, "Experimental and numerical study on progressive flooding in full-scale," *Trans. R. Inst. Nav. Archit. Part A Int. J. Marit. Eng.*, vol. 152, no. 4, pp. 197–208, 2010.

[30] H. Dankowski and H. Dilger, "Omae2013-10342," *Omae*, no. 1, pp. 1–10, 2013.

[31] H. Dankowski, P. Russell, and S. Krüger, "OMAE2014-23323 New Insights into the Flooding Sequence of the Costa Concordia Accident," pp. 1–10, 2014.

[32] H. Dankowski and S. Krüger, "Progressive Flooding Assessment of the Intermediate Damage Cases as an Extension of a Monte-Carlo based Damage Stability Method The Monte Carlo Approach for Damage Stabil-," pp. 650–657, 2013.

[33] S. Lee, J. M. You, H. H. Lee, T. Lim, S. H. Rhee, and K. P. Rhee, "Preliminary tests of a damaged ship for CFD validation," *Int. J. Nav. Archit. Ocean Eng.*, vol. 4, no. 2, pp. 172–181, 2012.

[34] C. Strasser, A. Jasionowski, and D. Vassalos, "Calculation of the Time-To-Flood of a Box-Shaped Barge By Using Cfd," *10th Int. Conf. Stab. Ships Ocean Veh.*, pp. 733–740, 2009.

[35] H. Sadat-Hosseini, D. H. Kim, P. M. Carrica, S. H. Rhee, and F. Stern, "URANS simulations for a flooded ship in calm water and regular beam waves," *Ocean Eng.*, vol. 120, pp. 318–330, 2016.

[36] T. Manderbacka and P. Ruponen, "The impact of the inflow momentum on the transient roll response of a damaged ship," *Ocean Eng.*, vol. 120, pp. 346–352, 2016.

[37] E. Ypma and T. Turner, "An approach to the validation of ship flooding simulation models," in *Proceedings of the 11th international ship stability workshop*, 2010.

[38] K. S. Kim, M. I. Roh, and J. S. Kim, "A method of dynamic flooding analysis in time domain for the compartment arrangement design of a ship," *Proc. Int. Offshore Polar Eng. Conf.*, pp. 862–866, 2017.

[39] T. Manderbacka, P. Ruponen, J. Kulovesi, and J. Matusiak, "Model experiments of the transient response to flooding of the box shaped barge," *J. Fluids Struct.*, vol. 57, pp. 127–143, 2015.

[40] O. Lorkowski, H. Dankowski, F. Kluwe, S. Krüger, and K. Frömming, "A Numerical and Experimental Approach for the Assessment of the Dynamic Damage Stability of Ships," vol. 2, pp. 205–219, 2015.

[41] G. J. Lee, "Dynamic orifice flow model and compartment models for flooding simulation of a damaged ship," *Ocean Eng.*, vol. 109, pp. 635–653, 2015.

[42] S. Debra, J. William, and F. Jeffery, "Leaking Tank Experiments with Orimulsion

and Canola Oil," U.S.A., 2001.

[43] T. R. Gruber, "A translation approach to portable ontology specification," *An Int. J. Knowl. Acquis. Knowledge-Based Syst.*, vol. 5, no. 2, pp. 199–220, 1993.

[44] N. F. Noy and L. M. Deborha, *Ontology development 101: A guide to creating yout first ontology*. Stanford University, 2001.

[45] C. S. Moore and J. R. Paulling, *The Principles of Naval Architecture Series: Intact Stability*. U.S.A.: The Sociery of Naval Architects and Marine Engineers, 2010.

[46] A. J. Brown and F. Deybach, "Towards a rational intact stability criteria for naval ships," *Nav. Eng. J.*, vol. 110, no. 1, pp. 65–77, 1998.

[47] T. H. Sarhin and L. L. Goldberg, "Stability and Buotancy Criteria for US Naval Surface Ships," *Trans. SNAME*, 1962.

[48] I. 92/26/add.1, "Revised recommensdation on a standard method for evaluating cross-flooding arrangements," vol. 362, no. June, pp. 1–13, 2013.

[49] IMO, "RESOLUTION MSC.245(83) (adopted on 12 October 2007) RECOMMENDATION ON A STANDARD METHOD FOR EVALUATING CROSS-FLOODING ARRANGEMENTS," vol. 245, no. October, 2007.

[50] P. Ruponen, T. Manderbacka, and D. Lindroth, "On the calculation of the righting lever curve for a damaged ship," *Ocean Eng.*, vol. 149, no. December 2017, pp. 313–324, 2018.

[51] R. A. Gingold and J. J. Monaghan, "Smoothed particle hydrodynamics: theory and application to non-spherical starts," *Mon. Not. R. Astron. Sociery*, vol. 181, no. 3, pp. 375–389, 1977.

[52] S. Koshizuka and Y. Oka, "Moving Particle Semi-Implicit Method for Fragmentation of Incompressible Fluid," *Nucl. Sci. Eng.*, vol. 123, pp. 421–434, 1996.

[53] M. Müller, B. Heidelberger, M. Hennix, and J. Ratcliff, "Position based dynamics," *J. Vis. Commun. Image Represent.*, vol. 18, no. 2, pp. 109–118, 2007.

[54] M. Muller, B. Heidelberger, M. Hennix, and J. Ratcliff, "Position based dynamics," *J. Vis. Commun. Image Represent.*, vol. 18, no. 2, pp. 109–118, 2007.

[55] M. Macklin and M. Müller, "Position based fluids," *ACM Trans. Graph.*, vol. 32, no. 4, p. 1, 2013.

[56] M. Ihmsen, N. Akinci, M. Becker, and M. Teschner, "A parallel SPH implementation on multi-core CPUs," *Comput. Graph. Forum*, vol. 30, no. 1, pp. 99–112, 2011.

[57] C. Ericson, *Real-Time Collision Detection*. Boston, USA., 2005.

[58] J. J. Monaghan, "Smoothed particle hydrodynamics," *Online*, vol. 68, pp. 1703–1759, 2005.

[59] S. H. Ham, M. I. Roh, H. Lee, J. W. Hong, and H. R. Lee, "Development and validation of a simulation-based safety evaluation program for a mega floating crane," *Adv. Eng. Softw.*, vol. 112, pp. 101–116, 2017.

[60] W. E. Cummins, "The Impulse Response Function and Ship Motions," *Schiffstechnik*, vol. 47, pp. 101–109, 1962.

[61] M. O. Said, "Theory and Practice of Total Ship Survivability for Ship Design," *Nav. Eng. J.*, vol. 107, no. 4, pp. 191–203, 1995.

[62] U. D. of the Army, "Structures to resist the effects of accidental explosions TM5-1300," Washington, DC., 1990.

[63] Y. S. Choi, S. K. Yeo, and H. Chung, "An optimal arrangement method of blast hardened bulkhead for surface warships using a simplified vulnerability," in *Advances in Structural Engineering and Mechanics*, 2015.

[64] E. Harmsen and M. Krikke, "A probabilistic damage stability calculation method for naval vessels," in *7th International Conference on Stability of Ships and Ocean Vehicles*, 2000, pp. 330–350.

[65] J. S. Przemieniecki, *Mathematical Methods in Defense Analyses*, 3rd Editio. Virginia: AIAA Education Series, 2000.

[66] J. S. Arora, *Introduction to Optimum Design*. Boston, USA.: Academic Press, 2004.

[67] G. N. Vanderplaats, *Numerical optimization techniques for engineering design: with applications*. New York, USA.: Ingenieria Mecanica, 1984.

[68] K. Deb, A. Member, A. Pratap, S. Agarwal, and T. Meyarivan, "A fast and elitist multi-objective genetic algorithm:NSGAII," vol. 6, no. 2, pp. 182–197, 2002.

[69] E. Zitzler, M. Laumanns, and L. Thiele, "SPEA2: Improving the Strength Pareto Evolutionary Algorithm," Zurich, Swiss, 2001.

[70] A. J. Nebro, J. J. Durillo, J. Garcia-Nieto, C. A. Coello, F. Luna, and E. Alba, "SMPSO : A New PSO Metaheuristic for Multi-objective Optimization," no. 2, 2009.

[71] K. M. T. Kleefsman, G. Fekken, A. E. P. Veldman, B. Iwanowski, and B. Buchner, "A Volume-of-Fluid based simulation method for wave impact problems," *J. Comput. Phys.*, vol. 206, no. 1, pp. 363–393, 2005.

[72] Z. Wang, K. Shibata, and S. Koshizuka, "Verification and validation of explicit moving particle simulation method for application to internal flooding analysis in nuclear reactor building," *J. Nucl. Sci. Technol.*, vol. 55, no. 5, pp. 461–477, 2018.

[73] S. U. Lee, M. I. Roh, J. H. Cha, and K. Y. Lee, "Ship compartment modeling based on a non-manifold polyhedron modeling kernel," *Adv. Eng. Softw.*, vol. 40, no. 5, pp. 108–126, 2009.

[74] F. D. James, *Computer Graphics: Principles and Practice*. Addison-Wesley, 1996.

# APPENDICES

# A. Quasi-static method for flooding analysis

Quasi-static flooding analysis involves several aspects, as shown Figure A-1. First, the calculation of the amount of fluid flowing through damaged holes or openings is highly important (Figure A-1-①) Secondly, the air pressure in the compartments, particularly fully flooded compartments, should be accurately calculated (Figure A-1-②). Thirdly, as the center of gravity (CoG) of the ship changes during the analysis and the free surface of the internal liquid cargo varies depending on the vessel attitude, it is necessary to accurately estimate the shape of the liquid cargo in the ship (Figure A-1-③). Fourthly, as there are various types of liquid and solid cargo as well as the hull and the compartments, these should be considered for realistic results (Figure A-1-④). Finally, as previously mentioned, it should always be verified that the ship meets the damage stability criteria during flooding.

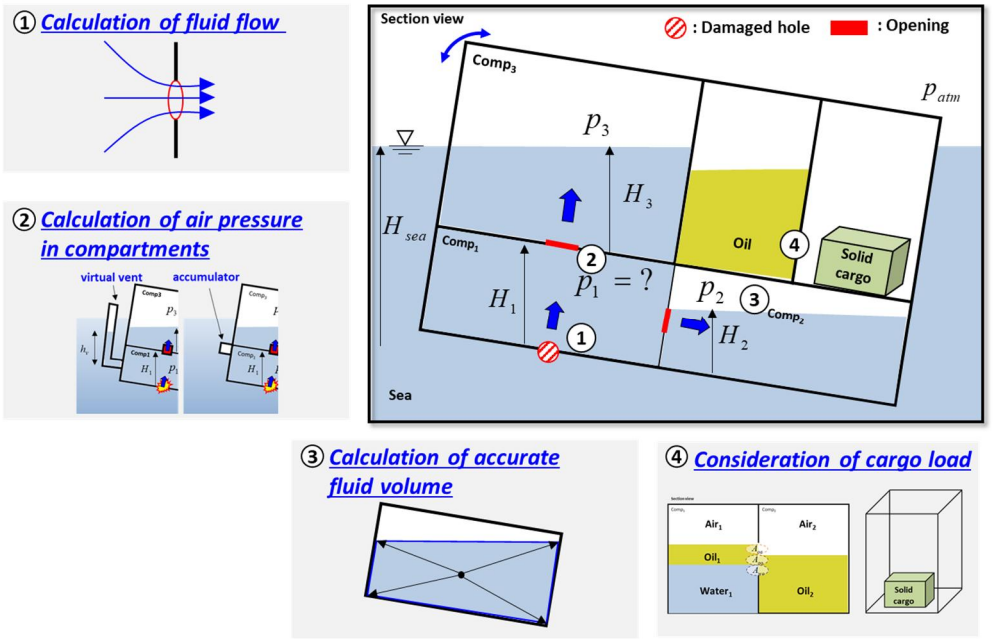


Figure A-1. Overview of quasi-static analysis

## A.1. Overall procedure of flooding analysis

It is a simple technique for simulating the flooding process. For each time step, the static position and orientation are determined considering weight and CoG changes due to flows. More precisely, Figure A-2 shows the overall procedure of the flooding analysis using the quasi-static method.

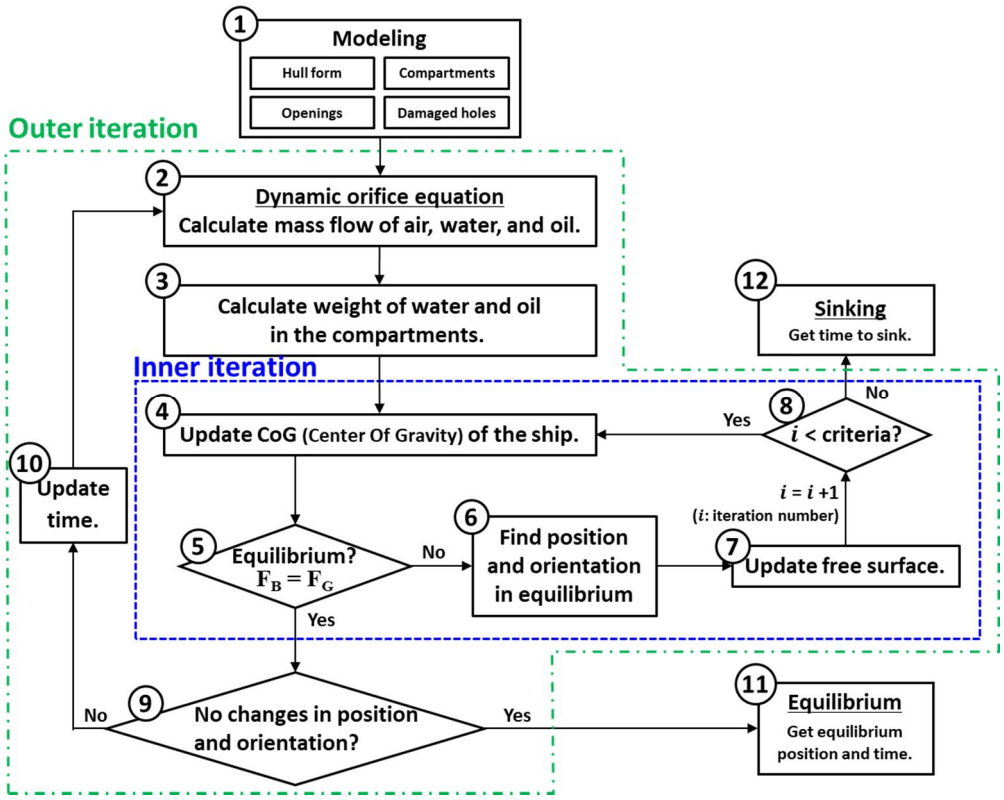


Figure A-2. Procedure of the flooding analysis using the quasi-static method

Before the analysis, data related to the damaged ship, such as hull form, compartments, openings, and damaged holes, should be collected (Figure A-2-①). Using the information on damaged holes and openings, the fluid mass flow rate at any time can be calculated using the dynamic orifice equation (Figure A-2-②), thus estimating water and oil weight changes in compartments (Figure A-2-③). Then, through the inner iterations, the static position and orientation of the ship can be determined in each step. First, the CoG of the ship is updated using the weight changes in each compartment (Figure A-2-④).

Subsequently, it is checked whether the ship is in equilibrium state or not (Figure A-2-⑤). If the buoyancy and the weight of the ship are not equal, the position and the orientation should be adjusted to achieve equilibrium (Figure A-2-⑥). Then, the free fluid surface effect should be considered in each compartment (Figure A-2-⑦), as this may change the CoG. Considering the CoG change and the free surface effect, the equilibrium position and orientation of the ship should be determined within an acceptable number of iterations (Figure A-2-⑧). The inner iteration process is schematically shown in Figure A-3. If the equilibrium state can be determined in a specific step, the process continues with outer iterations in the next step. The movement of the ship can be estimated by comparing its position and orientation between two consecutive steps (Figure A-2-⑨). If the position and orientation change, then there is still flooding, and the process continues to the next step (Figure A-2-⑩). There are two criteria for ending the simulation. In the outer iterations, if there are no changes in the position and orientation of the ship between two consecutive steps, then flooding has stopped. Therefore, the time and the final state of the ship can be obtained (Figure A-2-⑪). On the other hand, in the inner iterations, if there is no equilibrium within an acceptable number of iterations, then the ship is to sink, and the quasi-static analysis is terminated (Figure A-2-⑫).

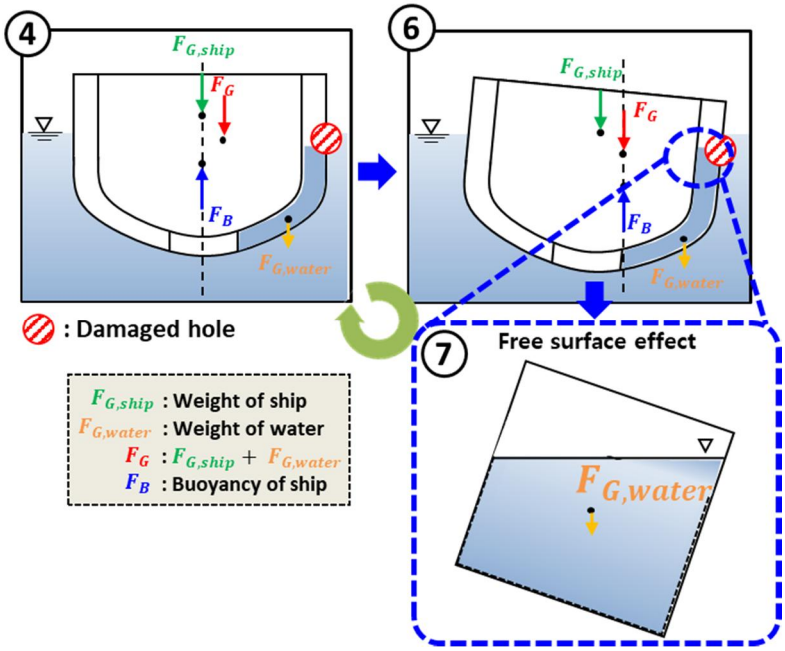


Figure A-3. Three steps of inner iterations

## A.2. Calculation of fluid flow using dynamic orifice equation

In several studies described in Section 1.2.2, the following hydraulic orifice equation, which is derived from the steady Bernoulli's equation, has been used to calculate the flow through an opening:

$$q = \rho C_D A v = \rho C_D A \sqrt{\frac{2\Delta p}{\rho}} \tag{91}$$

where q is the mass flux, $\rho$ is the density of the flow, v is the velocity at the opening,

$A$ is the area of the opening, $\Delta p$ is the pressure difference, and $C_D$ is the discharge coefficient. In Eq. (91), the rate of change with respect to the pressure difference tends to infinity as the pressure difference tends to zero. Accordingly, an unrealistic oscillation occurs when the pressure difference is small. Furthermore, it can be applied only in steady state conditions and to orifices of small cross section [41]. For this reason, Lee [41] introduced a dynamic orifice equation, which is adopted in the present study as well.

The dynamic orifice equation is derived under four physical assumptions: (1) The fluid is incompressible. (2) On the right side of the orifice (inlet), the velocity and pressure are uniformly distributed. (3) The flow is inviscid. (4) Only the normal direction of the opening is considered, and thus the control volume around the opening is accordingly defined (Fig. 4). In this figure, $p$ is the effective compartment pressure, $p_0$ is the outlet pressure, $p_1$ is the inlet pressure, $C_0$ is the outlet control volume, $C_1$ is the inlet control volume, $A_R$ is the area of the semi-sphere $C_0$, $A_{opening}$ is the opening area, $A_1$ is orifice area, and $R_0$ is the radius of $C_0$.

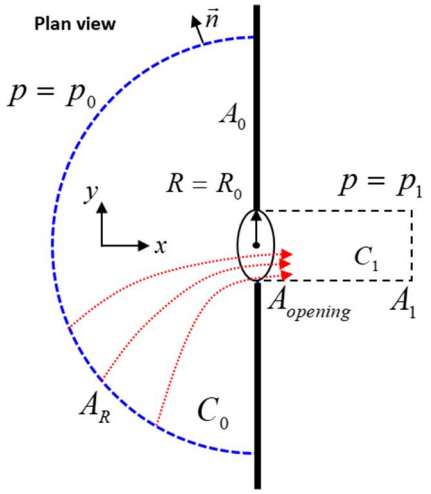


Figure A-4. Plan view for control volume of fluid around opening

To determine the fluid mass flow rate, the control volumes are set using a semi-sphere and an orifice around the openings. By applying mass conservation and momentum conservation to the control volume, the following dynamic orifice equation [41] is obtained:

$$\frac{\sqrt{A_{opening}}}{2}\frac{\partial u}{\partial t}+\frac{7}{8}(u)^2=\frac{(p_0-p_1)}{\rho} \tag{92}$$

## A.3. Calculation of air pressure for fully flooded compartments

When the ship is damaged, water comes in and propagates through openings. In this process, the air in the compartments also flows through openings or vents. Therefore, the air pressure in the compartments affects the water flow. If the compartment is not fully flooded, the air pressure can be easily calculated by Boyle's law as follows

$$p_{air}=\rho_{air}\frac{p_{atm}}{\rho_{atm}} \tag{93}$$

where $p_{air}$ is the compartment air pressure, $\rho_{air}$ is the compartment air density, $\rho_{atm}$ is the atmospheric air density, and $p_{atm}$ is the atmospheric air pressure. According to Eq. (93), if water continuously comes into the compartment, the air pressure increases

because the air density increases. However, if the compartment is fully flooded, the air pressure will drop to zero by Boyle's law. This leads to unrealistic results when flooding analysis is performed, as shown in Figure A-5.

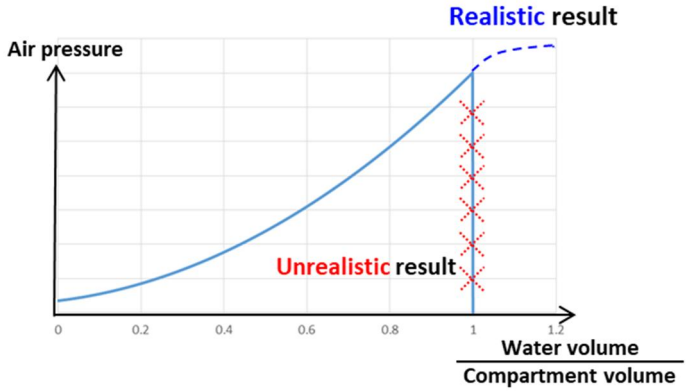


Figure A-5. Air pressure vs water volume/compartment volume ratio

To overcome this, Ruponen [27] proposed a pressure correction method, and Dankowski et al. [31] used a continuity equation considering the relation between the compartments. However, these methods require iteration schemes, and thus they are time consuming. In this study, the virtual vent and accumulator method, which was originally proposed by Lee [41], is used to resolve the problem. This method does not require iteration schemes and is therefore quite fast.

The virtual vent method is used to calculate the air pressure in compartment with vent hole or duct equipment (vented compartment). In this case, air freely flows through the vent or duct, so that the air density in the compartment is not significantly increased, whereas the accumulator method is used to calculate the air pressure in non-vented compartments (which have no vent hole at all). In this case, there is no vent or duct, so

that the air density in the compartment continuously increases as the flooding proceeds. To simulate this, a virtual vent is generated for the vented compartment and an accumulator for the airtight compartment, as shown in Fig. 6 [41].

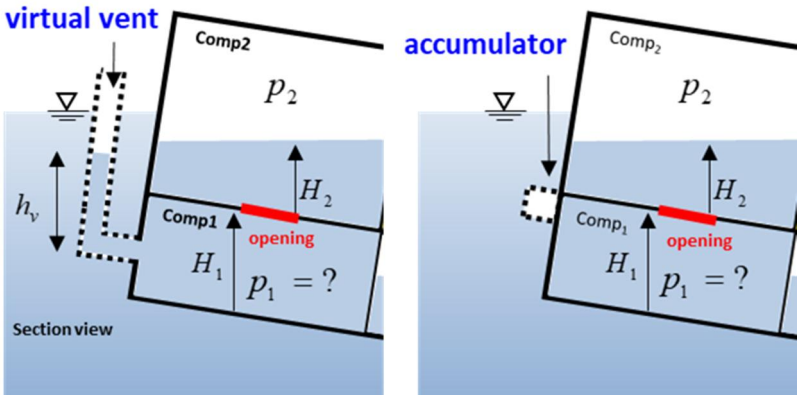


Figure A-6. Virtual vent and accumulator for fully flooded compartments

Thereby, the air pressure due to the actual airflow in the vent or duct can be determined. Then, the hydrostatic pressure due to the added water in the virtual vent is calculated, resulting in Eq. (94). Likewise, the air pressure in the non-vented compartment can be calculated by Eq. (95).

$$p_1 = \rho g h_v + p_{vent} \tag{94}$$

$$p_1 = \rho_{acc} \frac{p_{atm}}{\rho_{atm}} \tag{95}$$

where $g$ is the gravitational acceleration, $h_v$ is the height of the added water in the virtual vent, $p_{vent}$ is the pressure loss due to the flow through the vent, and $\rho_{acc}$ is the air density in the accumulator. By using the virtual vent and the accumulator, the air pressure inside fully flooded compartments can be calculated.

## A.4. Calculation of accurate fluid volume

As flooding proceeds, water comes into the compartments, and the position and orientation of the ship change. Accordingly, the volume of the water in the compartments continuously changes. Therefore, these changes should be tracked to calculate the accurate flow rate by the orifice equation. To this end, several studies (e.g., [39]) have used the fluid plane based method, whereby the water volume is calculated according to the fluid plane of the previous time step. However, this method is inaccurate when it is applied to compartments with complicated shape. Thus, in this study, polyhedral integration was used for volume calculation. The difference between the two methods is shown in Figure A-7.

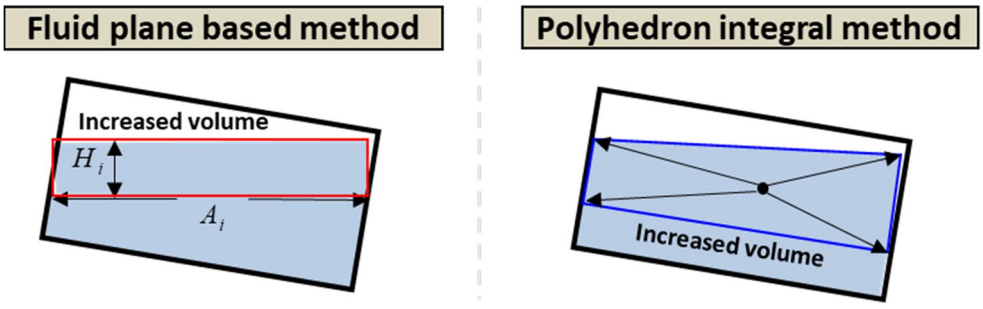


Figure A-7. Fluid plane based method and polyhedron integral method

Polyhedron integral method is used to obtain geometric properties of mesh objects [73]. In this study, triangle meshes were used to construct all models, including hull and compartments. Figure A-8 and Eq. (96) show a simple example of the calculation of the volume of a tetrahedron using polyhedral integration.

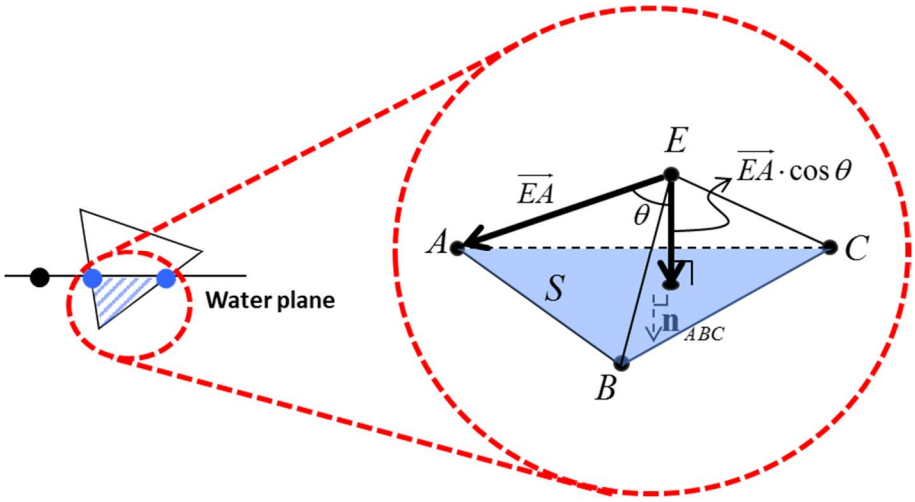


Figure A-8. Intersection between the water plane and triangle mesh of the body

$$V_{ABC-E} = \frac{1}{3} S_{ABC} \left|\overrightarrow{EA}\right| \cdot \cos\theta \tag{96}$$

where $S_{ABC}$ is the area of the triangle $ABC$ and $V_{ABC\text{-}E}$ is the volume of the tetrahedron $V_{ABC\text{-}E}$. To calculate fluid volume, information regarding the water plane, such as area or moment of inertia, and center of buoyancy (CoB) is important for accurate flooding analysis, as shown in Figure A-9. This data is used for determining the position of the

ship and for the damage stability criteria.

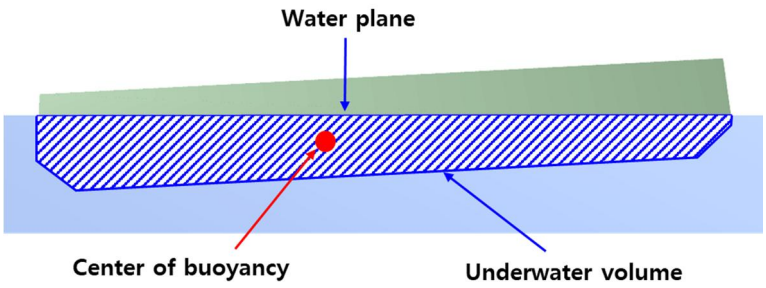


Figure A-9. Ship information for flooding analysis

## A.5. Cargo load

In most studies on flooding analysis, only the water and air flows have been considered. However, there is usually a large amount of cargo, liquid and solid. Therefore, in this study, the spilled oil is also considered (along with solid cargo items), as this is important for the evaluation of the environmental effect as well as the effect on the ship itself.

### A.5.1. Consideration of oil leakage

In Sections A.2 and A.3, the calculation of water and air flows in flooding analysis is discussed. If only consider water and air flows are considered, there are three types of interface at openings, as shown in Figure A-10.

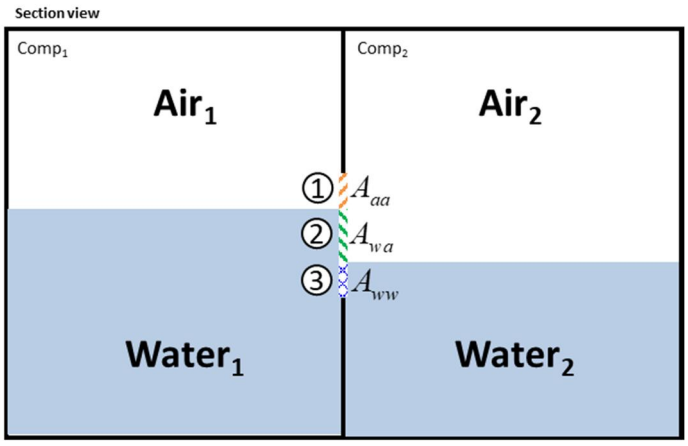


Figure A-10. Three types of interface by water and air in opening

Namely, air/air (Figure A-10-①), water/air (Figure A-10-②), and water/water (Figure A-10-③) interfaces. Then, the dynamic orifice equation can be applied individually in each case. At the air/air interface, the dynamic orifice equation has the following form:

$$\frac{\sqrt{A_{aa}}}{2}\frac{\partial u}{\partial t}+\frac{7}{8}(u)^2=\frac{(p_{Air_1}-p_{Air_2})}{\rho} \tag{97}$$

where $A_{aa}$ is the interface area, $p_{Air1}$ and $p_{Air2}$ are the section pressure in compartment 1 and compartment 2, respectively, and $\rho$ is the density of the fluid in the higher-pressure compartment. At the water/air interface, the dynamic orifice equation is applied as follows:

$$\frac{\sqrt{A_{wa}}}{2}\frac{\partial u}{\partial t}+\frac{7}{8}(u)^2=\frac{(p_{Water_1}-p_{Air_2})}{\rho} \tag{98}$$

where $A_{wa}$ is the interface area. Finally, at the water/water interface, the dynamic orifice equation is

$$\frac{\sqrt{A_{ww}}}{2}\frac{\partial u}{\partial t}+\frac{7}{8}(u)^2=\frac{(p_{Water_1}-p_{Water_2})}{\rho} \tag{99}$$

where $A_{ww}$ is the interface area. Using Eqs. (97)-(99), the corresponding flows can be calculated. Considering the height of the water in the compartments, there can be nine cases, as shown in Figure A-11. However, if oil is considered in flooding analysis, three interfaces are added. As shown in Figure A-12, the added interfaces are oil/air (Figure A-12-①), oil/oil (Figure A-12-②), water/oil (Figure A-12-③). Then, another form of the dynamic orifice equation should be applied.

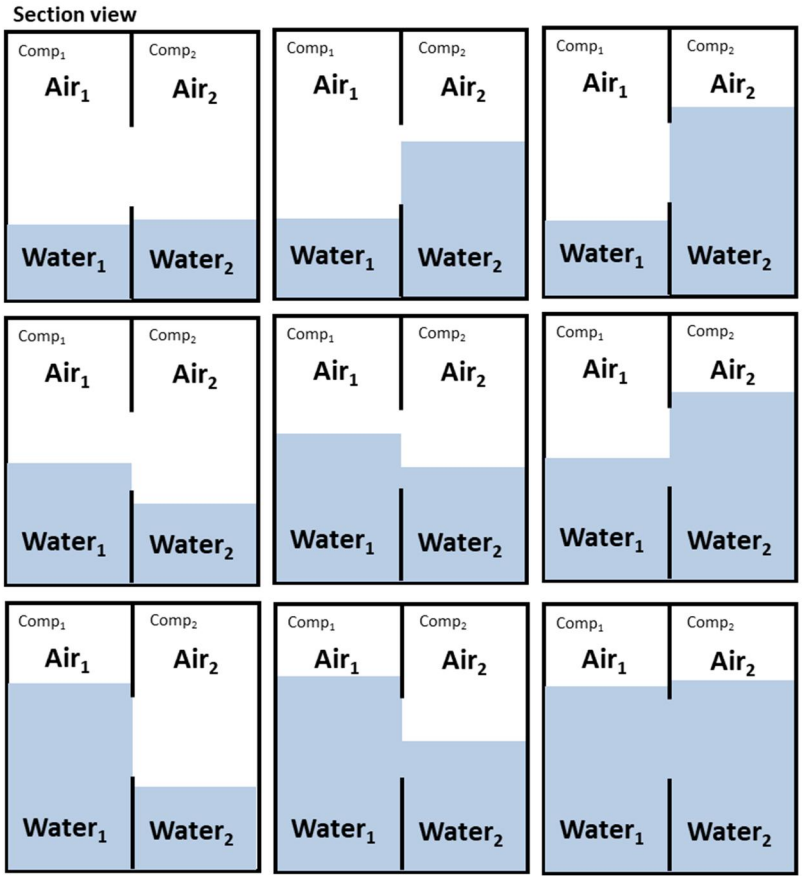


Figure A-11. Nine cases depending on water height

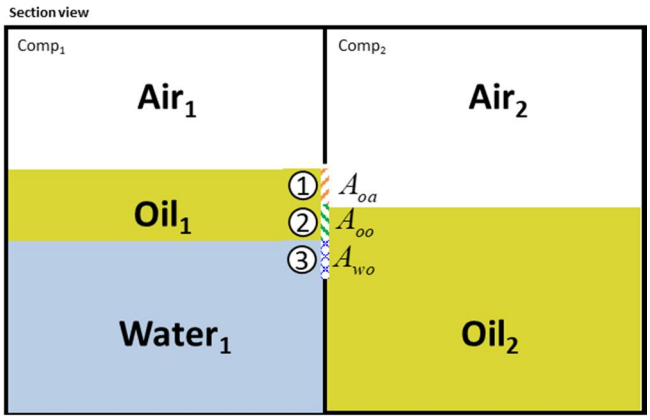


Figure A-12. Interface types between oil, water, and air

At the oil/air interface, the dynamic orifice equation is

$$\frac{\sqrt{A_{oa}}}{2}\frac{\partial u}{\partial t}+\frac{7}{8}(u)^2=\frac{(p_{Oil_1}-p_{Air_2})}{\rho} \tag{100}$$

where $A_{oa}$ is the interface area. At the oil/oil interface, the dynamic orifice equation is

$$\frac{\sqrt{A_{oo}}}{2}\frac{\partial u}{\partial t}+\frac{7}{8}(u)^2=\frac{(p_{Oil_1}-p_{Oil_2})}{\rho} \tag{101}$$

where $A_{oo}$ is the interface area. At the water/oil interface, the dynamic orifice equation is

$$\frac{\sqrt{A_{wo}}}{2}\frac{\partial u}{\partial t}+\frac{7}{8}(u)^2=\frac{(p_{Water_1}-p_{Oil_2})}{\rho} \tag{102}$$

where $A_{wo}$ is the interface area. Considering the height of water and oil in the compartments, there are additionally 35 cases, that is 44 cases in total, as shown in Figure A-13.

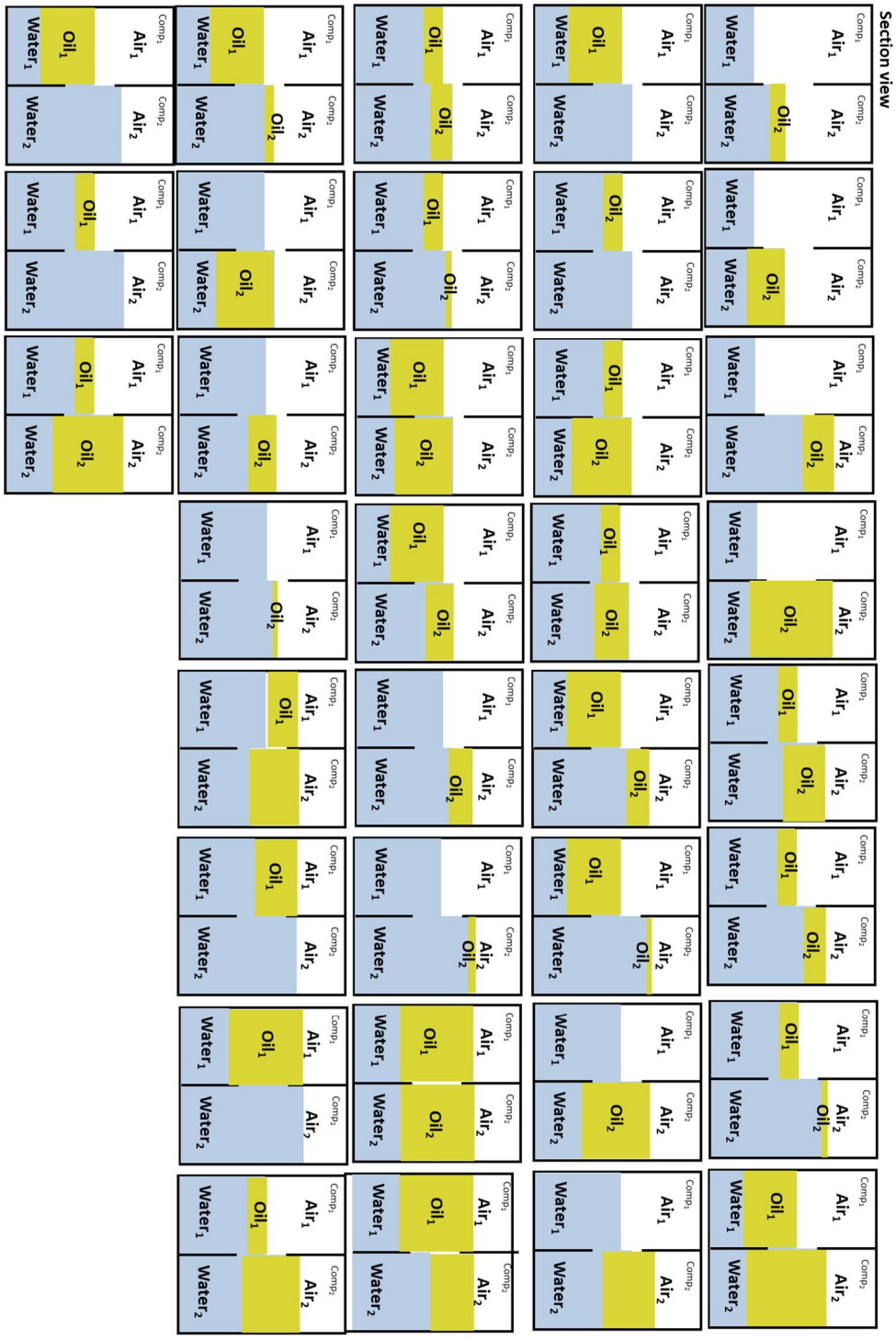


Figure A-13. Thirty-five cases depending on water and oil height

### A.5.2. Consideration of solid cargo items

Other studies on flooding analysis or damage stability have regarded solid cargo items as permeability of corresponding compartments, and thus the exact cargo shape could not be considered, resulting in inaccurate flooding analysis. Therefore, in this study, the exact cargo shape is taken into account in intermediate flooding analysis.

Solid cargo items, such as machinery equipment, piping, and accessories, have a fixed shape, and thus water or oil cannot take up their volume. To simulate this, each solid object in the fluid should be tracked. In this study, mesh models are used to express the shape of all components. To obtain the exact shape of solid objects in the fluid, and the shape of the fluid itself, constructive solid geometry (CSG) [74] was used, which is one of the techniques used in solid modeling. Using CSG, a Boolean operation was performed on the mesh models, so that the exact shape of all components could be obtained during flooding analysis.

# 국문 초록

## 침수를 고려한 함정의

## 초기 배치 설계의 적합성 평가 방법

함정의 초기 설계는 설계 요구 조건을 만족하기 위해 여러 단계를 거쳐 시행된다. 일반적으로 설계 요구 조건과 모선의 정보를 토대로 주요 제원 선정, 선형 설계, 주기관 선정, 배치 설계, 구조 설계 등의 단계를 거친다. 위의 과정 중 배치 설계는 모선의 정보와 설계자의 경험에 의존적이다. 이에 따라, 전통적으로 정량적인 평가보다는 정성적인 평가에 따라 배치 설계가 진행되었다. 그리고 설계자가 수작업으로 배치 설계를 진행하고 여러 안을 평가하기 때문에, 배치 설계를 위해 시간이 많이 소모된다. 따라서 본 연구에서는 함정의 초기 배치 설계를 위해, 정량적인 평가와 여러 안에 대한 검토를 자동화 및 최적화 하고자 하였다.

또한, 배치 설계 단계에서는 함정이 작전 도중 적절한 복원성을 가지고 있는지 확인하기 위해 선박 계산을 진행한다. 선박 계산은 정적 복원성과 손상 복원성 두 가지로 평가된다. 손상 복원성의 전통적으로 손상 이후 최종

자세만을 고려해 평가되어, 손상되어 침수가 진행되는 과정에 대한 평가가 부족하다. 또한, 선박 계산 프로그램을 통해 여러 가지 안에 대한 복원성 평가가 진행되어야 하기에 배치 설계와 마찬가지로 설계자의 공수가 많이 들어가는 과정이다. 따라서 본 연구에서는 기존 선박 계산의 한계점을 극복하기 위해, 비손상, 손상 복원성 평가뿐만 아니라 중간 단계 침수 해석을 진행하고, 이를 배치 설계 평가 과정에 적용함으로써, 함정 초기 배치 설계 및 선박 계산을 고도화, 자동화 하고자 하였다.

본 연구에서 초기 함정 배치 설계를 위해 복원성, 취약성, 운용성 세가지를 고려했다. 복원성 평가를 위해 정수 중 상태에서 정적 복원성을 검토하였다. 그리고 손상 복원성 평가는 일반적인 최종 상태에서의 손상 복원성과 더불어 중간 단계 침수를 고려해 진행되었다. 중간 단계 침수는 PBD (Position Based Dynamics)를 통해 손상부와 함정 내부의 개구부를 통해 흐르는 유량을 계산하고, 이를 통해 변경된 함정의 무게와 무게 중심을 갱신한다. 그리고 변경된 정보를 6 자유도 운동 방정식에 대입하여 매 시간마다 선박의 거동을 추적한다. 이를 통해, 손상을 통해 선박의 침수가 진행되는 과정과 그 과정에서의 손상 복원성을 평가할 수 있다. 정적 복원성 및 손상 복원성을 평가할 때, GZ 곡선 계산을 동반하게 되는데, 본 연구에서는 이를 고도화 하기 위해 기존의 상하

운동만을 고려한 GZ 값 계산에 더불어 종 경사 (trim)을 고려하였다.

함정의 취약성 평가는 격벽의 취약성과 격실의 취약성 두가지를 고려하였다. 격벽의 취약성은 다양한 손상이 격벽에 미치는 폭발 압력의 총합으로 고려되었으며, 격실의 취약성은 다양한 손상이 격실에 영향을 미칠 확률과 격실의 중요도를 곱한 값을 통해 고려되었다. 또한, 두 가지 취약성을 위해 관련 연구를 통해 다섯 가지 손상 종류 (대함 미사일, 어뢰, 기뢰, 충돌, 좌초)에 대한 함정의 길이, 폭, 높이 방향 손상 확률을 고려하였다.

함정의 운용성 평가를 정량적으로 진행하기 위해, 함정의 격실간 선원과 재화의 이동을 고려하였다. 이를 위해 각 격실간의 최단 거리와 격실간의 관계 고려하였다. 각 격실간의 관계는 가까이 있으면 좋은 격실간의 정도를 평가한 친밀성과, 서로 멀리 떨어져 있어야 하는 격실간의 적대성 두가지를 고려한 인접성을 통해 고려되었다.

위에 설명한 세가지 평가를 함정 초기 배치 설계를 위한 문제로 정식화 하였다. 최적화 문제를 설계 변수는 격벽과 갑판의 위치, 격실의 위치 및 복도의 위치로 설정되었으며, 목적 함수는 함정의 취약성을 최소화 하는것과 운용성을 최대화 하는 것으로 설정되었다. 그리고 복원성 향상을 위해 초기 GM 을 최대화 하는 것을 목적 함수로 고려하였다. 이 과정에서 각 격벽 및 갑판의 위치에

대한 제약과 기관부가 가져야 하는 길이 및 각 격실이 최소한 가져야 하는 넓이에 대한 제약이 고려되었으며, 또한 특정 격실이 가져야 하는 위치를 최적화 문제에서 제약 조건으로 고려하였다. 이를 통해 함정 초기 배치 설계의 최적 안을 도출하였으며, 도출된 최적 안은 중간 단계 침수를 포함해 손상 복원성을 만족하는지 평가되었다.

위에서 제시된 함정 초기 배치 설계 및 선박 계산 과정을 하나의 프로그램으로 개발하였으며, 이를 미 해군의 구축함에 적용하여 본 연구의 효용성을 확인하였다.

Keywords: 함정 초기 배치 설계, 복원성 평가, 중간 단계 침수 해석, PBD, 취약성 평가, 운용성 평가, 배치 최적화, 다목적 최적화

Student number: 2015-30240